

Laminar Flow Enhancement in Channels with Heat Transfer Analysis



By

Muhammad Nasir

DEPARTMENT OF MATHEMATICS

QUAID-I-AZAM UNIVERSITY

ISLAMABAD, PAKISTAN

2019

Laminar Flow Enhancement in Channels with Heat Transfer Analysis



By

Muhammad Nasir

Supervised By

Dr. Asif Ali

DEPARTMENT OF MATHEMATICS

QUAID-I-AZAM UNIVERSITY

ISLAMABAD, PAKISTAN

2019

Laminar Flow Enhancement in Channels with Heat Transfer Analysis

By

Muhammad Nasir

A THESIS SUBMITTED IN THE PARTIAL FULFILLMENT OF THE
REQUIREMENTS FOR THE DEGREE OF

DOCTOR OF PHILOSOPHY

IN

MATHEMATICS

Supervised by

Dr. Asif Ali

**DEPARTMENT OF MATHEMATICS
QUAID-I-AZAM UNIVERSITY
ISLAMABAD, PAKISTAN**

2019

DECLARATION

I Muhammad Nasir S/O Abdul Rauf, with Registration No. 031409134001, a student of Doctor of Philosophy at Quaid-i-Azam University, Islamabad Pakistan, do hereby solemnly declare that the thesis entitled "**Laminar Flow Enhancement in Channels with Heat Transfer Analysis**" submitted by me in partial fulfillment of the requirement for Doctor of Philosophy degree in Mathematics is my original work and has not been submitted and shall not, in future, be submitted by me for obtaining any degree from this or any other university or institution.

Date: 11-01-2019

Signature  _____

(Muhammad Nasir)

Plagiarism Undertaking

I solemnly declare that research work presented in the thesis titled “**Laminar Flow Enhancement in Channels with Heat Transfer Analysis**” is solely my research work with no significant contribution from any other person. Small contribution/help wherever taken has been acknowledged and complete thesis has been written by me.

I understand the zero tolerance policy of the HEC and Quaid-i-Azam University towards plagiarism. Therefore, I, as an author of the above title thesis declare that no portion of my thesis has been plagiarized and any material used as reference is properly referred/cited.

I undertake that I am found guilty of any formal plagiarism in the above titled thesis even afterward of PhD degree, the university reserves the rights to withdraw/revoke my PhD degree and that HEC and the university has the right to publish my name on the HEC/University Website on which names of students are placed who submitted plagiarized thesis.



Student/Author Signature:
Name: Muhammad Nasir

Laminar flow enhancement in channels with heat transfer analysis

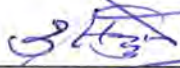
By

Muhammad Nasir


CERTIFICATE

A DISSERTATION SUBMITTED IN THE PARTIAL FULFILLMENT OF THE
REQUIREMENTS FOR THE DEGREE OF THE DOCTOR OF
PHILOSOPHY


We accept this dissertation as conforming to the required standard

1. 


Prof. Dr. Tasawar Hayat
(Chairman)

2. 

Dr. Asif Ali
(Supervisor)

3. 

Prof. Dr. Nazir Ahmad Mir
Department of Basics Sciences
Riphah International University I-14
Hajj Complex, Islamabad
(External Examiner)

4. 

Dr. Rahmat Ellahi
Associate Professor
Department of Mathematics & Statistics
International Islamic University
H-10 Sector, Islamabad
(External Examiner)

Department of Mathematics
Quaid-I-Azam University
Islamabad, Pakistan
2018

Certificate of Approval

This is to certify that the research work presented in this thesis entitled **Laminar flow enhancement in channels with heat transfer analysis** was conducted by Mr. **Muhammad Nasir** under the kind supervision of **Dr. Asif Ali**. No part of this thesis has been submitted anywhere else for any other degree. This thesis is submitted to the Department of Mathematics, Quaid-i-Azam University, Islamabad in partial fulfillment of the requirements for the degree of Doctor of Philosophy in field of Mathematics from Department of Mathematics, Quaid-i-Azam University Islamabad, Pakistan.

Student Name: **Muhammad Nasir**

Signature: _____


External committee:

a) **External Examiner 1:**

Name: **Dr. Nazir Ahmad Mir**

Designation: Professor

Office Address: Department of Basics Sciences Riphah International University I-14 Hajj Complex, Islamabad.

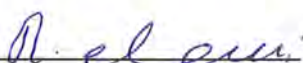
Signature: _____


b) **External Examiner 2:**

Name: **Dr. Rahmat Ellahi**

Designation: Associate Professor

Office Address: Department of mathematics, International Islamic University, H-10, Islamabad.

Signature: _____


c) **Internal Examiner**

Name: **Dr. Tasawar Hayat**

Designation: Professor


Office Address: Department of Mathematics, QAU Islamabad.

Supervisor Name:

Dr. Asif Ali

Name of Dean/ HOD

Prof. Dr. Tasawar Hayat

Signature: _____


Signature: _____


Signature: _____




Dedication

*To my father Hafiz Abdul Rauf
mother Ruqia Bagum
wife Tayyaba Aftab
brother Muhammad Nouman
and my sisters
for their enthusiasm,
compassion,
and patience*

Acknowledgement

Praise is to Allah Almighty, Creator and Sustainer of the heavens and the earth, and everything between them, Lord of lords, who gave me the potential and ability to complete this dissertation. All of my respect and veneration goes to the Holy Prophet Muhammad (Peace be upon him) who showed humanity the right path, brought the message of peace, love and emphasized the necessity and importance of knowledge. Respect is due for his family, friends, companions and all followers (Peace be upon all of them).

I owe my deepest gratitude to Prof. Dr. Asif Ali who not only supervised this dissertation but always been a source of stimulation for me. He always encouraged me to set prodigious goals and to find own ways to achieve them. His stimulating suggestions, conscious guidance and superb planning abetted me in the completion of this thesis. This dissertation could not have been completed without generous support and guidance of Prof. Waseem Siddiqui, Dr. Ahmar Mehmood and Dr. Sufian Munawar. Their fabulous provision, valuable suggestions and careful readings are extremely accredited in the completion of this work. I am also grateful to Prof. Dr. Tasawar Hayat, chair department of Mathematics, for providing research oriented environment and excellent facilities at the department. I would always be indebted to all my teachers of Quaid-I-Azam University by whom I gained marvelous skills and knowledge.

I gratefully acknowledge the marvelous company of my closest friends Dr. Adnan Saeed Butt, Dr. Attaullah, Dr. Sajjad Shoukat, Dr. Abdul Razaq and Dr. Nazim Tufail, we spent delightful moments together at QAU. I am thankful to my seniors (Dr. Sufian Munawar and Dr. Azeem) for their moral support and good wishes. Moreover, I am thankful to all those numerous well-wishers who prayed for my success, I am not being able to mention here all of them.

Finally, my sincere gratitude goes to my parents who supported me indirectly with great concern, generous support, love and prayers for my achievements. Words are countless to say thank to those benevolent hands that sincerely raised me with gentle love, care and patience. Without their prayers and sacrifices I could not be able to successfully complete whole of my educational career. Many thanks go to my brother Muhammad Nouman, my sisters, my nephews Farhan Ali, Aman Ali, Ayesha Bilal and Khedja Bilal for their great concern and encouragement. May almighty Allah reward all of them with great honor in this world and the world hereafter Ameen.

Muhammad Nasir
January, 2019

Abstract

Investigation of flow and heat transfer phenomena in a channel filled partially or fully with porous medium is of significant interest as it has numerous applications in heat exchangers, crude oil extraction, jet printers, petroleum reservoir, filtration mechanism, magnetic refrigerator, rocket propulsion etc. It is observed that the pressure gradient and temperature difference play vital role in the channel and pipe flows. Also, presence of porous medium has a significant effect on heat transfer phenomenon. Theoretical analysis of such flows is helpful to examine more complex problems related to flow and heat transfer phenomena. A lot of research has been conducted in this direction. However, characteristics of heat transfer in composite channel flows are yet to be explored as a few literature is available on this topic. Keeping this in mind, emphasis has been paid on the steady of flow and heat transfer characteristics in channels partially or fully filled with porous medium. Newtonian and non-Newtonian fluid known as Casson fluid have been considered and the impact of presence of magnetic field, unsteadiness and suction/injection on fluid flow and heat transfer are observed. The considered problems are mathematically modelled using momentum and energy equations. In some particular cases, entropy generation effects are also investigated to measure the energy losses during these processes.

Different techniques like numerical and analytical are used to solve partial differential equations which govern heat transfer and flow phenomena. Regular perturbation method is used to solve analytically the governing equations whereas finite difference scheme are employed to obtain the numerical solutions. The validity and accuracy level of the solutions have been determined either by comparing both the solutions or calculating the residual error.

The analysis carried out in this dissertation reveals that the presence of porous medium decreases the velocity of the fluid within the pipes or composite channels. Also, it is noticed that the flow and heat transfer strongly depend on the viscosity ratios, magnetic field parameter, thermal conductivity ratios, inclination angle and porosity parameter. Moreover, the Newtonian fluid velocity is higher than the Casson fluid velocity for irregular channel with convective boundary conditions. In case of composite channel, temperature enhancement is more in porous region as compared to clear region. Furthermore, presence of porous medium, magnetic field parameter and viscous dissipation effects are the major factor responsible for entropy generation.

Table of Contents

Chapter 1 Introduction and Preliminaries.....	14
1.1 Historical Background.....	14
1.2 Dynamics of Fluid	24
1.2.1 Newtonian Fluids	24
1.2.2 Non-Newtonian Fluids.....	25
1.3 Kinds of Flows.....	25
1.3.1 Laminar and Turbulent Flow.....	25
1.3.2 Steady and Unsteady Flow.....	25
1.3 Uniform and Varied Flow	25
1.4 Porosity and Porous Medium	26
1.4.1 Porous Medium	26
1.4.2 Porosity.....	26
1.4.3 Permeability	26
1.4.4 Shear Stress-Jump Condition	27
1.5 Governing Laws	27
1.5.1 Equation of Continuity.....	27
1.5.2 Navier-Stokes Equation.....	28
1.5.3 Energy Equation.....	29
1.5.4 Darcy Law	30
1.5.5 Darcy-Brinkman Equation.....	30
1.5.6 Second Law of Thermodynamics	30
1.6 Dimensionless Parameters.....	31
1.6.1 Eckert Number.....	31
1.6.2 Darcy Number	31
1.6.3 Grashof Number.....	32
1.6.4 Bejan Number.....	32
1.6.5 Biot Number.....	32
1.6.6 Schmidt Number.....	32
1.6.7 Skin Friction.....	33



1.6.8	Nusselt Number.....	33
1.6.9	Sherwood Number.....	33
Chapter 2	Heat Transfer and Time Dependent Flow through a Composite Channel having an Oscillating Wall.....	35
2.1	Introduction.....	35
2.2	Mathematical Formulation.....	35
2.2.1	Flow and Heat Transfer Phenomena.....	35
2.3	Solution Methodology.....	38
2.3.1	Regular Perturbation Method.....	38
2.3.2	Finite Difference Method.....	40
2.4	Comparison of Obtained Results.....	40
2.5	Results and Discussion.....	41
2.6	Concluding Remarks.....	48
Chapter 3	Unsteady Flow and Heat Transfer through a Composite Cylinder Partially Filled with Porous Medium.....	49
3.1	Introduction.....	49
3.2	Flow and Heat Transfer inside a Composite Porous Annulus with Time Dependent Injection.....	49
3.2.1	Mathematical Formulation.....	49
3.2.2	Solution Methodology.....	52
3.3	Results and Discussion.....	54
3.4	Concluding Remarks.....	62
3.5	Flow over a Permeable Cylinder Bounded by a Semi-Infinte Porous Medium.....	63
3.5.1	Mathematical Modeling.....	63
3.5.2	Solution of the Problem.....	65
3.5.3	Results and Discussion.....	65
3.5.4	Concluding Remarks.....	68
Chapter 4	Unsteady Chemically Reacting Casson Fluid Flow in an Irregular Channel with Convective Boundary Conditions.....	69
4.1	Introduction.....	69
4.2	Mathematical Formulation.....	69

4.2.1	Quantities of Physical Interest	72
4.3	Solution of the Problem	73
4.4	Results and Discussion.....	77
4.5	Concluding Remarks.....	85
Chapter 5	Unsteady Flow and Heat Transfer in an Inclined Composite Channel with an Oscillating Wall.....	86
5.1	Introduction.....	86
5.2	Mathematical Formulation	86
5.3	Solution of the Problem	89
5.3.1	Analytical Method.....	89
5.3.2	Numerical Method.....	91
5.4	Entropy Generation Analysis.....	92
5.5	Results and Discussion.....	94
5.6	Concluding Remarks.....	100
Chapter 6	Flow and Heat Transfer Analysis in an Inclined Channel with Embedded Region of Porous Medium.....	102
6.1	Introduction.....	102
6.2	Mathematical Modeling	102
6.3	Solution Methodologies	105
6.3.1	Analytical Solution.....	105
6.3.2	Numerical Scheme	107
6.4	Quantities of Physical Interest.....	108
6.4.1	Skin Friction.....	108
6.4.2	Nusselt Number.....	108
6.4.3	Entropy Generation.....	109
6.5	Results and Discussion.....	110
6.6	Concluding Remarks.....	119
Chapter 7	Conclusion and Future Work.....	121
7.1	Concluding Remarks.....	121
7.2	Future Work.....	122
Bibliography.....		123

List of Figures

Figure 2.1: Schematic flow diagram of the considered problem	36
Figure 2.2: The plots of velocity for various inputs of pressure gradient P	42
Figure 2.3: The plots of temperature for various inputs of pressure gradient P	42
Figure 2.4: The plots of velocity for various inputs of the ratio of viscosities m	43
Figure 2.5: The plots of temperature for various inputs of the ratio of viscosities m	43
Figure 2.6: The plots of velocity for various inputs of the porosity parameter σ	44
Figure 2.7: The plots of temperature for various inputs of the porosity parameter σ	44
Figure 2.8: The plots of velocity for various inputs of oscillatory parameter εA	45
Figure 2.9: The plots of temperature for various inputs of oscillatory parameter εA	45
Figure 2.10: The plots of velocity for various inputs of angular frequency ω	46
Figure 2.11: The plots of temperature for various inputs of angular frequency ω	46
Figure 2.12: The plots of temperature for various input of the ratio of the conductivities k	47
Figure 2.13: The plots of temperature for various inputs of the Eckert number Ec	47
Figure 2.14: The plots of temperature for various inputs of the ratio of the Prandtl number Pr ..	47
Figure 3.1: Schematic diagram and coordinate system	50
Figure 3.2: Velocity w versus r for various inputs of porosity parameter σ	55
Figure 3.3: Temperature θ versus r for various inputs of porosity parameter σ	55
Figure 3.4: Velocity w versus r for various inputs of the viscosities ratio parameter m	56
Figure 3.5: Temperature θ versus r for various inputs of viscosities ratio parameter m	56
Figure 3.6: Temperature θ versus r for various inputs of Prandtl number Pr	57
Figure 3.7: Temperature θ versus r for various inputs of ratio of conductivities k	57
Figure 3.8: Temperature θ versus r for various inputs of Eckert number, Ec	58
Figure 3.9: Velocity w versus r for various inputs of oscillation amplitude εA	58
Figure 3.10: Temperature θ versus r for various inputs of oscillation amplitude εA	59
Figure 3.11: Velocity w versus r for various inputs of pressure gradient P	59
Figure 3.12: Temperature θ versus r for various inputs of the pressure gradient P	60
Figure 3.13: Velocity w versus r for various inputs of frequency ω	60
Figure 3.14: Temperature θ versus r for various inputs of the frequency ω	61
Figure 3.15: Velocity w versus r for various inputs of Reynold number Re	61

Figure 3.16: Temperature θ versus r for various inputs of Reynold number Re	61
Figure 3.17: Schematic diagram of the considered problem	63
Figure 3.18: Plots of velocity w for various inputs of the ratio of viscosities m	65
Figure 3.19: Plots of velocity w for various inputs of pressure gradient P	66
Figure 3.20: Plots of velocity w for various inputs of stress jump parameter β_1	66
Figure 3.21: Plots of velocity w for various inputs of magnetic parameter M	67
Figure 3.22: Plots of velocity w for various inputs of suction Reynold parameter S	67
Figure 3.23: Plots of velocity w for various inputs of porosity parameter σ	68
Figure 4.1: Schematic flow diagram.....	70
Figure 4.2: Velocity distribution for various inputs of Biot number B_i	78
Figure 4.3: Velocity distribution for various inputs of radiation absorption parameter α_c	78
Figure 4.4: Velocity distribution for various inputs of thermal radiation parameter F	79
Figure 4.5: Velocity distribution for various inputs solutal Grashof number G_c	79
Figure 4.6: Velocity distribution for various inputs of thermal Grashof number G_r	80
Figure 4.7: Mass concentration distribution for various inputs of chemical reaction parameter K_r	80
Figure 4.8: Mass concentration distribution for various inputs of Schmidt number S_c	81
Figure 4.9: Temperature distribution for various inputs of Biot number B_i	81
Figure 5.1: Geometry of the considered problem	87
Figure 5.2: Influence of porosity parameter σ on the velocity profile	94
Figure 5.3: Influence of inclination angle α on the velocity profile.....	95
Figure 5.4: Influence of mixed convection parameter λ on the velocity profile	95
Figure 5.5: Influence of porosity parameter σ on the temperature profile.....	96
Figure 5.6: Influence of inclination angle α on the temperature profile	96
Figure 5.7: Influence of mixed convection parameter λ on the temperature profile.....	97
Figure 5.8: Influence of the Eckert number Ec on the temperature profile.....	97
Figure 5.9: Influence of inclination angle α on the entropy generation number.....	98
Figure 5.10: Influence of group parameter Br/Ω on the entropy generation number	98
Figure 5.11: Influence of mixed convection parameter λ on the entropy generation number.....	99

Figure 5.12: Influence of inclination angle α on the Bejan number	99
Figure 5.13: Influence of group parameter Br / Ω on the Bejan number	100
Figure 5.14: Influence of mixed convection parameter λ on the Bejan number	100
Figure 6.1: Schematic Diagram and coordinate system.....	103
Figure 6.2: Velocity profile for variation in the magnetic field M	110
Figure 6.3: Velocity profile for variation in the porosity parameter σ	111
Figure 6.4: Velocity profile for variation in the favorable pressure gradient P	111
Figure 6.5: Velocity profile for for variation in the adverse pressure gradient P	111
Figure 6.6: Velocity profile for variation in the inclination angle α	112
Figure 6.7: Temperature profile for variation in the favorable pressure gradient P	113
Figure 6.8: Temperature profile for variation in the Prantdl number Pr	113
Figure 6.9: Temperature profile for variation in magnetic field parameter M	113
Figure 6.10: Temperature profile for variation in the inclination angle α	114
Figure 6.11: Entropy generation for variation in group parameter Br / Ω	115
Figure 6.12: Bejan number for variation in group parameter Br / Ω	115
Figure 6.13: Entropy generation for variation in magnetic field parameter M	116
Figure 6.14: Bejan number for variation in magnetic field parameter M	116
Figure 6.15: Entropy generation for variation in porosity parameter σ	116
Figure 6.16: Bejan number for variation in porosity parameter σ	117
Figure 6.17: Entropy generation for variation in the inclination angle α	117
Figure 6.18: Bejan number for variation in the inclination angle α	117
Figure 6.19: Skin friction for variation in the both inclination angle and magnetic field	118
Figure 6.20: Skin friction for various inputs of the both porosity parameter and magnetic field	118
Figure 6.21: The Nusselt number for variation in the both inclination angle and magnetic field	119
Figure 6.22: The Nusselt number for various values of the both porosity parameter and magnetic field	119

List of Tables

Table 2.1: Comparison of values of velocity u , and temperature θ at different values of y .

The values of physical parameters $Ec = 2$, $Pr = 0.2$, $k = 0.25$, $P = -1$, $m = 0.25$

$\sigma = 1$, $\omega = 1$, $\omega t = \pi/3$, are kept constant.....41

Table 3.1: Shows the values for velocity w , temperature θ and at their derivatives by taking the

values of r between 1.0 and 2.0. Here $k = 0.25$, $Ec = 1$, $Pr = 1$, $\epsilon A = 0.2$, $Re = 1$

$\sigma = \frac{1}{2}$, $m = \frac{1}{4}$, $P = -2$, $\omega = 5$, $\omega t = \frac{\pi}{3}$, are kept fixed. 54

Table 4.1: Variation of shear stress at $y = 0$ and $y = 1$ while taking values of parameters

$S_c = 0.96$, $t = 2$, $G_c = 2$, $G_r = 2$, $Pr = 0.71$, $K_r = 2$, $\alpha_T = 2$, $\alpha_c = 2$, $M = 2$, $Bi = 0.2$. 83

Table 4.2: Variation of Nusselt number at $y = h$ and $y = 1$ while taking the values of parameters

are $S_c = 0.96$, $t = 2$, $G_c = 2$, $G_r = 2$, $Pr = 0.71$, $K_r = 2$, $\alpha_T = 2$, $M = 2$, $Bi = 0.2$,

$\alpha_c = 2$84

Table 4.3: Variation of Sherwood number at $y = h$ and $y = 1$ while taking values of the

parameters are $M = 2$, $Bi = 0.2$, $G_c = 2$, $G_r = 2$, $Pr = 0.71$, $K_r = 2$, $\alpha_T = 2$,

$S_c = 0.96$, $t = 2$, $\alpha_c = 2$84

Nomenclature

A	A positive constant	k'	Consistency index
A_1	First Rivlin-Ericksen tensor	K_r	Chemical radiation parameter
B_0	Dimensional magnetic field parameter	K_{eff}	Thermal conductivity in porous region
B_i	Biot number	$K_{\lambda 1w}$	Radiation absorption coefficient at the wall
Be	Bejan number	k	Ratio of thermal conductivities
Br	Brinkmann number	k_{11}	time steps for porous region
(b_x, b_y, b_z)	Body force component in (x, y, z)	k_{21}	time steps for clear region
(b_r, b_θ, b_z)	Body force component in (r, θ, z)	M	Magnetic field parameter
C_1	Mass concentration of wavy wall	m	Ratio of viscosities
C_2	Mass concentration of flat wall	M^2	Hartmann number
C_p	Specific heat at constant pressure	\dot{m}	Mass flow rate
D	Diffusion coefficient	n	Flow behavior index
D_a	Darcy number	Nu	Nusselt number
Ec	Eckert number	N_s	Entropy generation number
F	Thermal radiation	P	Pressure gradient
G_c	Solutal Grashof number	Pr	Prantdal number
G_r	Thermal Grashof number	q	Flow rate of the fluid
h	Vertical length of channel	q_w	Heat transfer rate
h_{11}	Space step for porous region	(r, θ, z)	Cylindrical coordinates
h_{21}	Space step for clear region	Re	Reynold number
h_f	Heat transfer coefficient	R_1	Radius of inner cylinder
I	Complex number	R_2	Radius of outer cyliner
\mathbf{I}	Identity tensor	$R_m = \frac{R_1 + R_2}{2}$	
K	Thermal conductivity of the fluid	S	Permeability of porous medium

S	Reynold suction/ injection parameter	u_{anal}	Analytical values of velocity
Sh	Sherwood number	u_{num}	Numerical values of velocity
S_c	Schmidt number	(u, v, w)	Velocity components in cartesian form
\dot{S}_{gen}	Entropy generation rate	V	Velocity vector
s'	Specific entropy	(w_r, w_θ, w_z)	Velocity components in cylindrical form
t	Time	(x, y, z)	Cartesian coordinates
T	Temperature of the fluid		
T	Cauchy Tensor		
T_∞	Temperature of the ambient fluid		
u_0	Reference velocity		

Greek Letters

α_T	Heat absorption parameter	θ	Dimensionless temperature
α_c	Heat-source/sink parameter	∇	Differential operator
$\chi = \begin{cases} 1 & \text{for porous matrix region} \\ 0 & \text{for clear fluid region} \end{cases}$		σ_1	Electrical conductivity
$\chi_\mu = \begin{cases} \mu_{eff} & \text{for porous matrix region} \\ \mu & \text{for clear fluid region} \end{cases}$		β_T	Thermal expansion coefficient
$\chi_k = \begin{cases} K_{eff} & \text{for porous matrix region} \\ K & \text{for clear fluid region} \end{cases}$		β_C	Concentration expansion coefficient
ρ	Fluid density	λ_1	Frequency parameter of the wavy wall
β	Coefficient of thermal expansion	ν	Kinematic viscosity
ε	Amplitude	γ	Casson fluid parameter
δ_{li}	Kronecker delta	μ	Dynamic viscosity
λ	Mixed convection parameter	μ_{eff}	Viscosity in porous region
σ^2	Dimensionless porosity parameter	ω	Frequency parameter
α	An inclination angle	Ω	Dimensionless temperature difference
		β_1	Stress jump parameter
		ΔT	Change in temperature
		θ_{anal}	Analytical values of temperature
		θ_{num}	Numerical values of temperature

Abbreviations

PDEs	Partial differential equations	BTCS	Backward time central spacing
ODEs	Ordinary differential equations	HAM	Homotopy analysis method
FDS	Finite difference scheme	MHD	Magnetohydrodynamics
3-D	Three Dimensional		

Chapter 1

Introduction and Preliminaries

This chapter includes the historical background of the flow and heat transfer in the channel. Also, the discussion is done related to the entropy generation effects in flow and heat transfer phenomena in different geometrical configurations. Moreover, this chapter comprises of the definitions and basic laws frequently used in this thesis besides the techniques to solve the non-linear PDEs.

1.1 Historical Background

The study of flows inside pipes or channels has historical significance. In the 19th century, Poiseuille (1797-1896) performed an experiment in pipe flow which on later, led to the development of equations for laminar flow in pipes. In literature, major contribution is associated with two scientists: Weisbach (1806-1871) and Henri Darcy (1803-1858). They made major contribution in the field by developing equations for frictional resistance in channel and pipe flows. During the last decades of the 19th century, experimental research played a vital role in the development of fluid mechanics; for example, the first towing tank for model testing of ships, wind tunnel and the first realistic attempt to model a tidal estuary. Reynold (1842-1912) explained the different types of flow such as cavitation problem and Darcy frictional law. The rapid growth of industries in the 19th and 20th centuries was due to better understanding of fluid flow phenomena. In 1901 Prandtl (1875-1953) proposed that flow regime can be divided into two parts: inviscid fluid and the transition layer at the fixed boundaries. Prandtl combined both disparate schools of thoughts and laid the foundation for the development of unified science of fluid mechanics. Prandtl published a series of papers in the third and fourth decades of 19th century, covering various aspects of boundary layer theory. In the 1930s the efforts of Nikuradse, Moody and others resulted in the clear understanding of pipe flows. This lead to the modern techniques to understand the flow behavior in pipes and channels.

After 1945, invention of electronic computers and advancements in data logging equipment led to better understanding of the nature of steady, turbulence and unsteady laminar flows in channels. The solutions of two dimensional Navier-Stokes equations provide better understanding in the flow behavior of the channel. Some of the applications of channel flow are, flow in blood oxygenators, the design of porous pipe, blood flow in capillaries and artificial kidney. Further applications of oscillatory channel flows are: the paper industry, manufacturing and processing of foods, oil drilling and many others. The most appropriate modeling and better understanding of different behavior of fluid in channel flows are required to understand the phenomenal results of these applications.

An ideal flow situation experienced in factual life is the assumption of laminar flow in a porous walled channel. Different literature reviews suggest that numerous research articles has been published in the field of porous walls channel due to its importance in gaseous diffusion and inspiration cooling. Pfitzner [1] described an analogy between laminar fluid flow along a tube and the flow of electrical current along a conductor. The pulsating laminar heat transfer behavior between parallel plates was observed by Siegel [2] for both thermal entrance and fully developed regions. These studies were used for two dimensional steady state incompressible laminar flow by Berman [3] and then by Terrill [4]. While two dimensional, viscous incompressible fluid flow in a parallel-walled channel was discussed in [5, 6]. For various Reynolds number taken on walls of channel, different conditions of large and small injection/suction velocities are discussed [7]. The magnitude of Reynolds number is of order 10 for practical applications such as boundary layer control and transpiration cooling problems. Brady [5] discussed the inlet velocity profile in a porous tube and channel. He proved that when $Re > 2.3$, the inlet velocity profile does not decay necessarily into the fully developed, similarity profile for an infinite tube. Using the power series solution in a uniform porous tube, White [8] addressed the laminar flow taken to be fully developed. Due to application in membrane separation processes, biological transport processes and filtration, one impermeable wall and one porous wall is very important, this laminar flow is discussed by Cox [9]. Cox [10] and Sellars [11] extended the idea of Berman [3] for high suction Reynold number. The obtained analytical results were compared with numerical solution. Asymptotic solution for the flows inside porous channel were obtained by Lu [12]. Taylor [13] solved the three-dimensional flow taken to be in

a channel which is porous. To establish the laminar flow in porous tube/pipe with permeable walls, both experimental and theoretical research [7-9] have been carried out. It was proved that under the axial flow Reynold number turbulent flow appeared and the regions of reverse flow were unstable. Andersson [14] determined that the time needed to attain a steady state is majorly lessened in the lesser porous channels. Skalak [15] found trivial solutions of laminar flow for porous tube/channel. Solutions for large suction Reynold number is presented by Terrill [16] in case of incompressible and electrically conducting porous channel due to transverse magnetic field. Wang [17] shown flow, through a finned porous channel, due to possible applications in bed reactors with enhanced catalysis through the fins. The heat transfer in a porous channel, due to MHD vibratory flow was considered by Choudhury and Das [18].

In the last few decades, the practical applications of porous media in different fields broadened this concept in the study of chemical catalytical reactors, direct-contact heat exchangers, building thermal insulation and petroleum reservoirs. However, this rapid usage of porous media demanded a detailed understanding of related transport procedures. In addition to this, some basic simplifications related to geometric complexities of the porous media are described. The oscillatory fluid flow between two parallel plates was discussed by Khodadadi [19] considered two impermeable parallel plates bounding the channel, filled with porous medium, having fully developed oscillatory fluid flow. To find the heat transfer characteristics, considering forced pulsating flow, Brinkman-Forchheimer-extended Darcy model was used by Kim et al. [20] in a saturated porous media filling the channel. Neale and Nader [21] presented that for boundary layer regions, Brinkman extension of Darcy's law can be used. So, in case of thin channel, lubrication processes and flow through fractures within petroleum reservoir formation, its effects on external flows can become significant. Moreover, the work was extended to various geometries and under different physical assumptions by [22, 23]. Batchelor [24] discussed different types of fluid flows in his book "*An Introduction to Fluid Dynamics*". Rectangular channel with laminar oscillatory flow was discussed by [25]. Taking isothermal boundary condition in a channel embedded with a porous medium, Chamkha [26] considered Non-Darcy, fully developed and mixed convection flow. The problem of Poiseuille and Couette-Poiseuille flow, under the effect of a horizontal Lorentz force, between parallel plates with porous medium was considered by Pantokratoras [27].

The unique relation in non-linearity between shear stress and the shear rate gave birth to the regime of non-Newtonian fluids. The rigorous research in the field of Non-Newtonian fluids is very fruitful due to its extensive applications in blood, oils, paints, ice cream, etc. Sarpkaya [28] discussed the non-Newtonian fluid subjected to constant pressure and magnetic field turned velocity distribution uniform and viscosity effects distinct near the boundary. The experiments were carried out by Chow and Fuller [29] for non-Newtonian Couette fluid flow. The obtained results were proved exact with those of theoretical. The non-linearity of shear rate with viscosity, time dependence and elongation effects make a new type of non-Newtonian fluids, called viscoelastic fluids, discussed by Ghosh [30]. Kasim et al. [31] discussed flow of viscoelastic fluid with Newtonian heating on a solid sphere by considering natural convection phenomena. These fluids, between porous parallel plates/cylindrical channel, have major contribution in several engineering technologies such as petroleum production, solar power collectors and chemical catalytic reactors. It was concluded by Kavitha and Murthy [32] that velocity of the second order flow in an inclined porous channel is inversely related to the Darcy's parameter by giving the fixed constant value to viscous elasticity parameter and Reynold no's. Laminar and second grade fluid flow through two flat walls and a cylindrical channel is considered by Ariel [33] by developing their solutions with the help of Perturbation method. It is proved that Perturbation technique does not produce suitable results for moderate values of Reynold number. A viscoelastic fluid, in the non-uniform channel, having MHD fluid flow (time-dependent) and conducting electrically was explained by Gireesha and Mahanthesh [34]. It was determined that the Hall Effect plays a vital role in controlling the fluid velocity. The boundary layer flows of these fluids with stretching flows make this field fruitful for plastic films, paper production and polymer extrusion etc. Also convective flow is an important property discussed by Hayat et al [35, 36]. It was noticed that thermal boundary layers are inversely related to mixed convection parameter within velocity field [35]. Dusty viscoelastic fluid flow with convective boundary was discussed by Sivaraj and Kumar [37, 38] and it resulted that the velocity field of dust particles is less peaked as compared to dusty fluid. To study the Soret and Dufour effects, HAM was used by Srinivasachary and Kalabhar [39] on free convection of a couple stress fluid flowing through a channel with heat and mass transfer. It was seen that both temeprature and mometum of the fluid decrease according to the lessening of Dufour number. Heat transfer characteristics were studied by Adesanya and Makinde [40] for MHD, oscillatory, non-Newtonian and couple stress

fluid flow with non-uniform wall temperature between parallel porous plates. The viscoelastic fluid flow in a channel saturated with porous medium was discussed by Adesanya [41] to examine the combined effects of radiative heat transfer.

During the past few years, significant work has been done on an important type of flow namely the composite channel flow with heat transfer due to its use in several engineering problems. The study of flow through channels and ducts partially filled with porous medium have profound implications in engineering such as crude oil extraction, thermal insulation and many other geophysical applications. First time Hassanizadeh and Gray [42] explained the fluid flow and transport at the clear/porous interface. Both theoretical and experimental results show that the mean filter velocity within the body of porous material is lesser than the tangential component of velocity of the free liquid at the porous boundary. The interfacial conditions between porous and homogenous fluid was derived by Ochoa- Tapia and Whitaker [43]. The purpose of conditions is to connect Darcy's law with the Brinkman correction to the Stokes equations and these are used by Deng [44] to model the two dimensional Newtonian flow, over and through a porous medium. It was known that Darcy law can be extended if a non-linear term is added. The term called Forchheimer term for speedy fluids in the porous medium. Beavers-Joseph [45] slip conditions are encountered in pulsating flows in a channel bounded between permeable beds with suction/injection.

The analytical solutions for the study of both parallel plate and cylindrical composite channel were discussed by Kuznetsov [46]. The Ochoa-Tapia and Whitaker [43] conditions were used to find the solution at the interface region. Kuznetsov [47] by using stress jump boundary condition in a composite region, gave an approximate solution for the steady channel flow, which was half filled with a porous medium. Kuznetsov [48, 49] elaborated analytical solutions of couette flow in a duct/channel. It was established that matching the Brinkamn-Darcy and Stokes equations preserves continuity of the tangential velocity but yields a jump in the shear stress at the interface. The problem of transient free convection in domains partially filled with porous substrates was explained analytically by Nimr and Khadrawi [50]. Chauhan and Agrawal [51] studied the consequences of the Hall current on MHD fluid flow in a composite channel. Also Chauhan and Kumar [52] discussed 3-D couette flow in a composite channel. In a parallel plate channel, Kuznetsov [53] elaborated fully developed, forced convection fluid flow partly

occupied by a porous material. The non-linear Brinkman-Forchheimer-extended Darcy equation was used to explain the flow. The roughness effects on turbulent flow in ducts were described by Kuznetsov [54]. It was observed that the roughness of the fluid/porous interface has an impact on the turbulent flow both for fluid region and overall heat transfer in the duct.

In general, major attention was paid on steady state composite flow and heat transfer phenomenon by authors. However, most of the fluid flow is unsteady in nature. Significant attention has not been given to the unsteady fully developed flow in composite channel problems. In this regard, Umavathi et al. [55] stressed on the unsteady flow in the horizontal composite channel having oscillatory injection velocity besides heat transfer of a viscous fluid. Thus the analytic solution was determined. Umavathi [56] analyzed the completely developed and free convection flow of immiscible fluids in a vertical channel occupied by a porous medium. Darcy-Lapwood Brinkmann equation is applied to formulate the Poiseuille Couette flow [57] in an inclined composite channel. Whereas, the Brinkman extended Darcy model was applied by Huang [58] to explore the porous region which allows to observe the effect of Darcy number. Li et al. [59] found the numerical results for the momentum and heat transfer characteristics in a channel containing staggered porous blocks. Gireesha et al. [60] elaborated 3-D, Couette and dusty fluid flow in a porous parallel plates which are placed horizontally and are infinitely long. Leong and Jin [61] considered vibratory flow in a channel which is occupied by aluminum foam to examine the heat transfer in a constant wall heat flux. An exact solution is calculated to describe the flow behavior at the interface by Vafai and Kim [62]. Huang and Vafai [63] carried a numerical investigation for forced convection in an isothermal channel consisting of porous cavity and block. Forced convection analysis is made by Chikh et al. [64] in an annular composite duct. It is shown that presence of a porous layer in a duct offers resistance to the flow.

A new model was developed by Geindreau and Auriault [65] for the tensorial filtration law in a porous medium for steady-state slow flow of an electrically conducting and incompressible flow of viscous fluid. The model proposed in Geindreau and Auriault [65] provides a better landscape of the porous media magnetic field interacting situation in which the results are valid for some moderate values of porosity which reflects more realistic situations. Marques et al [66] continue the research of Terrill [67] for Couette-Poiseuille flow in an annulus of infinite extent using similarity transformation. Vafai [68] considered the convective flow and

heat transfer in porous media to analyze the behavior of variable porosity and inertial forces. Hinch [69] and Holmes [70] studied in-detail the concept of regular perturbation method for partial differential equations. The investigation of magnetic field, frequency, Hall current effects on the motion of an incompressible conducting fluid flow have been discussed by Hayat et al [71] bounded between two parallel plates. It was concluded that both numerical and exact solutions show excellent agreement for the rotation parameter $K > 20$.

The thermal deficiency of engineering devices is greatly affected by irreversible losses that ultimately enhance the entropy. Thus, it is important to detect the parameters that augment the entropy production. Entropy, disorder and irreversibility are given by second law of thermodynamics. Viscous dissipation, heat exchange and convective heat transfer are responsible for finite entropy. The energy losses in daily life appliances like refrigerators, geothermal energy systems and solar panels are due to entropy production.

To improve the performance of heat transfer processes, entropy generation minimization has been considered as an effective tool. Bejan [72] remarked that by achieving information about the parameters that cause entropy production, the effects of energy losses due to entropy can be minimized. Eegunjobi and Makinde [73] examined that entropy generation could be minimized by choosing the suitable values of thermophysical parameters controlling the flow system. Adomian Decomposition Method was used by Adesanya and Makinde [74] to examine the couple stress effects on the entropy generation rate of the viscous and incompressible fluid flow with convective heating at the walls. Mahmud and Fraser [75] gave numerical and analytical analysis of momentum and heat transfer characteristics and investigated the factors that generate entropy in a porous parallel plates channel. Heat transfer reduction in an unsteady porous channel flow with Navier slip was observed by Chinyoka and Makinde [76]. Entropy generation due to forced convection was discussed by Hooman et al. [77] in a parallel plate channel containing porous medium. Morosuk [78] investigated the entropy generation due to laminar flow in a pipe fully/half occupied by a porous medium. He elaborated that how rate of entropy generation is affected by the thickness and permeability of the porous layer. Darcy and energy equations were used by Cimpean and Pop [79] to analyze the measure of disorder due to mixed convection flow in an inclined porous channel. Chauhan and Kumar [80] concluded that entropy generation number give the extreme values near the circular channel wall, occupied with a porous medium saturated with a rare field gas. Srinivasacharya [81] studied micropolar fluid

velocity and heat transfer in an inclined channel. The obtained equations of momentum and heat transfer were used to calculate the entropy production inside the inclined channel.

Many researchers worked on hydromagnetic channel flow due to vast applications in engineering for example: geothermal reservoirs, crystal growth, magnetic filtration, jet printers and petroleum reservoirs. Various studies have been done for MHD fluid flow under various physical situations. Sparrow and Cess [82] found free convection heat transfer to liquid metals is influenced by the magnetic field. While, very little effect can be experienced by other fluids. Two dimensional steady, incompressible, viscous fluid flow through a porous medium confined by an infinite vertical porous surface was discussed by Raptis and Kafousias [83].

The laws of thermodynamics were applied by Tasnim et al [84] inside the vertical porous channel in transverse magnetic field. The steady and fully developed fluid flow in a half filled porous channel in the presence of transverse magnetic field effecting entropy generation was discussed by Kumar et al. [85]. It was observed that entropy generation remains maximum near the centerline due to magnetic field.

Generally, the analytical solution for non-linear differential equations is not available in all cases. Therefore, one is forced to obtain the approximate solution using available methods either analytical or numerical. The presence of inertial term in Navier Stokes equations makes it non-linear. Thus, obtaining the analytical solution of Navier Stokes equation is a cumbersome if not impossible. The analytical solutions are always more fruitful due to their exactness and thus to obtain the correct interpretation of the entire mathematical mechanism. This enables to understand the interaction between the variables and their effective role in the conclusion clearly. Analytical results verify the authenticity of the numerical results besides giving the qualitative picture of the channel flow and the characteristic of the flow. Due to the complexity of the problems, mathematical model become more troublesome and it is vital to find some appropriate numerical techniques. Though numerical results are the approximation to the analytical yet this estimation leads to exact interpretation. Perturbation technique is one of the analytical method, widely discussed in various books by Hinch and Holmes [69, 70] and in the various review papers by [34, 55, 56, 86, 87] to investigate dynamics of fluids. However, analytical methods are not always useful and we have to move towards numerical techniques to solve the highly non-linear differential equations. Traditionally, finite difference method are best to use for highly

non-linear differential equations [88, 89]. Finite difference technique were applied to investigate the unsteady, incompressible, periodic and transversal flow of a viscous fluid through the channel by Kaur et al. [87]. An implicit finite difference method was applied by Shanker [88] to study the flow of blood through a porous channel in magnetic field and different pressure gradients. Jha et al. [89] discussed both steady and unsteady Couette flow for reactive viscous fluid flow through a vertical porous plate channel. Also, Jha [90] studied the unsteady Couette flow in a clear/porous channel using finite difference method. Umavathi [56] used the techniques of regular perturbation and finite difference methods for the natural convection flow of different fluids in a vertical porous channel in the presence of source/sink. Heat transfer and velocity characteristics of two immiscible fluids [57] in an inclined composite channel is analyzed by analytically and numerically. However, the results are dependent on the variation of the values of the parameters.

In this thesis, the problems have been solved by finite difference method and regular perturbation techniques. The results obtained by two different techniques are compared with each other which confirm the results. Also, the comparison has been made with the already available results in the literature.

Chapter one includes the literature review of the channel flow and the related definitions are also included. The fundamental flow equations are presented along with the explanation of the perturbation method and implicit finite difference technique.

Chapter two discusses unsteady fluid flow and temperature gradient effects in a composite channel having oscillating upper wall. The Darcy Brinkman model is incorporated to model the system. The analytical series solution is got for momentum and energy equations. To compare the results obtained by perturbation method, implicit finite difference scheme is used. The behavior of different pertinent parameters are elaborated with the help of plots. The numerical values of velocity and temperature with their derivatives for different parameters are also calculated. The major contents of this chapter have been published in *Journal of Porous Media*.

Chapter three comprises of two sections. The first section is about the study of unsteady MHD fluid momentum and heat transfer in a composite annulus. An analytical solution for both

momentum and heat transfer equations by using perturbation method is presented. The annulus injects the time dependent oscillatory velocity normal to its surface. A parametric analysis is performed for the velocity and temperature profile. The major contents of this article are published in *Zeitschrift für Naturforschung A*. In second part of this chapter, we extend our analysis to viscous fluid electrically conducting over a permeable cylinder, bounded by semi-infinite porous medium. Various physical parameters are discussed with the help of graphs. This article is published in the *Journal of Porous Media*.

Chapter four deals with the Casson fluid taken in an irregular channel under convective boundary. The obtained PDEs are converted into system of ODEs by using regular perturbation technique. The exact solution is calculated for the obtained ordinary differential equations of fluid flow, heat transfer and mass concentration. The graphical results of various physical parameters are presented. This work has been published in *Zeitschrift für Naturforschung A*.

The fifth chapter in this thesis deals with the fully developed laminar flow in an inclined composite channel discussing unsteady flow, heat transfer characteristics and entropy generation. An asymptotic solution of the problem is found for fluid velocities, temperature by regular perturbation method. The results are compared with the implicit finite difference scheme. An excellent agreement is found between series and numerical solution. Entropy generation effects are computed by using the results of velocity and temperature profiles. Interpretation of various physical parameters is explained with the help of plots for velocity, entropy generation rate, temperature and Bejan number. The major material of this chapter has been accepted by *Journal of Porous media* for publication.

Chapter 6 reports the theoretical analysis of unsteady, laminar and incompressible MHD fluid flow in an inclined channel in which porous medium is embedded between two viscous fluid layers. The obtained results of momentum and heat transfer are used to study the entropy generation. The perturbation method is employed to convert the nonlinear PDEs into system of ODEs. These differential equations are also solved numerically and the results are compared by using graphs. This work has been accepted by *Journal of Porous media* for the publication.

1.2 Dynamics of Fluid

Fluid is the form of matter, that varies its shape and state according to the forces applied on it and circumstantial conditions. Liquids and gases are called fluids due to their characteristic of flow. The fluids having no viscosity are termed as inviscid or ideal fluids. The fluid possessing non-zero viscosity are called viscous fluid. Such fluids are also called real fluids. The viscous fluids are further partitioned into compressible and incompressible fluids according to their constant and variable densities during the motion, respectively.

The two major kinds of real fluids are as follows

1.2.1 Newtonian Fluids

Newton's law of viscosity is given as rate of velocity gradient/ angular deformation is directly proportional to the shear stress. The fluids which follow the law given above are Newtonian fluids.

Mathematically,

$$\text{Shear stress} \propto \frac{\partial u}{\partial y}, \quad (1.1)$$

and

$$\text{Shear stress} = \mu \frac{\partial u}{\partial y}, \quad (1.2)$$

where μ and u are the absolute/dynamic viscosity and horizontal component of velocity respectively.

For Newtonian fluid, the Cauchy stress tensor, \mathbf{T} fulfills the equation.

$$\mathbf{T} = -p \mathbf{I} + \mu \mathbf{A}_1, \quad (1.3)$$

where, \mathbf{I} , p and \mathbf{A}_1 are identity tensor, hydrostatic pressure and first Rivlin-Ericksen tensor respectively. \mathbf{A}_1 is given as

$$\mathbf{A}_1 = \text{grad}V + (\text{grad}V)^T, \quad (1.4)$$

where V represent the velocity.

1.2.2 Non-Newtonian Fluids

The fluids not obeying Newton's viscosity law (1.2) are termed as non-Newtonian fluids. In such fluids, non-linearity in shear stress and shear strain rate completes the definition. Mathematically

$$\text{Shear stress} = \sigma_{yx} = k' \left(\frac{\partial u}{\partial y} \right)^n \quad n \neq 1, \quad (1.5)$$

where n and k' are given in nomenclature. For $n=1$ and $k'=\mu$, Newtonian fluids can be obtained. Some well-known examples of non-Newtonian fluids are ketchup, blood, tomato, yogurt and honey.

1.3 Kinds of Flows

The major classifications of the fluid flows are as follows

1.3.1 Laminar and Turbulent Flow

A fluid flow where the path of each particle of the fluid follows a particular pattern is called laminar flow otherwise it is called turbulent flow.

1.3.2 Unsteady and steady Flow

The fluid flow is called steady according as the flow pattern remains unchanged with respect to time. On the other hand, when the characteristics and flow behavior of the fluid depending on time, that fluid is called unsteady.

1.3.3 Uniform and Varied Flow

The flow in which fluid velocity remains constant in every part of channel/annulus is uniform flow whereas the fluid in which fluid have different velocities in every part of the annulus/channel is known as varied or non-uniform flow.

1.4 Porosity and Porous Medium

1.4.1 Porous Medium

The substance resembling matrix re-presentation with interconnected pores are known as porous medium. The pores make the flow convenient through the specific material. Due to different shapes and dimensions, these pores are called irregular pores. Some of the well-known examples of porous medium are wood, foam, bread and lime stone etc.

In a porous medium, fluid flow is an ordered one in an irregular geometrical pattern. It is dependent on the specific physical characteristics of fluids and the porous matrix. The accurate form is complicated and varies from medium to medium. It may consist of large variety of particles such as sand, gravel, mud and other solid particles. Whenever the fluid is drained/filtered using a porous material, the exact path of the fluid particle cannot be studied analytically, which happens because pores have complex behavior. If this happens, then it is necessary to determine the overall result of the phenomenon. This can be done by taking a macroscopic view of the masses taken large enough as compared to the size of the pore of medium. This can be explained by equilibrium condition of forces. There are two types of forces, one is the driving force applied to move fluid at a given speed across a porous medium in equilibrium with the second force i.e resistive/drag force produced by friction between the fluid and pores.

1.4.2 Porosity

Porosity is given by

$$\text{porosity} = \frac{\text{volume of pores}}{\text{total volume of porous matrix}} \quad (1.6)$$

It is a non-dimensional quantity.

1.4.3 Permeability

The quantity of the fluid, which is permissible to pass through its interconnected pore network. Its dimension is a length squared. It is observed that, for unidirectional flow, flow rate and applied pressure gradient has a special connection, given by

$$\mathbf{q} = -\frac{s}{\mu} \nabla p, \quad (1.7)$$

here ∇p , \mathbf{q} and s are the pressure gradient, the flow rate of the fluid and the coefficient of permeability respectively, s being specific permeability of a porous medium, is independent of nature of fluid whereas dependent on shape of the medium.

The permeability of porous medium, porosity and certain properties of fluids determine the rigidity and nature of fluid flow. Moreover, effects of elasticity are not taken into account. Darcy-Brinkman law is applied to formulate the problem in porous region.

1.4.4 Shear Stress-Jump Condition

The interfacial boundary conditions between clear fluid regions and porous region in composite channel/annulus are known as stress jump boundary condition.

1.5 Governing Laws

1.5.1 Equation of Continuity

The continuity equation is followed by mass conservation of basic unit of considered volume in the fluid. It is defined as

$$\frac{\partial \rho}{\partial t} + \nabla \cdot (\rho \mathbf{V}) = 0. \quad (1.8)$$

For a homogenous and incompressible fluid, the equation (1.8) reduces to

$$\text{div} \mathbf{V} = 0. \quad (1.9)$$

Physically, the continuity equation states that the total mass of the continuous medium is conserved during its flow in any channel/annulus.

1.5.1.1 Continuity Equation in Cartesian Coordinates

The continuity equation for unsteady and compressible fluid flow in Cartesian coordinates can be written as

$$\frac{\partial \rho}{\partial t} + \frac{\partial(\rho u)}{\partial x} + \frac{\partial(\rho v)}{\partial y} + \frac{\partial(\rho w)}{\partial z} = 0. \quad (1.10)$$

For incompressible ($\rho = \text{constant}$) and steady state, flow equation (1.10) reduces to

$$\frac{\partial u}{\partial x} + \frac{\partial v}{\partial y} + \frac{\partial w}{\partial z} = 0. \quad (1.11)$$

1.5.1.2 Continuity Equation in Cylindrical Coordinates

The continuity equation for unsteady and compressible flow in cylindrical coordinates is given by

$$\frac{\partial \rho}{\partial t} + \frac{1}{r} \frac{\partial(\rho r w_r)}{\partial r} + \frac{1}{r} \frac{\partial(\rho w_\theta)}{\partial \theta} + \frac{\partial(\rho w_z)}{\partial z} = 0. \quad (1.12)$$

For steady and incompressible flow (1.12) takes the form

$$\frac{1}{r} \frac{\partial(r w_r)}{\partial r} + \frac{1}{r} \frac{\partial(w_\theta)}{\partial \theta} + \frac{\partial(w_z)}{\partial z} = 0. \quad (1.13)$$

1.5.2 Navier-Stokes Equation

1.5.2.1 Navier-Stokes Equation in Cartesian Coordinates

Navier-Stokes equations play a vital role in the study of fluid flow. In components form the Navier-Stokes equations for viscous incompressible fluid is

$$\frac{\partial u}{\partial t} + u \frac{\partial u}{\partial x} + v \frac{\partial u}{\partial y} + w \frac{\partial u}{\partial z} = \nu \left[\frac{\partial^2 u}{\partial x^2} + \frac{\partial^2 u}{\partial y^2} + \frac{\partial^2 u}{\partial z^2} \right] - \frac{1}{\rho} \frac{\partial p}{\partial x} + b_x, \quad (1.14)$$

$$\frac{\partial v}{\partial t} + u \frac{\partial v}{\partial x} + v \frac{\partial v}{\partial y} + w \frac{\partial v}{\partial z} = \nu \left[\frac{\partial^2 v}{\partial x^2} + \frac{\partial^2 v}{\partial y^2} + \frac{\partial^2 v}{\partial z^2} \right] - \frac{1}{\rho} \frac{\partial p}{\partial y} + b_y, \quad (1.15)$$

$$\frac{\partial w}{\partial t} + u \frac{\partial w}{\partial x} + v \frac{\partial w}{\partial y} + w \frac{\partial w}{\partial z} = \nu \left[\frac{\partial^2 w}{\partial x^2} + \frac{\partial^2 w}{\partial y^2} + \frac{\partial^2 w}{\partial z^2} \right] - \frac{1}{\rho} \frac{\partial p}{\partial z} + b_z. \quad (1.16)$$

1.5.2.2 Navier-Stokes Equation in Cylindrical Coordinates

In cylindrical coordinates, the Navier-Stokes equations for viscous incompressible flow with body force are given by

$$\begin{aligned} \frac{\partial w_r}{\partial t} + w_r \frac{\partial w_r}{\partial r} + \frac{w_\theta}{r} \frac{\partial w_r}{\partial \theta} - \frac{w_\theta^2}{r} + w_z \frac{\partial w_r}{\partial z} = -\frac{1}{\rho} \frac{\partial p}{\partial r} \\ + \frac{\nu}{r} \frac{\partial}{\partial r} \left(r \frac{\partial w_r}{\partial r} \right) - \frac{\nu w_r}{r^2} + \frac{\nu}{r^2} \frac{\partial^2 w_r}{\partial \theta^2} - \frac{2\nu}{r^2} \frac{\partial w_\theta}{\partial \theta} + \nu \frac{\partial^2 w_r}{\partial z^2} + b_r, \end{aligned} \quad (1.17)$$

$$\begin{aligned} \frac{\partial w_\theta}{\partial t} + w_r \frac{\partial w_\theta}{\partial r} + \frac{w_\theta}{r} \frac{\partial w_\theta}{\partial \theta} + \frac{w_\theta w_r}{r} + w_z \frac{\partial w_\theta}{\partial z} = -\frac{1}{\rho r} \frac{\partial p}{\partial \theta} \\ + \frac{\nu}{r} \frac{\partial}{\partial r} \left(r \frac{\partial w_\theta}{\partial r} \right) - \frac{\nu w_\theta}{r^2} + \frac{\nu}{r^2} \frac{\partial^2 w_\theta}{\partial \theta^2} + \frac{2\nu}{r^2} \frac{\partial w_r}{\partial \theta} + \nu \frac{\partial^2 w_\theta}{\partial z^2} + b_\theta, \end{aligned} \quad (1.18)$$

$$\begin{aligned} \frac{\partial w_z}{\partial t} + w_r \frac{\partial w_z}{\partial r} + \frac{w_\theta}{r} \frac{\partial w_z}{\partial \theta} + w_z \frac{\partial w_r}{\partial z} = -\frac{1}{\rho} \frac{\partial p}{\partial z} \\ + \frac{\nu}{r} \frac{\partial}{\partial r} \left(r \frac{\partial w_z}{\partial r} \right) + \frac{\nu}{r^2} \frac{\partial^2 w_z}{\partial \theta^2} + \nu \frac{\partial^2 w_z}{\partial z^2} + b_z. \end{aligned} \quad (1.19)$$

1.5.3 Energy Equation

The law of conservation of energy is given by

$$\rho C_p \frac{DT}{Dt} = \mathbf{T} \cdot \mathbf{L} + K \nabla^2 T, \quad (1.20)$$

where T , C_p , K and ρ represent the Cauchy tensor, specific heat, thermal conductivity and

density of the fluid respectively. $\frac{D}{Dt}$ represents the total derivative which is

$\frac{\partial}{\partial t} + u \frac{\partial}{\partial x} + v \frac{\partial}{\partial y} + w \frac{\partial}{\partial z}$, here $\frac{\partial}{\partial t}$ represents local derivative and $\frac{\partial}{\partial t} + u \frac{\partial}{\partial x} + v \frac{\partial}{\partial y} + w \frac{\partial}{\partial z}$

represents convective derivative.

1.5.3.1 Energy Equation in Cartesian Coordinates

The energy equation in cartesian form is given by

$$\rho C_p \left(\frac{\partial T}{\partial t} + u \frac{\partial T}{\partial x} + v \frac{\partial T}{\partial y} + w \frac{\partial T}{\partial z} \right) = K \left[\frac{\partial^2 T}{\partial x^2} + \frac{\partial^2 T}{\partial y^2} + \frac{\partial^2 T}{\partial z^2} \right]. \quad (1.21)$$

1.5.3.2 Energy Equation in Cylindrical Coordinates

The heat transfer equation in cylindrical coordinates is as follow

$$\rho C_p \left(\frac{\partial T}{\partial t} + w_r \frac{\partial T}{\partial r} + \frac{w_\theta}{r} \frac{\partial T}{\partial \theta} + w_z \frac{\partial T}{\partial z} \right) = K \left[\frac{1}{r} \frac{\partial}{\partial r} \left(r \frac{\partial T}{\partial r} \right) + \frac{1}{r^2} \frac{\partial^2 T}{\partial \theta^2} + \frac{\partial^2 T}{\partial z^2} \right]. \quad (1.22)$$

1.5.4 Darcy Law

The Darcy law is applicable to unbounded, slow viscous fluid present in porous medium. It links the reduction in pressure caused by the drag force and velocity parameters. Moreover, the boundary effects on the flow are ignored in the relation. Therefore the induced pressure reduction is proportional to velocity. Darcy's law states that

$$\nabla p = -\frac{\mu}{s} q. \quad (1.23)$$

1.5.5 Darcy-Brinkman Equation

According to Brinkamn, Darcy's law can be extended to Darcy-Brinkman equation, proposed in 1949. He added a body force in the Navier Stokes equations which results from the solid matrix drag exerted on fluid. It is given by

$$\nabla p = -\frac{\mu}{s} q + \mu \nabla^2 q, \quad (1.24)$$

The additional term in Eq. (1.23) is linear in both viscosity and velocity. Boundary conditions, at the junction of composite channels are solved using Brinkman's equation.

1.5.6 Second Law of Thermodynamics

It can be stated as

$$\dot{S}_{gen} = \frac{\partial S}{\partial t} - \frac{\dot{Q}}{T} - \sum_{in} \dot{m} s' + \sum_{out} \dot{m} s' \geq 0, \quad (1.25)$$

where \dot{S}_{gen} , \dot{Q} , \dot{m} , s' and T are the entropy generation rate, heat transfer rate, mass flow rate, specific entropy and boundary temperature of the system, respectively.

Rate of change of entropy generation measures the irreversibility in the system. Equation (1.25) shows that irreversibility cannot be circumvented, but can be minimized. Second law of thermodynamics/entropy generation rate can be used to determine the disorder in any thermal system. The thermodynamics irreversibility or entropy generation related to fluid flow is usually combination of heat transfer across finite temperature difference and viscous friction. The entropy generation rate per unit volume in the medium is a combination of viscous and heat effects. The viscous and heat transfer effects can be calculated by momentum equation and energy equation respectively. Physical behavior of fluid such as density, thermal conductivity, viscosity and specific heat remain independent of temperature.

1.6 Dimensionless Parameters

1.6.1 Eckert Number

It is defined as,

$$Ec = \frac{u_0^2}{C_p \Delta T}, \quad (1.26)$$

where u_0 , C_p and ΔT denote the reference velocity, the specific heat at constant temperature and temperature difference respectively. The Eckert number usually appears in the non-dimensional heat equation, if the viscous dissipation is present in the problem. Eckert number has no unit.

1.6.2 Darcy Number

The dimensionless number D_a , Darcy number is the ratio between medium permeability s and the square of the domain thickness h^2 .

$$D_a = \frac{s}{h^2}. \quad (1.27)$$

1.6.3 Grashof Number

The fraction of buoyancy of fluid to viscous force is termed as Grashof number. Mathematically,

$$Gr = \frac{g \beta \Delta T h^3}{\nu^2}, \quad (1.28)$$

where the symbols used in equation (1.28) are given in the nomenclature. Grashof number is a dimensionless number.

1.6.4 Bejan Number

The Bejan number, Be is the fraction of entropy because of heat transfer to the total entropy in a given volume.

$$Be = \frac{\text{Entropy due to heat generation}}{\text{Total entropy}}.$$

1.6.5 Biot Number

The Biot number is defined by

$$Bi = \frac{h_f d}{K}, \quad (1.29)$$

where h_f is the heat transfer coefficient.

1.6.6 Schmidt Number

The Schmidt number is defined by

$$Sc = \frac{\nu}{D}, \quad (1.30)$$

where D and ν are the molecular diffusivity and kinematic viscosity respectively.



1.6.7 Skin Friction

The viscous force acting at the surface per unit area is called skin friction and is denoted by τ_f^* .

Mathematically,

$$\tau_f^* = \mu \left. \frac{\partial u}{\partial y} \right|_{y=h}. \quad (1.31)$$

The local skin friction, τ_f acting on the wall is given by

$$\tau_f = \frac{\tau_f^* d}{\mu u_0}, \quad (1.32)$$

where reference velocity is denoted by u_0 and dynamic viscosity is given by μ .

1.6.8 Nusselt Number

The Nusselt number is given by

$$Nu = \frac{q_w d}{K \Delta T}, \quad (1.33)$$

where channel length, thermal conductivity of the fluid and temperature difference of the wall are represented by d, K and ΔT respectively. q_w represents the heat transfer rate at the surface, and can be written as

$$q_w = -K \left. \frac{\partial T}{\partial y} \right|_{y=h}. \quad (1.34)$$

1.6.9 Sherwood Number

It is defined as

$$Sh_0^* = -DC', \quad (1.35)$$

$$Sh = \frac{Sh_0^* d}{D \Delta C} = -\frac{\partial \varphi}{\partial y}. \quad (1.36)$$

The symbols used in Eqs. (1.35)-(1.36) are given in the nomenclature.

Chapter 2

Heat Transfer and Time Dependent Flow through a Composite Channel having an Oscillating Wall

2.1 Introduction

In this chapter, a unidirectional oscillatory flow in a channel having half porous space with an oscillatory upper plate is discussed. The Darcy-Brinkman model is used to model the flow in porous region of the channel. The continuous velocities and shear stresses are assumed at the interface of porous medium and clear fluid. An analytical series solution is calculated for the complete analysis of the velocity and the temperature profiles. To validate the analytical series solution, a numerical solution of the problem is also calculated. The effects of sinusoidal oscillatory plate on the flow and the heat transfer in a composite channel for various physical parameters are analyzed through graphical illustrations.

2.2 Mathematical Formulation

2.2.1 Flow and Heat Transfer Phenomena

Consider the laminar, unsteady, fully developed, incompressible and viscous fluid flow passing through a composite channel which is infinitely long. The region-1 ($y \in]-h, 0[$) and region-2 ($y \in]0, h[$) are occupied by porous matrix and clear viscous fluid respectively as shown in figure 2.1. The upper and lower walls of the channel are maintained at constant temperatures T_{w1} and T_{w2} with $T_{w1} > T_{w2}$ respectively.

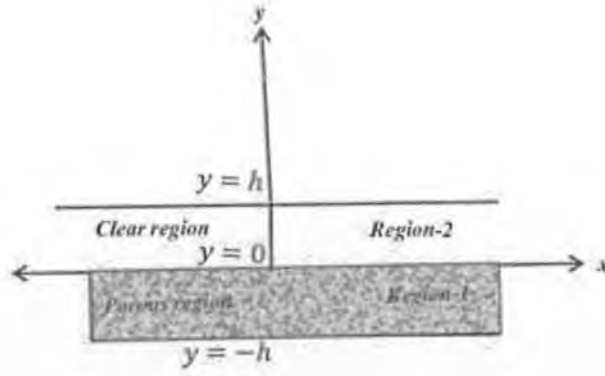


Figure 2.1: Schematic flow diagram of the considered problem

Since we supposed that the plates are infinite, placed horizontally along x -axis and all variables other than pressure depending upon y and t . In addition to this, a constant pressure gradient is supposed to derive the flow through both the regions. Initially, both the fluid and plates are assumed to be in the state of rest and at $t > 0$ the upper plate starts vibratory motion with velocity $U = u_0(1 + \varepsilon A e^{i\omega t})$. Using these assumptions, the equations corresponding to motion and the heat transfer are

$$\rho \left(\frac{\partial u_i}{\partial t} \right) = -\frac{\partial p}{\partial x} + \chi_\mu \left(\frac{\partial^2 u_i}{\partial y^2} \right) - \chi \frac{\chi_\mu}{s} u_i, \quad (2.1)$$

$$\rho C_p \left(\frac{\partial T_i}{\partial t} \right) = \chi_k \frac{\partial^2 T_i}{\partial y^2} - \chi_\mu \left(\frac{\partial u_i}{\partial y} \right)^2 + \chi \frac{\chi_\mu}{s} u_i^2, \quad (2.2)$$

where the index $i=1$ gives equations for region-1 and $i=2$ gives equations for region-2, $T_i(y, t)$ represents the temperature field, $u_i(y, t)$ denotes the horizontal component of the fluid velocity.

No-slip boundary conditions are taken into account for the velocity field and walls are assumed to be isothermal. Moreover, velocity, shear stress and the temperature are continuous at interfacial point. The boundary and interface conditions can be written as

$$u_1(-h) = 0, \quad T_1(-h) = T_{w1}, \quad u_2(h) = U = u_0(1 + \varepsilon A e^{i\omega t}), \quad T_2(h) = T_{w2}, \quad (2.3)$$

$$u_1(0) = u_2(0), \quad \mu_{eff} \left. \frac{\partial u_1}{\partial y} \right|_{y=0} = \mu \left. \frac{\partial u_2}{\partial y} \right|_{y=0}, \quad T_1(0) = T_2(0), \quad K_{eff} \left. \frac{\partial T_1}{\partial y} \right|_{y=0} = K \left. \frac{\partial T_2}{\partial y} \right|_{y=0}, \quad (2.4)$$

where ω is the frequency parameter, A a positive real constant and ε is the amplitude, such that, $\varepsilon A < 1$.

Introducing non-dimensional variables

$$y^* = \frac{y u_0}{\nu}, \quad u_i^* = \frac{u_i}{u_0}, \quad t^* = \frac{t u_0^2}{\nu}, \quad \theta = \frac{T - T_{w_2}}{T_{w_1} - T_{w_2}}, \quad (2.5)$$

where u_0 and ν are the reference velocity and kinematic viscosity respectively. Using equation (2.5) and dropping asterisk for simplicity, equations (2.1) and (2.2) in dimensionless form become

$$\frac{\partial u_i}{\partial t} = -P + A_i \frac{\partial^2 u_i}{\partial y^2} - \chi \sigma^2 u_i, \quad (2.6)$$

$$\frac{\partial \theta}{\partial t} = B_i \frac{\partial^2 \theta}{\partial y^2} + Ec A_i \left(\frac{\partial u_i}{\partial y} \right)^2 + \chi Ec \sigma^2 u_i^2, \quad (2.7)$$

where

$$A_i = \begin{cases} m, & i = 1, \\ 1, & i = 2, \end{cases}$$

$$B_i = \begin{cases} \frac{k}{Pr}, & i = 1, \\ \frac{1}{Pr}, & i = 2, \end{cases}$$

$P = \frac{\mu}{\rho^2 u_0^3} \frac{\partial p}{\partial x}$ is the pressure gradient, $Pr = \frac{\rho \nu C_p}{k}$ is the Prandtl number, $m = \frac{\mu_{eff}}{\mu}$ and

$k = \frac{K_{eff}}{K}$ represent the ratios of viscosities and the thermal conductivities respectively.

Whereas, $\sigma^2 = \frac{\nu^2}{S u_0^2}$ and $Ec = \frac{u_0^2}{C_p \Delta T}$ are porosity parameter and Eckert number

respectively. The dimensionless boundary and interface conditions are

$$u_1(-1) = 0, \quad u_2(1) = 1 + \varepsilon A e^{I\omega t}, \quad \theta_1(-1) = 1, \quad \theta_2(1) = 0, \quad (2.8)$$

$$u_1(0) = u_2(0), \quad \theta_1(0) = \theta_2(0), \quad m \frac{\partial u_1}{\partial y} \Big|_{y=0} = \frac{\partial u_2}{\partial y} \Big|_{y=0}, \quad k \frac{\partial \theta_1}{\partial y} \Big|_{y=0} = \frac{\partial \theta_2}{\partial y} \Big|_{y=0}. \quad (2.9)$$

2.3 Solution Methodology

The solution of dimensionless non-linear PDEs (2.6)-(2.7) along with boundary and interface conditions (2.8)-(2.9) can be obtained numerically by finite difference technique and analytically by regular Perturbation method. The obtained results are plotted for different pertinent parameters in the next section.

2.3.1 Regular Perturbation Method

The solution of coupled PDEs (2.6)-(2.7), can not be found in closed form. However, these PDEs can be transformed into system of ODEs by expanding the series for momentum and temperature fields as

$$u_i(y, t) = u_{i0}(y) + \varepsilon A e^{I\omega t} u_{i1}(y) + O(\varepsilon A)^2, \quad (2.10)$$

$$\theta_i(y, t) = \theta_{i0}(y) + \varepsilon A e^{I\omega t} \theta_{i1}(y) + O(\varepsilon A)^2. \quad (2.11)$$

This assumption is valid due to the selection of u_i at the upper boundary as defined in (2.8) with the condition that $\varepsilon A < 1$. By substituting (2.10) and (2.11) into (2.6) and (2.7), comparing the

periodic, non-periodic terms and ignoring the terms of order $O(\varepsilon A)^2$ and higher, one can obtain pair of equations for (u_{i0}, θ_{i0}) and (u_{i1}, θ_{i1}) .

Non-Periodic Coefficient $O(\varepsilon A)^0$

$$A_i \frac{\partial^2 u_{i0}}{\partial y^2} - \chi \sigma^2 u_{i0} = P, \quad (2.12)$$

$$B_i \frac{\partial^2 \theta_{i0}}{\partial y^2} + \text{Ec} A_i \left(\frac{\partial u_{i0}}{\partial y} \right)^2 + \chi \text{Ec} \sigma^2 u_{i0}^2 = 0. \quad (2.13)$$

Periodic Coefficient $O(\varepsilon A)^1$

$$A_i \frac{\partial^2 u_{i1}}{\partial y^2} - \chi \sigma^2 u_{i1} - i \omega u_{i1} = 0, \quad (2.14)$$

$$B_i \frac{\partial^2 \theta_{i1}}{\partial y^2} - i \omega \theta_{i1} + 2 \text{Ec} A_i \left(\frac{\partial u_{i0}}{\partial y} \right) \left(\frac{\partial u_{i1}}{\partial y} \right) + 2 \chi \text{Ec} \sigma^2 u_{i0} u_{i1} = 0. \quad (2.15)$$

Using (2.10) and (2.11), the interface and boundary conditions can be rewritten as

$$\begin{cases} u_{1i}(-1) = 0, & u_{20}(1) = 1, & u_{21}(1) = 1, \\ \theta_{1i}(-1) = 1 - \delta_{1i}, & \theta_{2i}(1) = 0, \end{cases} \quad (2.16)$$

$$\begin{cases} m \frac{\partial u_{1i}}{\partial y} \Big|_{y=0} = \frac{\partial u_{2i}}{\partial y} \Big|_{y=0}, & u_{1i}(0) = u_{2i}(0), \\ k \frac{\partial \theta_{1i}}{\partial y} \Big|_{y=0} = \frac{\partial \theta_{2i}}{\partial y} \Big|_{y=0}, & \theta_{1i}(0) = \theta_{2i}(0), \end{cases} \quad (2.17)$$

where δ_{1i} is the Kronecker delta, $i=1$ gives interface and boundary conditions for periodic $O(\varepsilon A)^1$ coefficients whereas $i=0$ gives these conditions for non-periodic $O(\varepsilon A)^0$ coefficients.

2.3.2 Finite Difference Method

The differential equations (2.6) and (2.7) with boundary conditions (2.8)-(2.9) are discretized by using BTCS (Backward time central spacing).

$$\frac{u_1(l,n)-u_1(l,n-1)}{k_{11}} + P - m \frac{u_1(l+1,n)-2u_1(l,n)+u_1(l-1,n)}{h_{11}^2} + \sigma^2 u_1(l,n) = 0, \quad (2.18)$$

$$\frac{u_2(l,n)-u_2(l,n-1)}{k_{12}} + P - \frac{u_2(l+1,n)-2u_2(l,n)+u_2(l-1,n)}{h_{12}^2} = 0, \quad (2.19)$$

$$\frac{\theta_1(l,n)-\theta_1(l,n-1)}{k_{21}} - \frac{k}{Pr} \frac{\theta_1(l+1,n)-2\theta_1(l,n)+\theta_1(l-1,n)}{h_{21}^2} - Ec m \left(\frac{u_1(l,n)-u_1(l+1,n)}{h_{11}} \right)^2 - Ec \sigma^2 u_1^2(l,n) = 0, \quad (2.20)$$

$$\frac{\theta_2(l,n)-\theta_2(l,n-1)}{k_{22}} - \frac{1}{Pr} \frac{\theta_2(l+1,n)-2\theta_2(l,n)+\theta_2(l-1,n)}{h_{22}^2} - Ec \left(\frac{u_2(l,n)-u_2(l+1,n)}{h_{12}} \right)^2 = 0, \quad (2.21)$$

$$\begin{cases} u_1(-1,n) = 0, & u_2(1,n) = 1 + \epsilon A e^{l\omega n}, \\ \theta_1(-1,n) = 1, & \theta_2(1,n) = 0, \end{cases} \quad (2.22)$$

$$\begin{cases} u_1(0,n) = u_2(0,n), & u_2(l-1,n) - m u_1(l-1,n) + (m-1)u_1(l+1,n) = 0, \\ \theta_1(0,n) = \theta_2(0,n), & \theta_2(l-1,n) - k \theta_1(l-1,n) + (k-1)\theta_1(l+1,n) = 0. \end{cases} \quad (2.23)$$

The symbolic software Mathematica is used to do the computation by taking $k_{11} = k_{21} = 5$, $\sigma = 2$, $\omega = 1$, $\omega t = \pi/3$, $Ec = 2$, $Pr = 0.2$, $k = 0.5$, $P = -2$, $m = 2$, $h_{11} = h_{21} = 0.1$. The system of algebraic equations that are formed are then solved by using Gauss Seidel method.

2.4 Comparison of Obtained Results

In order to compare the solutions obtained by perturbation method and finite difference technique, the tabulated values for the momentum and the temperature are compared in the table 2.1. The resemblance in both solutions can be observed from table 2.1.

Table 2.1: Comparison between numerical and analytical values of velocity u and temperature θ at various values of y . The values of parameters $Pr = 0.2$, $k = 0.25$, $P = -1$, $m = 0.25$, $Ec = 2$, $\sigma = 1$, $\omega = 1$, $\omega t = \pi / 3$, are kept constant.

y	u_{anal}	u_{num}	absolute error $E = u_{anal} - u_{num} $	θ_{anal}	θ_{num}	absolute error $E = \theta_{anal} - \theta_{num} $
-1	0.00000	0.00000	0.00000	1.00000	1.00000	0.00000
-0.8	0.38493	0.37963	0.00530	0.88003	0.92340	-0.04336
-0.6	0.67000	0.66022	0.00978	0.74385	0.81717	-0.07331
-0.4	0.90096	0.88802	0.01293	0.59447	0.68301	-0.08853
-0.2	1.1139	1.10060	0.01330	0.43127	0.51384	-0.08257
0.0	1.34045	1.33299	0.00746	0.25348	0.29653	-0.04305
0.2	1.38003	1.36426	0.01577	0.20716	0.23816	-0.03099
0.4	1.37657	1.35662	0.01995	0.16033	0.17959	-0.01928
0.6	1.32936	1.31005	0.01931	0.11168	0.12087	-0.00919
0.8	1.23753	1.22454	0.0130	0.05921	0.06140	-0.00219
1.0	1.10000	1.00000	0.10000	1.562×10^{-9}	0.00000	0.00000

2.5 Results and Discussion

The effects of physical parameters on momentum and heat transfer profiles are discussed graphically in this section. The obtained results are illustrated through graphs. The pertinent parameters $\sigma = 2$, $\omega = 1$, $\omega t = \pi / 3$, $Ec = 2$, $Pr = 0.2$, $k = 0.5$, $P = -2$, $m = 2$ are kept constant except the varying one.

The variations of non-dimensional velocity and temperature fields for different values of favorable pressure gradient are given in figures 2.2 and 2.3 respectively. The velocity field and favorable pressure gradient are directly related. The temperature profile also augments as the favorable pressure gradient increases which is only due to the augmentation of the phenomenon of convection.

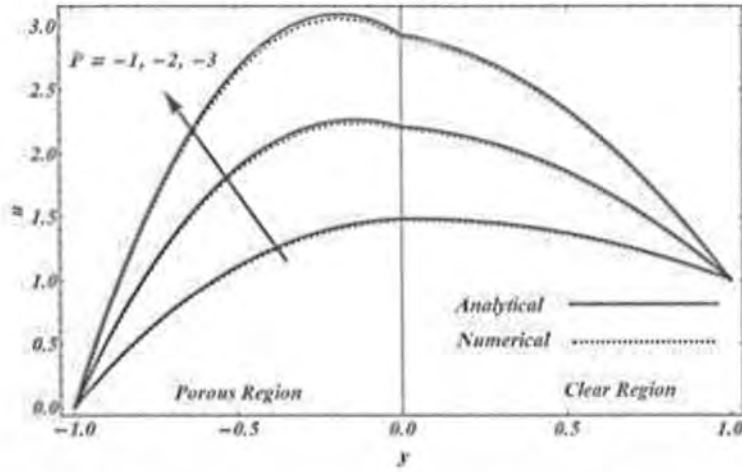


Figure 2.2: The plots of velocity for various inputs of pressure gradient P

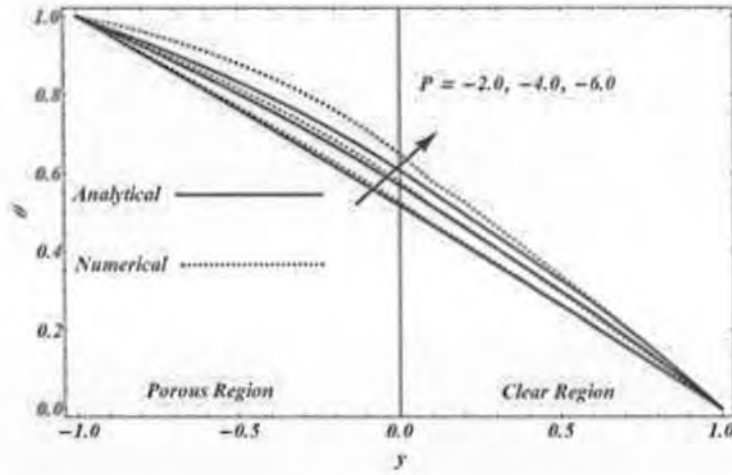


Figure 2.3: The plots of temperature for various inputs of pressure gradient P .

The influence of the viscosity ratio parameter m on the temperature and velocity fields are given in figures 2.4 and 2.5. It can be viewed that both velocity and temperature fields are inversely related to m . This behavior of the flow is due to the thickness of fluid for which the process of convection becomes slow and hence the momentum and temperature profiles decrease. It is found that the velocity profile in clear region is large as compared to the porous region. This shows that the momentum transport in porous region is small due to the presence of large resistive force.

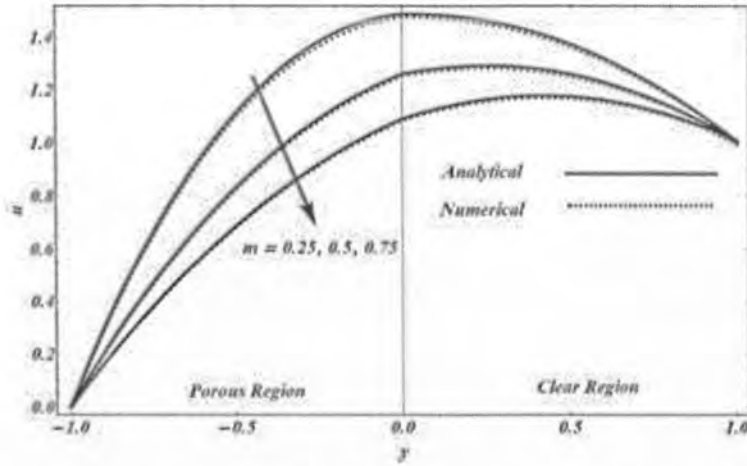


Figure 2.4: The plots of velocity for various inputs of the ratio of viscosities m

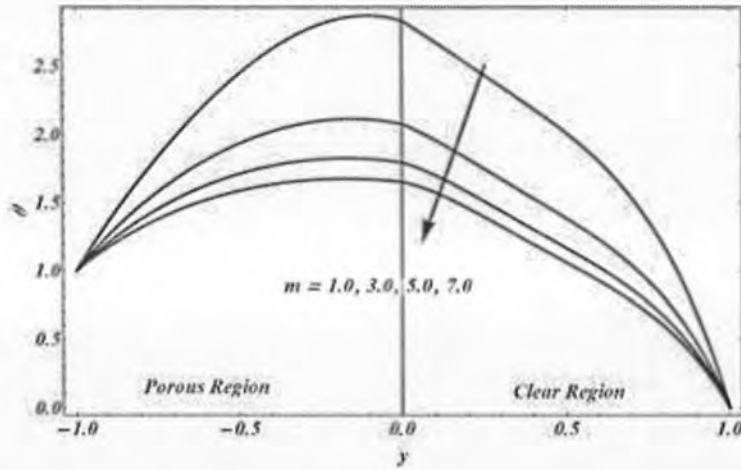


Figure 2.5: The plots of temperature for various inputs of the ratio of viscosities m

Figures 2.6 and 2.7 demonstrate the effects of porosity parameter σ on the temperature and velocity profiles. The large value of σ corresponds to small permeability. The figures indicate that velocity and temperature fields are inversely related to σ in both the regions. However, it is noticed that this fall in temperature and velocity profiles is more prominent in the region-2 than that of the region-1 which is due to the occurrence of large resistive force in region-2.

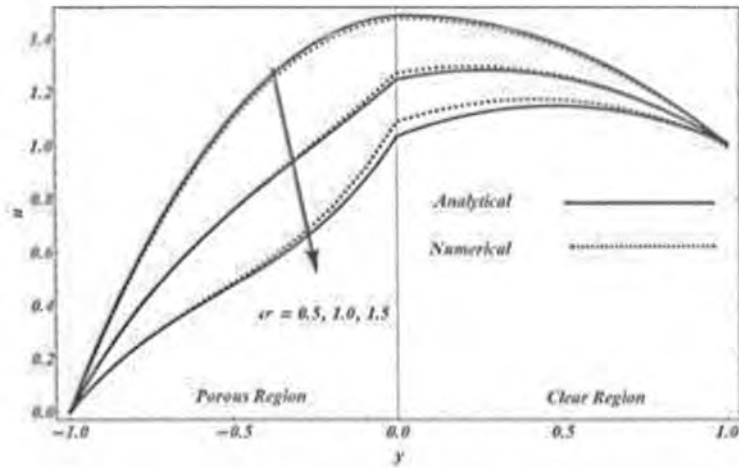


Figure 2.6: The plots of velocity for various inputs of the porosity parameter σ

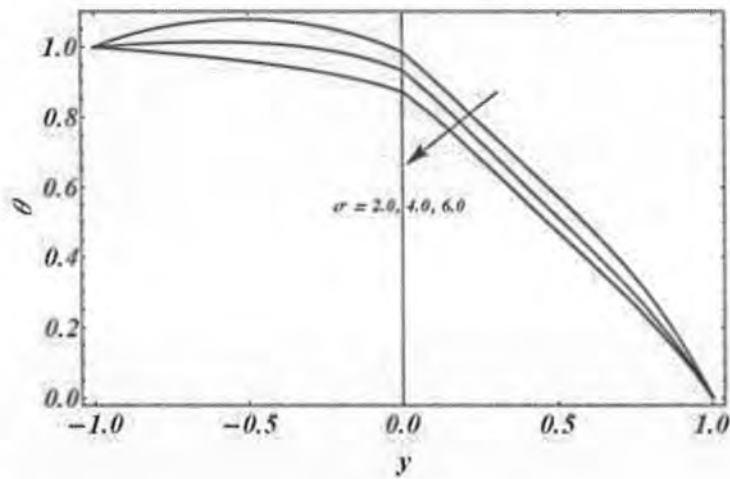


Figure 2.7: The plots of temperature for various inputs of the porosity parameter σ

Figures 2.8 and 2.9 show the effects of amplitude of oscillations of upper plate on the temperature and velocity profiles. Here it can be viewed that as ϵA increases the velocity profile also enhances near the upper plate but this enhance is not significant in region-2. This behavior is expected because as upper plate oscillates with high amplitude, the velocity of the particles near the upper plate also increases. The temperature profile also rises as the amplitude of oscillation increases, although, this increase is more significant in porous region as compared to clear region.

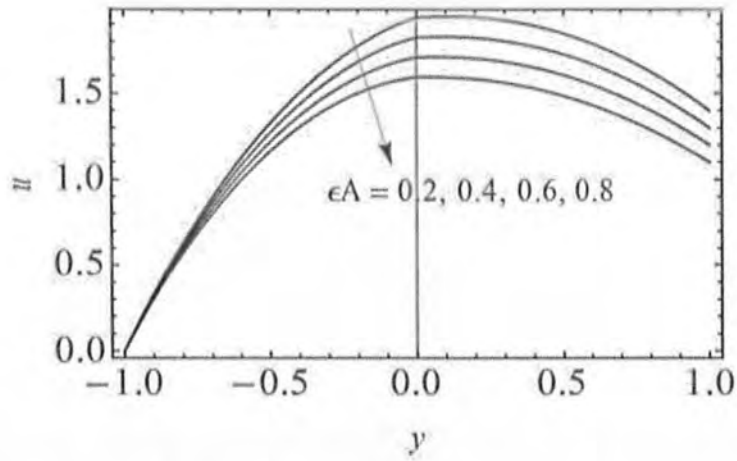


Figure 2.8: The plots of velocity for various inputs of oscillatory parameter ϵA

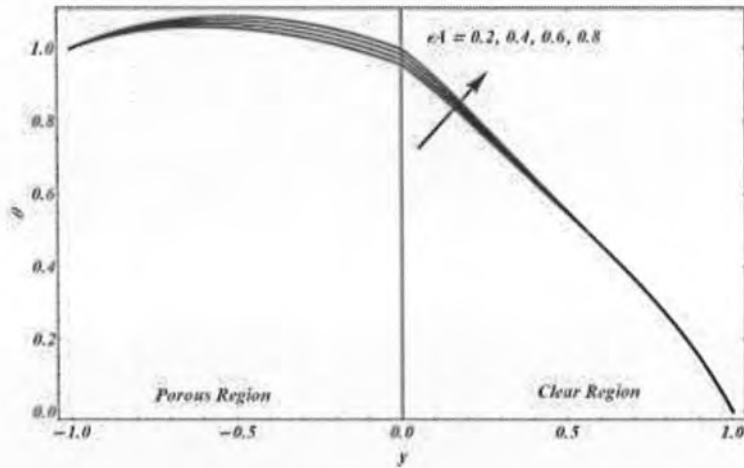


Figure 2.9: The plots of temperature for various inputs of oscillatory parameter ϵA

Figures 2.10 and 2.11 indicate the momentum and the temperature fields for different values of angular frequency ω . From here it is noted that by increasing angular frequency ω the momentum and temperature profiles decrease.

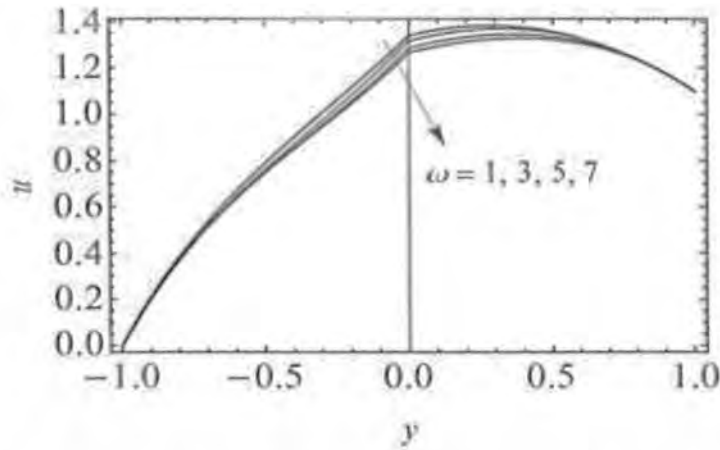


Figure 2.10: The plots of velocity for various inputs of angular frequency ω

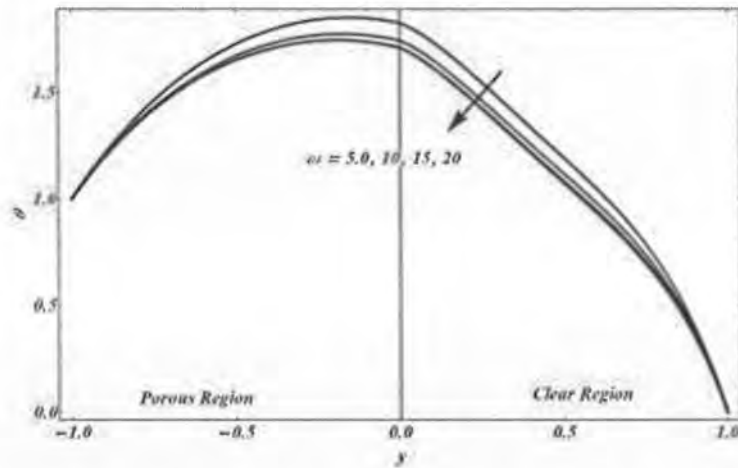


Figure 2.11: The plots of temperature for various inputs of angular frequency ω

Figure 2.12 illustrates the graph of temperature field for the different inputs of k . The graph indicates that the temperature profile enhances with the value of thermal conductivity k . This is quite expected behavior of temperature profile on increasing the thermal conductance of the fluid. The change in temperature profile due to Eckert number is depicted in figure 2.13. The viscous dissipation in the fluid is represented by the Eckert number. This is analyzed that rise in the value of Ec also augments the temperature profile which is because of the increasing heat due to fluid frictional effects. Figure 2.14 shows the temperature profile for the different inputs of the Prandtl number Pr . It is seen that the temperature enhances as Prandtl number Pr rises.

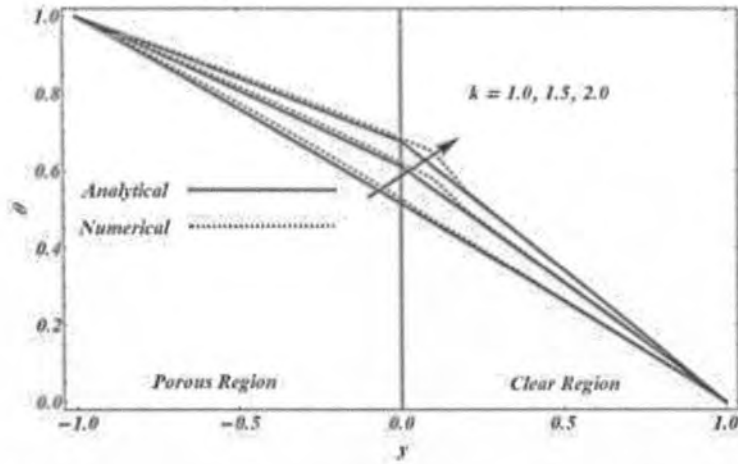


Figure 2.12: The plots of temperature for various input of the ratio of the conductivities k

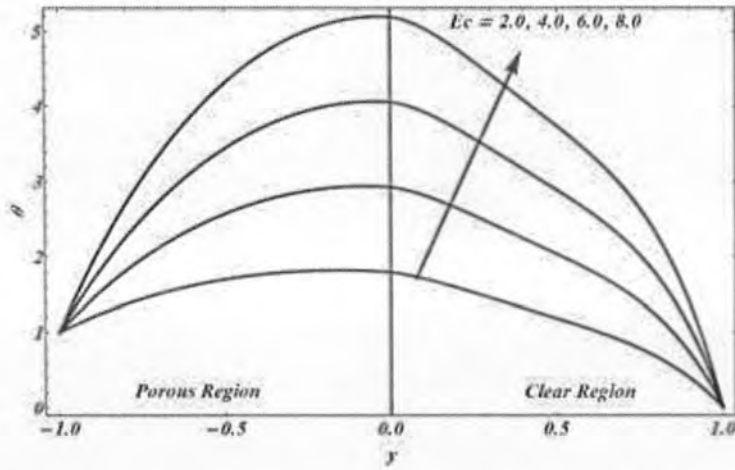


Figure 2.13: The plots of temperature for various inputs of the Eckert number Ec

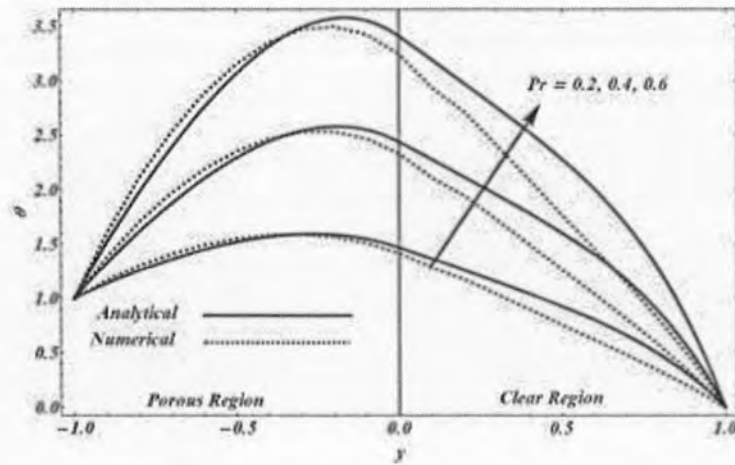


Figure 2.14: The plots of temperature for various inputs of the ratio of the Prandtl number Pr

2.6 Concluding Remarks

An unsteady and viscous fluid flow between two parallel infinite plates whose half space is occupied with porous medium and upper plate is oscillating, is analyzed analytically and numerically. The obtained solutions for the momentum and heat transfer equations are plotted graphically for different physical parameters and following conclusions are made from the analysis done above.

- With the increase in ratio of viscosities the profiles of both temperature and the velocity decreases.
- Behavior of momentum and temperature profiles remains same for different physical parameters.
- The favorable pressure gradient helps in augmentation of convection.
- It can be viewed that the velocity graph shows an increase near the oscillating plate more significantly as compared to the lower plate when amplitude of oscillations increases.
- The behavior of velocity and temperature is inversely related to that of angular frequency. Whereas oscillation amplitude is proportional to temperature.
- This can also be seen that the temperature is directly related to the Eckert number, the Prandtl number and the thermal conductivity.



Chapter 3

Unsteady Flow and Heat Transfer through a Composite Cylinder Partially Filled with Porous Medium

3.1 Introduction

In present chapter we have analyzed the flow and heat transfer effects of viscous fluid through composite cylindrical annulus partially occupied with uniform porous media. Two different flow situations have been analyzed which are described in two upcoming sections. The next section is about the non-steady flow and heat transfer inside a annulus. Third section is devoted to discuss the heat transfer and momentum in a cylinder taken to be permeable, bounded by semi-infinite porous medium. A clear fluid is filled between the cylinder and the porous medium. Perturbation series method is used to give the analytical solution. A brief parametric analysis is performed for the momentum and the temperature fields.

3.2 Flow and Heat Transfer inside a Composite Porous Annulus with Time-Dependent Injection

3.2.1 Mathematical Formulation

Take two concentric cylinders consisting of incompressible, non-steady, fully developed and laminar flow of a viscous fluid in a composite annulus. The system is illustrated in figure 3.1. The region $R_1 < r < (R_1 + R_2)/2$ contains a porous medium and the region $(R_1 + R_2)/2 < r < R_2$ is occupied by a clear viscous fluid.

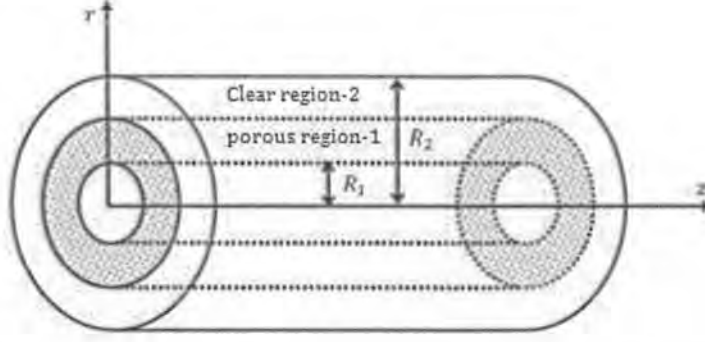


Figure 3.1: Schematic diagram and coordinate system

Both the cylinders are assumed to be infinite and placed horizontally; therefore all physical variables depend on r and t except pressure. The inner cylinder is at constant temperature T_{w1} , while the outer cylinder is fixed at the temperature T_{w2} with $T_{w2} > T_{w1}$. The heat transfer in the annulus is due to constant temperature difference $\Delta T = T_{w2} - T_{w1}$. The viscous dissipation are also assumed to be present. Under these considerations, the equations of motion and heat transfer are

$$\frac{u_i}{r} + \frac{\partial u_i}{\partial r} = 0, \quad (3.1)$$

$$\rho \left(\frac{\partial w_i}{\partial t} + u_i \frac{\partial w_i}{\partial r} \right) = -\frac{\partial p}{\partial z} + \frac{\chi_\mu}{r} \frac{\partial}{\partial r} \left(r \frac{\partial w_i}{\partial r} \right) - \chi \frac{\mu}{s} w_i, \quad (3.2)$$

$$\rho C_p \left(\frac{\partial T_i}{\partial t} + u_i \frac{\partial T_i}{\partial r} \right) = \chi_k \frac{\partial^2 T_i}{\partial r^2} + \frac{\chi_k}{r} \frac{\partial T_i}{\partial r} + 2\chi_\mu \left(\frac{\partial u_i}{\partial r} \right)^2 + \chi_\mu \left(\frac{\partial w_i}{\partial r} \right)^2 + 2\chi_\mu \left(\frac{u_i}{r} \right)^2 + \chi \frac{\mu}{s} w_i^2, \quad (3.3)$$

where region-1 (porous region) and region-2 (clear region) can be obtained by putting $i = 1$ and $i = 2$ respectively. Similarly, $w_i(r, t)$, u_i and $T_i(r, t)$ are the axial velocity, the radial components of velocity of the fluid and the temperature respectively.

The isothermal and no slip boundary conditions have been taken into account at the surfaces. Moreover, the shear stress and velocity at the interface are assumed to be continuous, unlike Kuznetsov [47], where the jump condition was taken on the shear stress. The boundary and interface conditions are given by

$$w_1(R_1) = 0, \quad w_2(R_2) = 0, \quad (3.4)$$

$$\begin{cases} w_1(R_m) = w_2(R_m) \\ \mu_{eff} \frac{\partial w_1}{\partial r} \Big|_{r=R_m} = \mu \frac{\partial w_2}{\partial r} \Big|_{r=R_m} \end{cases}, \quad (3.5)$$

$$T_1(R_1) = T_{w1}, \quad T_2(R_2) = T_{w2}, \quad (3.6)$$

$$\begin{cases} T_1(R_m) = T_2(R_m) \\ K_{eff} \frac{\partial T_1}{\partial r} \Big|_{r=R_m} = K \frac{\partial T_2}{\partial r} \Big|_{r=R_m} \end{cases}, \quad (3.7)$$

where $R_m = \frac{R_1 + R_2}{2}$. The mass conservation law (3.1) shows that u_1 and u_2 are depending on r and t . Therefore, we take

$$u_i = \frac{f(t)}{r}, \quad (3.8)$$

which gives

$$u_i = \frac{u_0 R_1 (1 + \varepsilon A e^{i\omega t})}{r}, \quad (3.9)$$

Introducing non-dimensional variables

$$r^* = \frac{r u_0}{\nu}, \quad w_i^* = \frac{w_i}{u_0}, \quad t^* = \frac{t u_0^2}{\nu}, \quad (3.10)$$

where u_0 is the reference velocity. Using (3.10) and dropping asterisks, (3.2) and (3.3) in dimensionless form become

$$\frac{\partial w_i}{\partial t} + \frac{Re(1 + \varepsilon A e^{i\omega t})}{r} \frac{\partial w_i}{\partial r} = -P + A_i \frac{\partial^2 w_i}{\partial r^2} + \frac{C_i}{r} \frac{\partial w_i}{\partial r} - \chi \sigma^2 w_i, \quad (3.11)$$

$$\frac{\partial \theta_i}{\partial t} + \frac{Re(1 + \varepsilon A e^{i\omega t})}{r} \frac{\partial \theta_i}{\partial r} = B_i \frac{\partial^2 \theta_i}{\partial r^2} + \frac{B_i}{r} \frac{\partial \theta_i}{\partial r} + 4 \frac{A_i Re^2 Ec (1 + \varepsilon A e^{i\omega t})^2}{r^4} + Ec A_i \left(\frac{\partial w_i}{\partial r} \right)^2 + \chi Ec \sigma^2 w_i^2, \quad (3.12)$$

where

$$A_i = \begin{cases} m & i=1 \\ 1 & i=2 \end{cases},$$

$$B_i = \begin{cases} \frac{k}{\text{Pr}} & i=1 \\ \frac{1}{\text{Pr}} & i=2 \end{cases},$$

and $\text{Re} = \frac{R_1 u_0}{\nu}$ is the Reynold number. The dimensionless form of the boundary and interface conditions (3.4)-(3.7) reduce to

$$w_1(1) = 0, \quad w_2(2) = 0, \quad (3.13)$$

$$\begin{cases} w_1(R_m) = w_2(R_m) \\ m \frac{\partial w_1}{\partial r} \Big|_{r=R_m} = \frac{\partial w_2}{\partial r} \Big|_{r=R_m} \end{cases}, \quad (3.14)$$

$$\theta_1(1) = 1, \quad \theta_2(2) = 0, \quad (3.15)$$

$$\begin{cases} \theta_1(R_m) = \theta_2(R_m) \\ k \frac{\partial \theta_1}{\partial r} \Big|_{r=R_m} = \frac{\partial \theta_2}{\partial r} \Big|_{r=R_m} \end{cases}. \quad (3.16)$$

3.2.2 Solution Methodology

The coupled non-linear PDEs for momentum and energy equations (3.11) and (3.12) respectively, cannot be found in closed form. However, (3.11) and (3.12) can be converted to a set of ODEs by expanding the series for the momentum and temperature fields as

$$w_i(r,t) = w_{i0}(r) + \varepsilon A e^{I\omega t} w_{i1}(r) + O(\varepsilon A)^2 + \dots \quad i=1,2. \quad (3.17)$$

$$\theta_i(r,t) = \theta_{i0}(r) + \varepsilon A e^{I\omega t} \theta_{i1}(r) + O(\varepsilon A)^2 + \dots \quad i=1,2. \quad (3.18)$$

It is an effective consideration due to the choice of u_i in equation (3.9) that the amplitude $\varepsilon A < 1$. By plugging equations (3.17) and (3.18) into equations (3.11) and (3.12), comparing the coefficient of $(\varepsilon A)^0$ and $(\varepsilon A)^1$ terms and neglecting the higher order terms, the following non-periodic and periodic coefficients can be attained.

Non-Periodic Coefficient $O(\varepsilon A)^0$

$$C_i \frac{\partial^2 w_{i0}}{\partial r^2} + \frac{(C_i - Re)}{r} \frac{\partial w_{i0}}{\partial r} - \chi \sigma^2 w_{i0} = P, \quad (3.19)$$

$$B_i \frac{\partial^2 \theta_{i0}}{\partial r^2} + \frac{(B_i - Re)}{r} \frac{\partial \theta_{i0}}{\partial r} + \frac{4C_i Re^2 Ec}{r^4} + Ec C_i \left(\frac{\partial w_{i0}}{\partial r} \right)^2 + \chi Ec \sigma^2 w_{i0}^2 = 0. \quad (3.20)$$

Periodic Coefficient $O(\varepsilon A)^1$

$$C_i \frac{\partial^2 w_{i1}}{\partial r^2} + \frac{(C_i - Re)}{r} \frac{\partial w_{i1}}{\partial r} - \chi \sigma^2 w_{i1} - I \omega w_{i1} - \frac{A Re}{r} \frac{\partial w_{i0}}{\partial r} = 0, \quad (3.21)$$

$$B_i \frac{\partial^2 \theta_{i1}}{\partial r^2} + \frac{(B_i - Re)}{r} \frac{\partial \theta_{i1}}{\partial r} - I \omega \theta_{i1} - \frac{A Re}{r} \frac{\partial \theta_{i0}}{\partial r} + \frac{8C_i Ec Re^2 A}{r^4} + 2Ec C_i \left(\frac{\partial w_{i0}}{\partial r} \right) \left(\frac{\partial w_{i1}}{\partial r} \right) + 2\chi Ec \sigma^2 w_{i0} w_{i1} = 0. \quad (3.22)$$

Using equations (3.17) and (3.18), the boundary and interface conditions take the form

$$\begin{cases} w_{1i}(R_1) = 0, & w_{2i}(R_2) = 0, \\ \theta_{1i}(R_1) = 1 - \delta_{1i}, & \theta_{2i}(R_2) = 0, \end{cases} \quad (3.23)$$

$$\begin{cases} w_{1i}(R_m) = w_{2i}(R_m) \\ m \frac{\partial w_{1i}}{\partial r} \Big|_{r=R_m} = \frac{\partial w_{2i}}{\partial r} \Big|_{r=R_m} \\ \theta_{1i}(R_m) = \theta_{2i}(R_m) \\ k \frac{\partial \theta_{1i}}{\partial r} \Big|_{r=R_m} = \frac{\partial \theta_{2i}}{\partial r} \Big|_{r=R_m} \end{cases}, \quad (3.24)$$

where δ_{1i} is the Kronecker delta.

3.3 Results and Discussion

The non-linear PDEs (3.19)-(3.22) with boundary conditions (3.23)-(3.24) are solved analytically. As the solutions of these equations are quite lengthy and complicated, therefore we are giving tabulated values for velocity, temperature and at their derivatives. These values are given in the Table 3.1.

Table 3.1: Shows the inputs for temperature θ , velocity w and at their derivatives by taking the values of r between 1.0 and 2.0. Here $k = 0.25$, $Ec = 1$, $Pr = 1$, $\varepsilon A = 0.2$, $Re = 1$

$\sigma = \frac{1}{2}$, $m = \frac{1}{4}$, $P = -2$, $\omega = 5$, $\omega t = \frac{\pi}{3}$ are kept fixed.

r	w	w'	θ	θ'
1.0	5.0610×10^{-21}	1.74912	1.0	0.509117
1.1	0.163302	1.50011	1.02005	-0.107671
1.2	0.296212	1.13674	0.978537	-0.721948
1.3	0.385923	0.631519	0.875794	-1.33288
1.4	0.416864	-0.04322	0.711444	-1.96136
1.5	0.370724	-0.91452	0.480286	-0.67267
1.6	0.337674	-0.43261	0.407571	-0.780192
1.7	0.28416	-0.63783	0.324296	-0.886192
1.8	0.210079	-0.84391	0.229949	-1.00366
1.9	0.115365	-1.05041	0.122795	-1.14417
2.0	-1.443×10^{-10}	-1.25683	2.458×10^{-9}	-1.31811

The effects of various physical parameters are analyzed by plotting graphs. When $m = \frac{1}{4}$, $P = -1$,

$\omega = 5$, $\omega t = \pi/3$, $Re = 1$, $\sigma = 1/2$ are kept fixed.

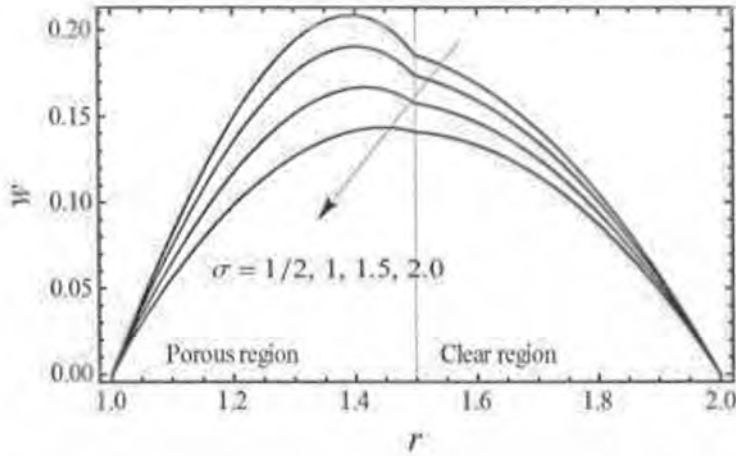


Figure 3.2: Velocity w versus r for various inputs of porosity parameter σ

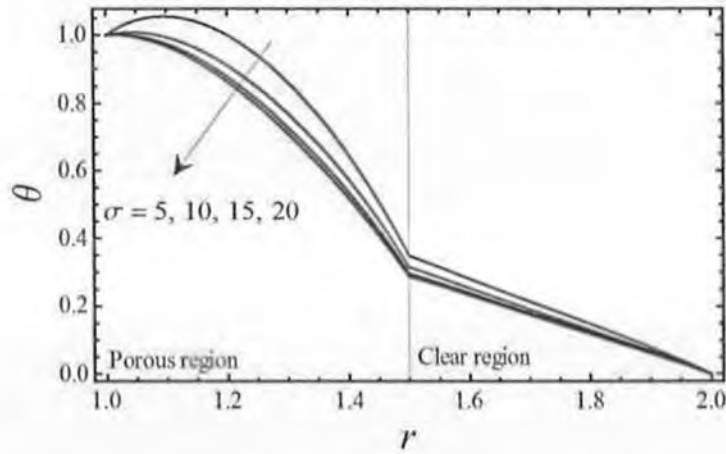


Figure 3.3: Temperature θ versus r for various inputs of porosity parameter σ

Figures 3.2 and 3.3 display the effect of porosity parameter on the velocity and temperature fields, respectively. It is noticed from the figures that the velocity and temperature profiles are inversely related to σ . This is because of the shrinking of the pores area due to which momentum transport reduces and as a result, velocity as well as temperature profile decreases. It is also observed from here that porous medium parameter σ has significant effects in both porous and non-porous regions and the velocity profile reduces in both regions, however, this reduction is more significant in the porous region.

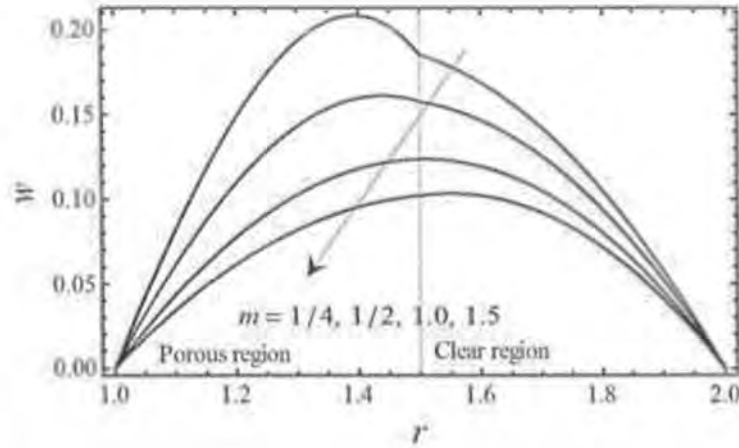


Figure 3.4: Velocity w versus r for various inputs of the viscosities ratio parameter m

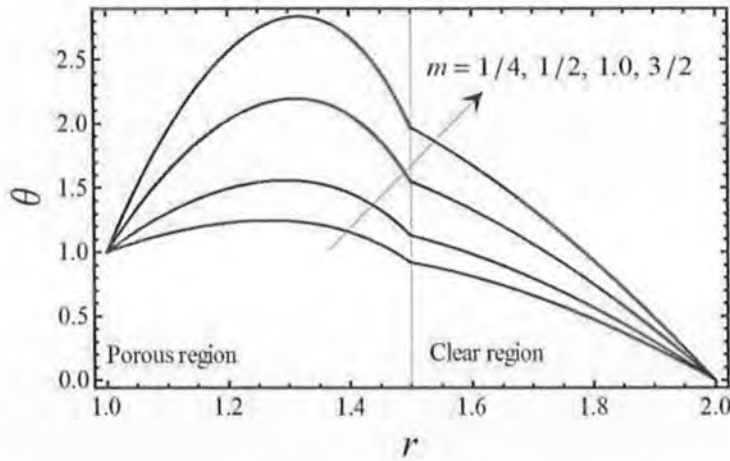


Figure 3.5: Temperature θ versus r for various inputs of viscosities ratio parameter m

Figures 3.4 and 3.5 elaborate the influence of the viscosities ratio m on the momentum and temperature profile respectively. As the value of viscosities ratio parameter m enhances, the velocity drops whereas temperature profile rises. This conduct of the flow is due to the increasing field viscosity by which the process of internal heat generation enhances and due to the thickness of fluid the velocity profile decreases. It can be viewed that the decrease in velocity profile in the porous region is more prominent as compared to the clear region. Similarly, the increase in temperature profile by increasing m is more significant in porous region. This is due to the presence of resistive force which amplifies the temperature and reduces the velocity more significantly as compared to the clear region.

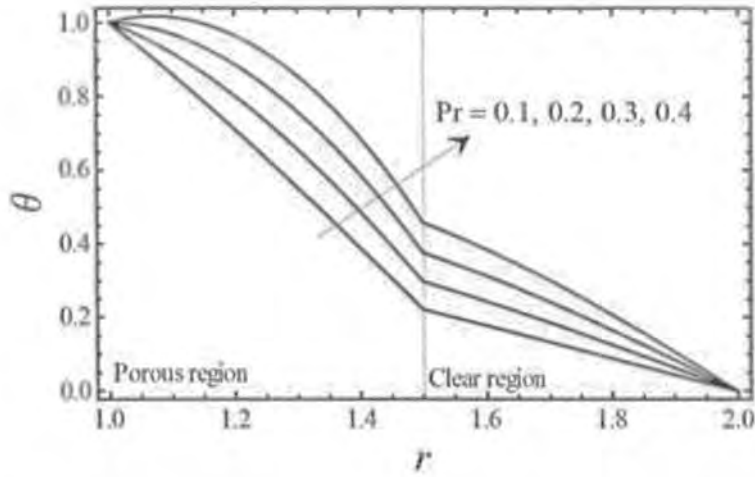


Figure 3.6: Temperature θ versus r for various inputs of Prandtl number Pr

The temperature field under the effect of Prandtl number can be seen in figure 3.6. This can be viewed that the temperature profile and Pr are directly related. Increase of viscous diffusion in dissipation enhances heat generation inside the annulus, which directly affects the temperature profile shown.

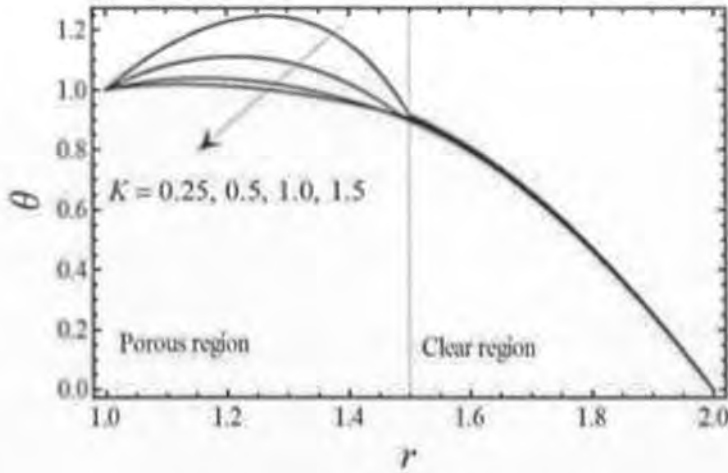


Figure 3.7: Temperature θ versus r for various inputs of ratio of conductivities k

The temperature profile is given in figure 3.7, for different values of thermal conductivity, k . The temperature profile also decreases for porous region for the increase of thermal conductivity and remains constant for clear region in the fluid.

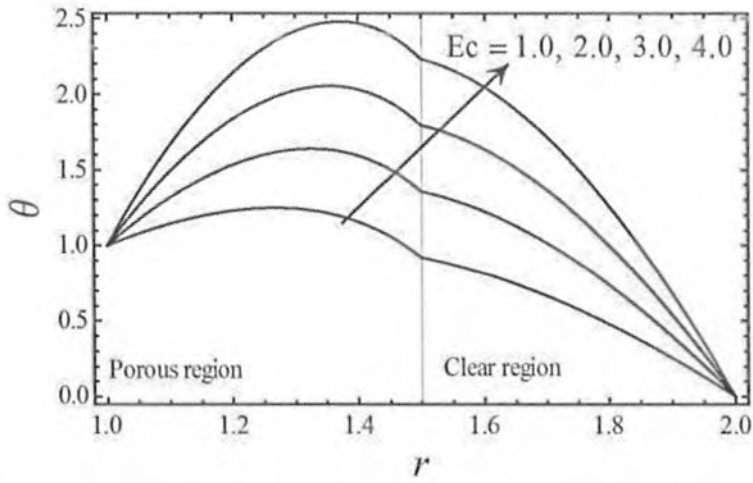


Figure 3.8: Temperature θ versus r for various inputs of Eckert number, Ec

The role of Eckert number on the temperature profile can be seen in Figure 3.8. A rise in Ec augments the temperature profile which is due to the rise of fluid frictional effects.

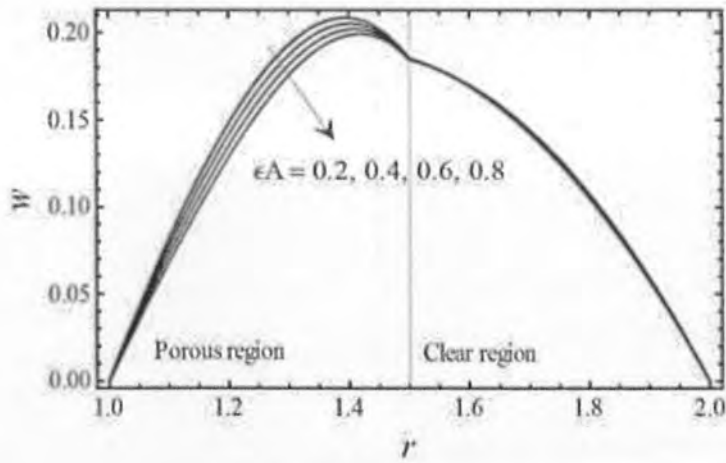


Figure 3.9: Velocity w versus r for various inputs of oscillation amplitude ϵA

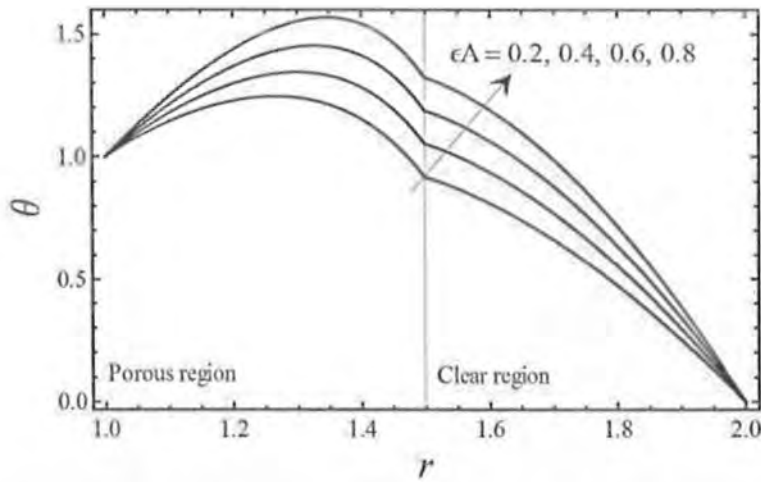


Figure 3.10: Temperature θ versus r for various inputs of oscillation amplitude εA

Figures 3.9 and 3.10 show the effect of the amplitude of oscillation εA on the velocity and temperature fields, respectively. Oscillation amplitude is taken to be small for analytical solutions i.e. $\varepsilon A \leq 1$ and $\varepsilon A = 0$ corresponds to the steady state solutions. It is vivid in the figure 3.9 that with increase in amplitude, velocity decreases for porous region but remains constant for clear region. On the other hand, increase in amplitude has an increasing effect on the temperature profile for both the region of the channel, which is quite expected behavior of the profile.

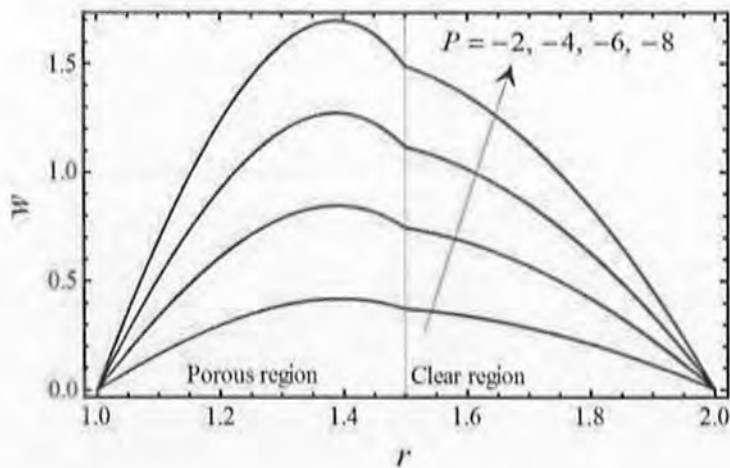


Figure 3.11: Velocity w versus r for various inputs of pressure gradient P

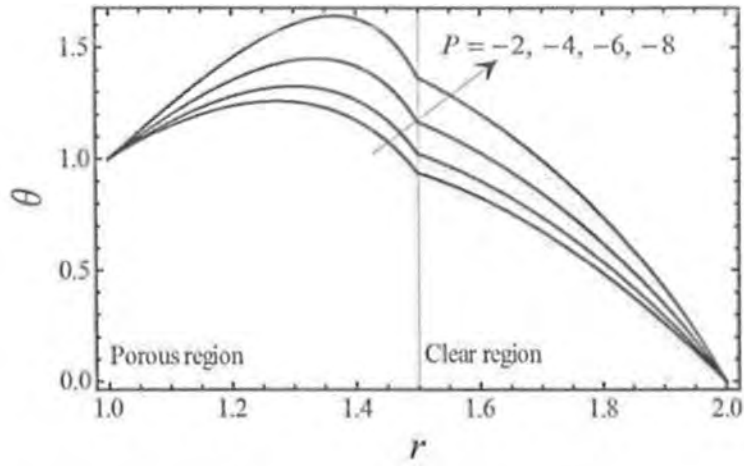


Figure 3.12: Temperature θ versus r for various inputs of the pressure gradient P

Figures 3.11 and 3.12 depict the role of pressure gradient on both temperature and velocity. Both the momentum and the temperature fields are inversely related to pressure, which was expected because of favorable pressure. Figures 3.13 and 3.14 show the effects of angular frequency for both momentum and temperature. With the rise of angular frequency, velocity increases while temperature decreases.

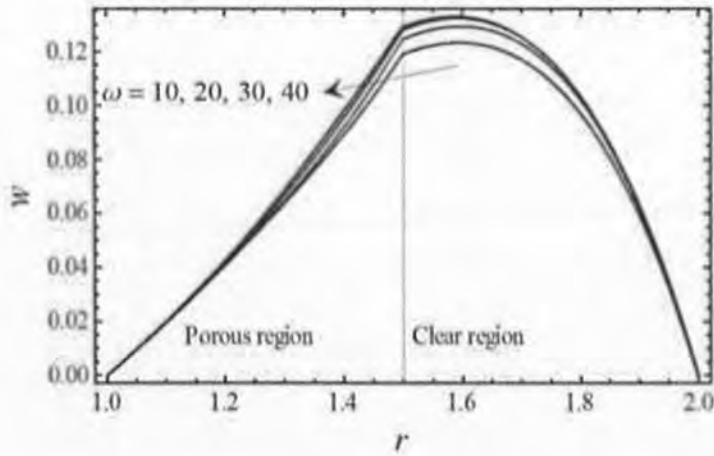


Figure 3.13: Velocity w versus r for various inputs of frequency ω

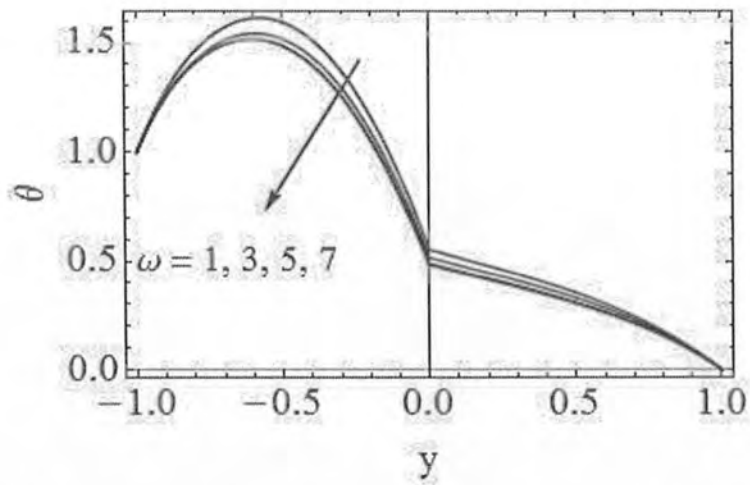


Figure 3.14: Temperature θ versus r for various inputs of the frequency ω

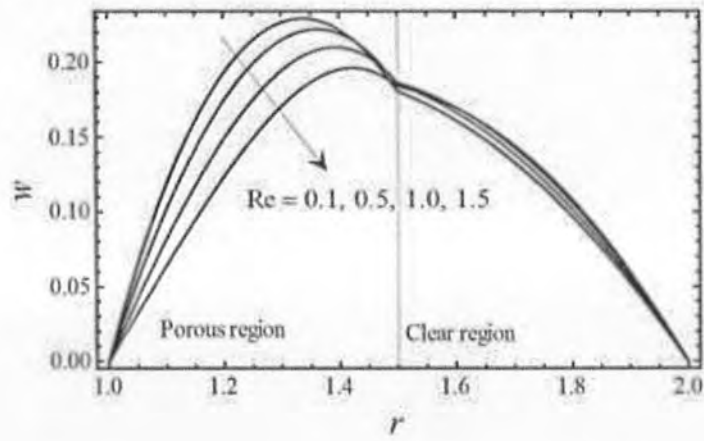


Figure 3.15: Velocity w versus r for various inputs of Reynold number Re

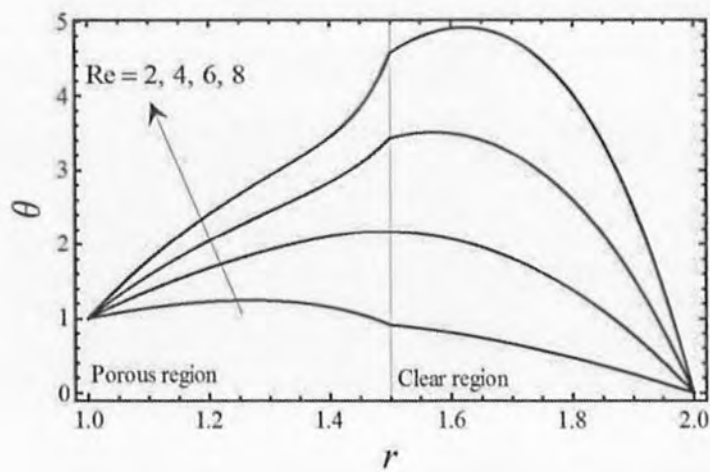


Figure 3.16: Temperature θ versus r for various inputs of Reynold number Re

Figures 3.15 and 3.16 are the plots of velocity and temperature fields on Reynold number, velocity decreases by increase of Reynold number due to the decrease of inertial forces, while temperature increases by increase of Reynold number.

3.4 Concluding Remarks

The effects of viscous fluid flow (taken to be unsteady) and transfer of heat between two concentric cylinders is analyzed analytically. Taking viscous dissipation into account for both regions in the permeable channel, the heat transfer analysis is also made. The computed solutions are displayed for different values of parameters and the following concluding observations are noticed from the above analysis.

- It is concluded that by increasing the permeability of pores, the velocity as well as temperature profile fall in both parts of permeable channel. However, the fall is more significant in porous region.
- The velocity profile drops with the rise of viscosity ratio parameter, although this decrease is prominent in lower region. On the other hand, the temperature profile exhibits inverse behavior of the said parameter.
- The temperature field is directly proportional Prandtl number and Eckert number while for thermal conductivity temperature profile decreases.
- It is noted that amplitude in the velocity decreases for porous region and remains constant for clear region while the temperature profile is increasing functions for amplitude.
- Both the velocity and the temperature are directly related with pressure.
- It is observed that the effects of angular frequency were found to increase the velocity profile while decreases the temperature.
- By increasing the Reynold number velocity decreases while the temperature increases.

3.5 Flow over a Permeable Cylinder Bounded by a Semi-Infinite Porous Medium

3.5.1 Mathematical Modeling

Consider a permeable cylinder of radius R_1 filled with fully developed, electrically conducting, viscous fluid with laminar flow. The cylinder is bounded by a semi-infinite porous medium from its top at $R_2 \leq r < \infty$. The region between the cylinder and the porous medium $R_1 \leq r \leq R_2$ is filled by the clear fluid, as displayed in figure 3.17.

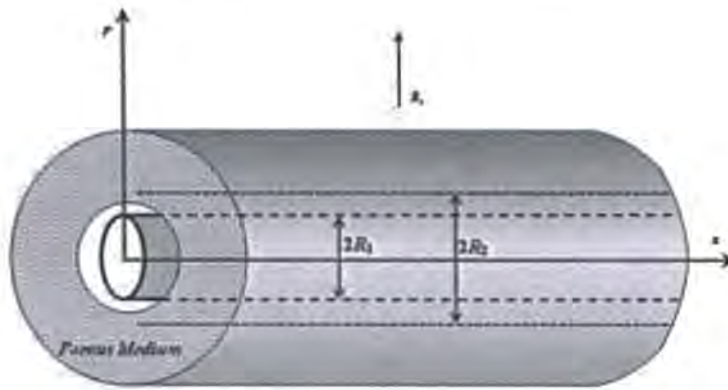


Figure 3.17: Schematic diagram of the considered problem

The cylinder injects a constant velocity u_0 into the fluid normal to its surface. The porous medium is taken to be uniform. The Darcy-Brinkman model is used to develop the governing equations for the flow phenomenon. A magnetic field B_0 is taken to be uniform and along radius. The induced magnetic field is considered to be insignificant under the assumption of small magnetic Reynold number. Under these suppositions, the set of governing equations becomes

$$u_0 \frac{\partial w_1}{\partial r} = -\frac{1}{\rho} \frac{\partial p}{\partial z} + \frac{\mu}{\rho r} \frac{\partial w_1}{\partial r} + \frac{\mu}{\rho r} \frac{\partial^2 w_1}{\partial r^2} - \frac{\sigma_1 B_0^2}{\rho} w_1, \quad \text{for } R_1 \leq r \leq R_2, \quad (3.25)$$

$$u_0 \frac{\partial w_2}{\partial r} = -\frac{1}{\rho} \frac{\partial p}{\partial z} + \frac{\mu_{\text{eff}}}{\rho r} \frac{\partial w_2}{\partial r} + \frac{\mu_{\text{eff}}}{\rho r} \frac{\partial^2 w_2}{\partial r^2} - \frac{\mu_{\text{eff}}}{\rho s} w_2 - \frac{\sigma_1 B_0^2}{\rho} w_2, \quad \text{for } R_2 \leq r < \infty, \quad (3.26)$$

where (3.25) represents the momentum transport in clear region and (3.26) for porous region, w_1 and w_2 are the axial velocities in clear and porous regions respectively, B_0 and σ_1 are the magnetic field and the electrical conductivity, respectively. The following boundary and interface conditions as suggested by Kuznetsov [47], are used for the two fluids.

$$w_1(R_1) = 0, \quad \frac{dw_2}{dr} = 0, \quad \text{at } r \rightarrow \infty, \quad (3.27)$$

$$w_1(R_2) = w_2(R_2), \quad \mu_{eff} \frac{\partial w_1}{\partial r} - \mu \frac{\partial w_2}{\partial r} = \beta_1 \frac{\mu w_1}{K^{1/2}}, \quad \text{at } r = R_2, \quad (3.28)$$

where β_1 is the stress jump parameter. It is noted that we are considering the constant ambient velocity and the stress jump condition which were used in Beaver and Joseph [45]. Introducing the following dimensionless quantities

$$r^* = \frac{r}{R_1}, \quad w_i^* = \frac{w_i}{u_0}, \quad i = 1, 2. \quad (3.29)$$

Using (3.29) in (3.25) -(3.26) and dropping the asterisks we left with the following set of ordinary differential equations.

$$\frac{d^2 w_1}{dr^2} + \frac{1}{r} \frac{dw_1}{dr} - S \frac{dw_1}{dr} - M^2 w_1 - P = 0, \quad (3.30)$$

$$m \frac{d^2 w_2}{dr^2} + \frac{m}{r} \frac{dw_2}{dr} - S \frac{dw_2}{dr} - (M^2 + \sigma^2) w_2 - P = 0, \quad (3.31)$$

where $S = u_0 \rho R_1 / \mu$, $M^2 = \sigma_1 B_0^2 R_1^2 / \mu$, $\sigma^2 = R_1^2 / K$ and $P = \frac{R_1^2}{\mu u_0} \frac{\partial p}{\partial z}$ are the Reynold suction/

injection parameter, magnetic field parameter, porosity parameter and the nondimensional pressure gradient, respectively. The dimensionless form of the interface and boundary conditions are

$$w_1(1) = 0, \quad \text{and} \quad \frac{dw_2}{dr} = 0, \quad \text{at } r \rightarrow \infty, \quad (3.32)$$

$$w_1(2) = w_2(2), \quad m \frac{\partial w_1}{\partial r} \Big|_{r=2} - \frac{\partial w_2}{\partial r} \Big|_{r=2} = \beta_1 \frac{\mu w_1}{K^{1/2}}. \quad (3.33)$$

3.5.2 Solution of the Problem

The symbolic computing software MATHEMATICA is used to find the solution of linear ODEs (3.30) and (3.31) along with conditions (3.32) and (3.33) by using the built-in command “NDSolve”. The semi-infinite domain is adjusted at appropriate place where the ambient conditions are met. In order to calculate the numerical solution, we have adjusted $R_2 = 2$ and the semi-infinite domain is trimmed at $r_\infty = 10$.

3.5.3 Results and Discussion

The obtained solutions for the velocity in both the regions are plotted for different inputs of physical parameters in present section. The values of physical parameters $m = 2.0$, $P = -1$, $\beta_1 = 1/5$, $\sigma^2 = 1$, $S = -0.2$, $M = 0.2$ are kept constant except the varying one.

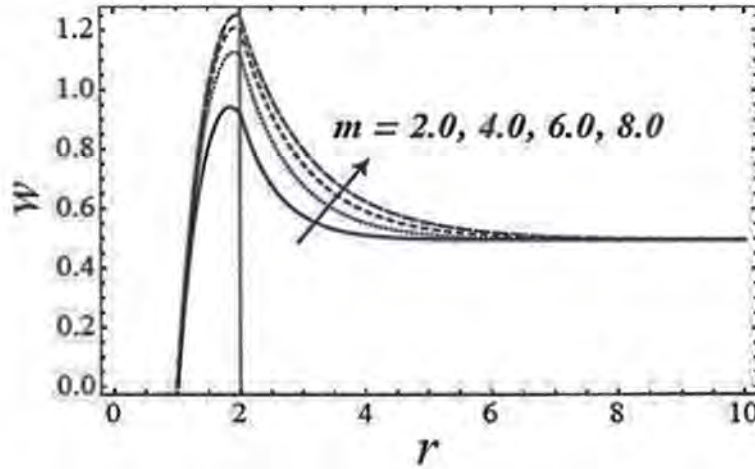


Figure 3.18: Plots of velocity w for various inputs of the ratio of viscosities m .

Figure 3.18 shows that the velocity is directly related to viscosities ratio parameter m and this increase is more significant near the interfacial region. It is also noticed from the figure that magnitude of velocity of fluid in clear region is greater than porous region and as one goes downstream, the velocity continuously decreases and becomes constant.

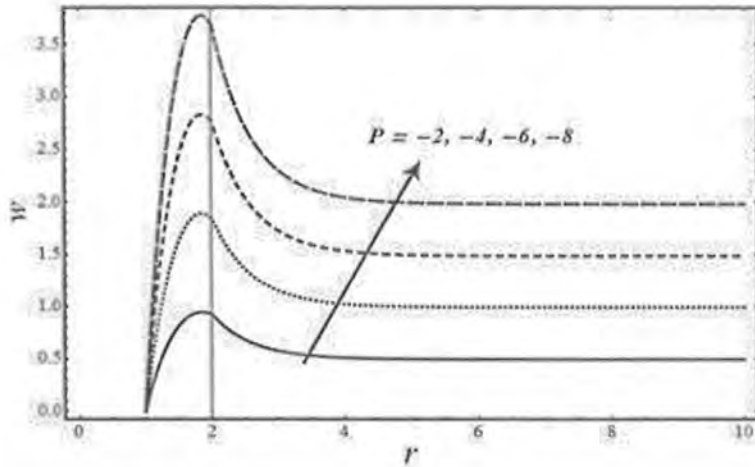


Figure 3.19: Plots of velocity w for various inputs of pressure gradient P

Figure 3.19 illustrates the velocity distribution for the influence of constant pressure gradient P . Here negative values of P indicate the favorable pressure gradient. It is noteworthy that the velocity field rises as favorable pressure gradient decreases.

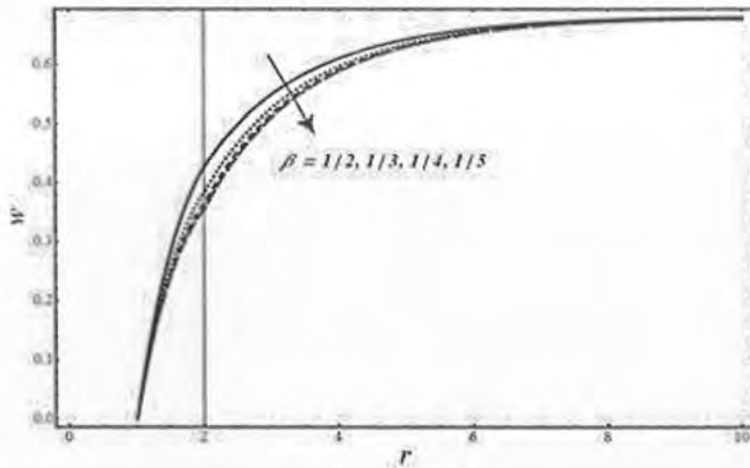


Figure 3.20: Plots of velocity w for various inputs of stress jump parameter β_1

Figure 3.20 demonstrates the effects of stress jump parameter β_1 on the velocity field. This shows that as β_1 decreases, velocity lessens in both regions. However, this change in velocity profile is more significant close to the interface region as compared to other regions of flow.

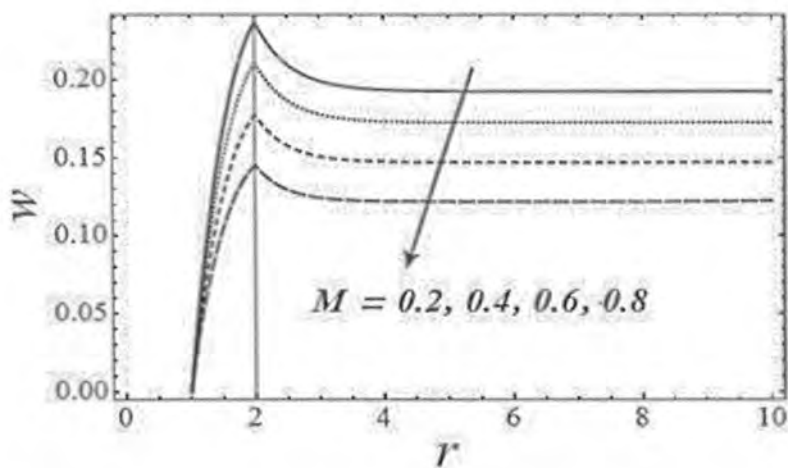


Figure 3.21: Plots of velocity w for various inputs of magnetic parameter M

Figure 3.21 demonstrates the effects of magnetic field on the velocity profile. Magnetic field parameter are inversely related to velocity field which is due to increasing viscous effects in the flow.

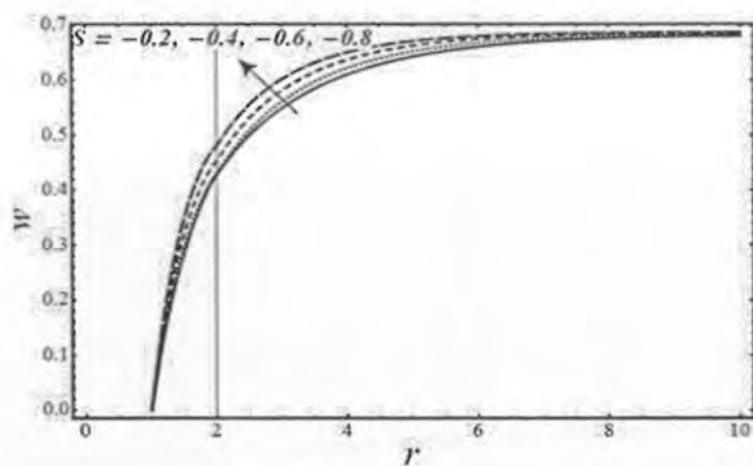


Figure 3.22: Plots of velocity w for various inputs of suction Reynold parameter S

Figure 3.22 displays the velocity field for numerous inputs of suction Reynold parameter. As the suction Reynolds number S accelerates, velocity decelerates which is quite expected due to the escaping of fluid particles from the surface of the cylinder.

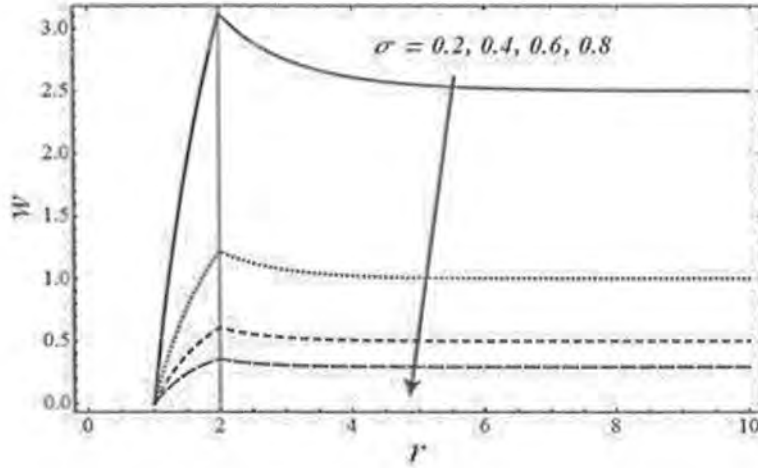


Figure 3.23: Plots of velocity w for various inputs of porosity parameter σ

Figure 3.23 displays the effects of porous medium parameter σ on the velocity profile. It can be seen that by raising σ , the velocity profile reduces significantly.

3.5.4 Concluding Remarks

A study is carried out to explore the behavior of flow in half porous and half clear region over an infinite cylinder. A numerical solution of the problem has been calculated and an analysis has been made through various graphs. The major findings are as follows

- In porous region the velocity of fluid is less than in clear region under the effect of m .
- It is noted that in clear region the velocity augments with the reduction of pressure gradient but remains constant for porous region.
- A decrease in the stress jump coefficient β_1 results in the decrease in velocity.
- The flow velocity is reduced with the magnetic field.
- It is noted that velocity reduces for the increase of suction Reynolds number.
- Rise in porosity parameter causes fall of velocity profile.

Chapter 4

Unsteady Chemically Reacting Casson Fluid Flow in an Irregular Channel with Convective Boundary Conditions

4.1 Introduction

The present chapter deals with the unsteady, chemically reacting Casson fluid in an irregular vertical channel with convective boundary conditions. The dimensionless PDEs that govern the momentum, temperature and mass concentration are converted into ODEs by using regular perturbation method. The closed form solutions are obtained. The effects of various parameters such as the thermal radiation parameter, chemical reaction parameter, thermal Grashof number, Solutal Grashof number, Nusselt number, local skin friction, Sherwood number, Soret number and Biot number have been discussed with the help of tables and graphs.

4.2 Mathematical Formulation

Consider an unsteady, two dimensional incompressible Casson fluid flow in a long vertical channel where one wall is wavy while another is lying flat as schematically shown in figure 4.1. The x^* - axis is assumed to be taken along the wavy wall. The wavy wall ($y^* = 0$) is maintained at temperature T_{w1} and mass concentration C_1 while the flat wall ($y^* = d$) is at temperature T_{w2} and mass concentration C_2 . The electrically conducting fluid passes through a uniform porous medium having permeability s . Furthermore, it is supposed that the convective heat exchange from the wall obeys Newton's law of cooling. The fluid flow is exposed to the influence of heat absorption, radiation absorption, first order chemically reactive species and uniform magnetic field of strength B_0 .

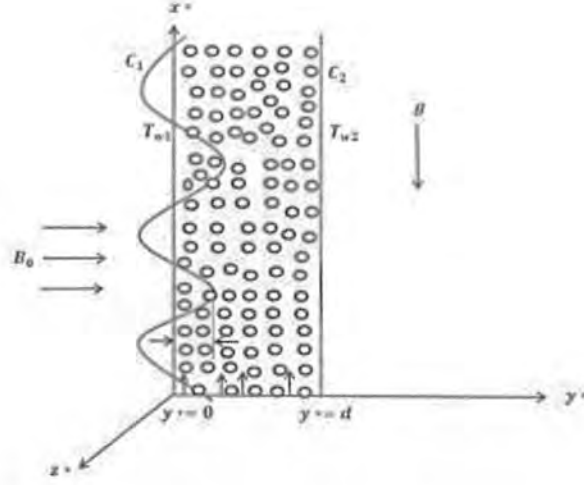


Figure 4.1: Schematic flow diagram

Under these assumptions, model equations for velocity, heat transfer and mass concentration are given by [38]

$$\frac{\partial u^*}{\partial t^*} = \nu \left(1 + \frac{1}{\gamma} \right) \frac{\partial^2 u^*}{\partial y^{*2}} - \frac{\nu}{s} u^* - \frac{\sigma_1 B_0^2}{\rho} u^* + g \beta_T (T^* - T_1) + g \beta_c (C^* - C_1), \quad (4.1)$$

$$\frac{\partial T^*}{\partial t^*} = \frac{k}{\rho C_p} \frac{\partial^2 T^*}{\partial y^{*2}} - \frac{Q_l}{\rho C_p} (T^* - T_1) - \frac{1}{\rho C_p} \frac{\partial q_r}{\partial y^*} + \frac{\nu}{C_p} \left(1 + \frac{1}{\gamma} \right) \left(\frac{\partial u^*}{\partial y^*} \right)^2 + \frac{\sigma B_0^2}{\rho C_p} u^{*2} + \frac{Q_c}{\rho C_p} (C^* - C_1), \quad (4.2)$$

$$\frac{\partial C^*}{\partial t^*} = D \frac{\partial^2 C^*}{\partial y^{*2}} - K_R (C^* - C_1). \quad (4.3)$$

The corresponding boundary and initial conditions [37] are

$$t^* = 0: \quad u^* = 0, \quad T^* = T_1, \quad C^* = C_1, \quad \text{for } h(x) < y^* < d, \quad (4.4)$$

$$t^* > 0: \quad \begin{cases} u^* = 0, & -k \frac{\partial T^*}{\partial y^*} = h_f (T_1 - T^* + (T_2 - T_1) \varepsilon A e^{-h^* t^*}), \\ C^* = C_1 + (C_2 - C_1) \varepsilon A e^{-h^* t^*}, \end{cases} \quad \text{for } y^* = \varepsilon A \cos(k_2 x^*), \quad (4.5)$$

Using the relation used in [38], radiative heat flux q_r is given by

$$\frac{\partial q_r}{\partial y^*} = 4(T_1 - T^*)I', \quad I' = \int k_{\lambda_1 w} \frac{\partial e_{b\lambda_1}}{\partial T} d\lambda_1, \quad (4.6)$$

where γ , $k_{\lambda_1 w}$, β_c , $e_{\lambda_1 w}$, β_T , Q_c , g and Q_t are the Casson fluid parameter, radiation absorption coefficient at the wall, concentration expansion coefficient, Planck's constant, thermal expansion coefficient, dimensional mass concentration absorption coefficient, gravitational acceleration and dimensional heat absorption coefficient respectively.

Non-dimensional quantities can be written as

$$x = \frac{x^*}{d}, \quad y = \frac{y^*}{d}, \quad u = \frac{u^*}{U_0}, \quad \theta = \frac{T^* - T_1}{T_2 - T_1}, \quad \varphi = \frac{C^* - C_1}{C_2 - C_1},$$

$$M^2 = \frac{\sigma_1 B_0^2 d^2}{\mu}, \quad \frac{1}{K} = \frac{d^2}{k^*}, \quad G_r = \frac{g\beta_T(T_2 - T_1)d^2}{\nu u_0}, \quad G_c = \frac{g\beta_c(C_2 - C_1)d^2}{\nu u_0},$$

$$\text{Pr} = \frac{\mu C_p}{K}, \quad \alpha_T = \frac{Q_t d^2}{K}, \quad F = \frac{4I' d^2}{K}, \quad h = \epsilon \cos(\lambda_1 x)$$

$$\alpha_c = \frac{Q_c(C_2 - C_1)d^2}{K(T_2 - T_1)}, \quad S_c = \frac{\nu}{D}, \quad B_i = \frac{h_f d}{K}, \quad K_r = \frac{K_R d^2}{\nu}, \quad \lambda_1 = K_2 d.$$

$$t = \frac{\nu t^*}{d^2}, \quad n = \frac{n^* d^2}{\nu}.$$

Applying the above dimensionless quantities in equations (4.1)-(4.3) we get

$$\frac{\partial u}{\partial t} = \left(1 + \frac{1}{\gamma}\right) \frac{\partial^2 u}{\partial y^2} - \left(M^2 + \frac{1}{K}\right) u + G_r \theta + G_c \varphi, \quad (4.7)$$

$$\frac{\partial^2 \theta}{\partial y^2} - \text{Pr} \frac{\partial \theta}{\partial t} + (F - \alpha_T) \theta + \text{Pr} Ec \left(1 + \frac{1}{\gamma}\right) \left(\frac{\partial u}{\partial y}\right)^2 + \text{Pr} Ec M^2 u^2 + \alpha_c \varphi = 0, \quad (4.8)$$

$$\frac{\partial^2 \varphi}{\partial y^2} - S_c \frac{\partial \varphi}{\partial t} - S_c K_r \varphi = 0. \quad (4.9)$$

Boundary conditions (4.4)-(4.5) become

$$t = 0: \quad u = 0, \quad \theta = 0, \quad \varphi = 0, \quad \text{for } y \in (h, 1), \quad (4.10)$$

$t > 0$:

$$\begin{cases} u = 0, & \theta' = B_i(\theta - \varepsilon A e^{-lm}), & \varphi = \varepsilon A e^{-lm}, & \text{at } y = h, \\ u = 0, & \theta' = B_i(\theta - 1 - \varepsilon A e^{-lm}), & \varphi = 1 + \varepsilon A e^{-lm}, & \text{at } y = 1, \end{cases} \quad (4.11)$$

where prime (') represents the derivative with respect to y . The constants $\gamma, M^2, S_c, G_r, G_C, Pr, K, F, \alpha_T, Ec, \alpha_c$, and K_r are the Casson fluid parameter, Hartman number, Schmidt number, thermal Grashof number, the solutal Grashof number, Prantdl number, coefficient of thermal conductivity, thermal radiation parameter, heat absorption parameter, Eckert number, heat-source/sink parameter and chemical reaction parameter, respectively.

4.2.1 Quantities of Physical Interest

The physical quantities such as Nusselt number, shear stress and Sherwood number at $y = h$ and $y = 1$ are defined by

$$\begin{aligned} \tau_{f0}^* &= -\mu \left. \frac{\partial u^*}{\partial y} \right|_{y=h}, \\ Nu_0^* &= -\mu \left. \frac{\partial T^*}{\partial y} \right|_{y=h}, \\ Sh_0^* &= -D \left. \frac{\partial C^*}{\partial y} \right|_{y=h}, \end{aligned} \quad (4.12)$$

and

$$\begin{aligned} \tau_{f1}^* &= -\mu \left. \frac{\partial u^*}{\partial y} \right|_{y=1}, \\ Nu_1^* &= -\mu \left. \frac{\partial T^*}{\partial y} \right|_{y=1}, \\ Sh_1^* &= -D \left. \frac{\partial C^*}{\partial y} \right|_{y=1}, \end{aligned} \quad (4.13)$$

which in diemnsionless form read as

$$\begin{aligned}
C_{f0} &= \frac{\tau_{f0}^* d}{\mu u_0} = -\left. \frac{\partial u}{\partial y} \right|_{y=h}, \\
Nu_0 &= \frac{Nu_0^* d}{K \Delta T} = -\left. \frac{\partial \theta}{\partial y} \right|_{y=h}, \\
Sh_0 &= \frac{Sh_0^* d}{D \Delta C} = -\left. \frac{\partial \varphi}{\partial y} \right|_{y=h},
\end{aligned} \tag{4.14}$$

$$\begin{aligned}
C_{f1} &= \frac{\tau_{f1}^* d}{\mu u_0} = -\left. \frac{\partial u}{\partial y} \right|_{y=1}, \\
Nu_1 &= \frac{Nu_1^* d}{\mu \Delta T} = -\left. \frac{\partial \theta}{\partial y} \right|_{y=1}, \\
Sh_1 &= \frac{Sh_1^* d}{D \Delta C} = -\left. \frac{\partial \varphi}{\partial y} \right|_{y=1}.
\end{aligned} \tag{4.15}$$

4.3 Solution of the Problem

The equations (4.7)-(4.9) represent the set of coupled PDEs can be reduced to a system of ODEs by expanding series in terms of εA as

$$u(y,t) = u_0(y) + \varepsilon A e^{-\lambda t} u_1(y) + o(\varepsilon A)^2, \tag{4.16}$$

$$\theta(y,t) = \theta_0(y) + \varepsilon A e^{-\lambda t} \theta_1(y) + o(\varepsilon A)^2, \tag{4.17}$$

$$\varphi(y,t) = \varphi_0(y) + \varepsilon A e^{-\lambda t} \varphi_1(y) + o(\varepsilon A)^2. \tag{4.18}$$

Now by substituting (4.16)-(4.18) into (4.7)-(4.9), then comparing harmonic, non-harmonic terms and ignoring higher powers of εA we have

$$u_0'' - \left(M^2 + \frac{1}{K} \right) \left(\frac{\gamma}{\gamma+1} \right) u_0 + \frac{\gamma G_r}{\gamma+1} \theta_0 + \frac{\gamma G_c}{\gamma+1} \varphi_0 = 0, \tag{4.19}$$

$$\theta_0'' + (F - \alpha_r) \theta_0 + \alpha_c \varphi_0 = 0, \tag{4.20}$$

$$\varphi_0'' - S_c K_r \varphi_0 = 0, \tag{4.21}$$

$$u_1'' - \left(M^2 + \frac{1}{K} - n \right) \left(\frac{\gamma}{\gamma+1} \right) u_1 + \frac{\gamma G_r}{\gamma+1} \theta_1 + \frac{\gamma G_c}{\gamma+1} \varphi_1 = 0, \quad (4.22)$$

$$\theta_1'' + (F - \alpha_r + n P_r) \theta_1 + \alpha_c \varphi_1 = 0, \quad (4.23)$$

$$\varphi_1'' + n S_c \varphi_1 - S_c K_r \varphi_1 = 0. \quad (4.24)$$

The corresponding boundary conditions (4.10)-(4.11) take the form

$$u_0 = 0, \quad \theta_0' = B_i \theta_0, \quad \varphi_0 = 0, \quad u_1 = 0, \quad (4.25)$$

$$\theta_1' = B_i (\theta_1 - 1), \quad \varphi_1 = 1 \quad \text{at } y = h, \quad (4.26)$$

$$u_0 = 0, \quad \theta_0' = B_i (\theta_0 - 1), \quad \varphi_0 = 1, \quad u_1 = 0, \quad (4.27)$$

$$\theta_1' = B_i (\theta_1 - 1), \quad \varphi_1 = 1 \quad \text{at } y = 1. \quad (4.28)$$

The exact solutions of equations (4.19)-(4.24) with boundary conditions (4.25)-(4.28) consist of lengthy mathematical expressions and are given below.

$$\begin{aligned} u(y, t) = & e^{-\gamma(2(A_1+A_3)+A_5)} (C_2 e^{\gamma((A_1+2A_3)+A_5)} A_6 A_7 + C_1 e^{\gamma(3A_1+2A_3+A_5)} A_6 A_7 \\ & - (A_3^2 - A_1^2) \left(K(1+\gamma)(A_5^2 - A_1^2) \left(C_6 e^{\gamma(2A_1+A_3+A_5)} G_r K \gamma + C_5 e^{\gamma(2A_1+3A_3+A_5)} G_r K \gamma \right) + A_7 e^{2\gamma(A_1+A_3+A_5)} C_9 + e^{2\gamma(A_1+A_3)} C_{10} \right. \\ & / (A_3^2 - A_1^2) (K(1+\gamma)(A_5^2 - A_1^2) A_7 - \varepsilon e^{-nt} (e^{-\gamma(4(A_1-A_2)+2A_4+A_8)} (-C_4 e^{\gamma(3(A_1-A_2)+2A_4+A_8)} k A_9 A_{10}) \\ & - C_3 e^{\gamma(5(A_1-A_2)+2A_4+A_8)} K A_9 A_{10} - (A_1^2 - A_2^2 - A_4^2) (K(1+\gamma)(A_5^2 - A_1^2) + (1+\beta) A_2^2 \\ & - n\gamma))) \left(C_6 e^{\gamma(4(A_1-A_2)+A_4+A_8)} \right) G_r K \gamma + C_5 e^{\gamma(4(A_1-A_2)+3A_4+A_8)} G_r K \gamma + \\ & e^{2\gamma(2(A_1-A_2)+A_4)} \left(\frac{1}{\gamma} A_{10} (e^{2\gamma A_8} C_{11} + C_{12}) \right) \left. \right) / (A_1^2 - A_2^2 - A_4^2) \\ & \frac{1}{\beta} A_{10} (K(1+\gamma)(A_5^2 - A_1^2) + (1+\gamma) A_2^2 - n\beta) \left. \right), \end{aligned} \quad (4.29)$$

$$\theta(y,t) = \frac{1}{A_1^2 - A_3^2} e^{-y(A_1+A_3)} - \left(C_2 e^{yA_3} \alpha_c - C_1 e^{y(2A_1+A_3)} \alpha_c + e^{A_1 y} (A_1^2 - A_3^2) (e^{2yA_3} C_5 + C_6) \right) \\ - \frac{\varepsilon e^{-nt} \left(e^{-y(A_1-A_2+A_4)} \left(-C_4 e^{yA_4} \alpha_c - C_3 e^{y(2(A_1-A_2)+A_4)} \alpha_c + e^{(A_1-A_2)y} (A_1^2 - A_2^2 - A_4^2) (e^{2yA_4} C_7 + C_8) \right) \right)}{-A_1^2 + A_2^2 + A_4^2}, \quad (4.30)$$

$$\varphi(y,t) = e^{A_1 y} C_1 + e^{-A_2 y} C_2 + \varepsilon e^{-nt} (e^{(A_1-A_2)y} C_3 + e^{-(A_1+A_2)y} C_4), \quad (4.31)$$

where

$$A_1 = \sqrt{Ks}, \quad A_2 = \sqrt{ns}, \quad A_3 = \sqrt{-F + \alpha_T}, \quad A_4 = \sqrt{-F + \alpha_T - nPr},$$

$$A_5 = \sqrt{\frac{\gamma + KM^2\gamma}{K(1+\gamma)}}, \quad A_6 = K(-G_r \alpha_c + G_c(F + k_s - \alpha_T)),$$

$$A_7 = \gamma(\gamma + K(F - \alpha_T + (F + M^2 - \alpha_T)\gamma)),$$

$$A_8 = \sqrt{\frac{\gamma(1 + KM^2 - kn)}{K(1+\gamma)}},$$

$$A_9 = (-G_r \alpha_c + G_c(F + n(Pr - s) + k_s - \alpha_T)),$$

$$A_{10} = \gamma(\gamma + K(F + nPr - \alpha_T + (F + M^2 + n(-1 + Pr) - \alpha_T)\gamma)),$$

$$C_1 = \frac{e^{A_1}}{e^{2A_1} - e^{2hA_1}},$$

$$C_2 = \frac{e^{A_1+2hA_1}}{e^{2A_1} - e^{2hA_1}},$$

$$C_3 = \frac{1}{e^{A_1-A_2} + e^{h(A_1-A_2)}},$$

$$C_4 = \frac{e^{(A_1-A_2)+h(A_1-A_2)}}{e^{A_1-A_2} + e^{h(A_1-A_2)}},$$

$$C_5 = \frac{1}{(e^{2A_3} - e^{2hA_3})(B^2 - A_3^2) \left(-A_3 \left((C_2(e^{hA_1+A_3} - e^{A_1+hA_3}) + C_1(-e^{(2+h)A_1+A_3} + e^{(1+2h)A_1+hA_3}) \right)^2 + A_1^2 \right)} e^{-(1+h)A_1} A_1 \alpha_c$$

$$+ B \left(C_2 \alpha_c (e^{hA_1+A_3} - e^{A_1+hA_3}) + C_1 \alpha_c (e^{(2+h)A_1+A_3} - e^{(1+2h)A_1+hA_3}) + C_1 e^{(1+h)A_1+A_3} (A_1^2 - A_3^2) \right) (B + A_3),$$

$$C_6 = (e^{-(1+h)A_1+A_3} \left(-C_2 e^{hA_1+2hA_3} - e^{A_1+(1+h)A_3} \right) + C_1 \left(-e^{(2+h)A_1+2hA_3} + e^{(1+2h)A_1+(1+h)A_3} \right) A_1 \alpha_c$$

$$- B \left(C_2 (e^{hA_1+2hA_3} - e^{A_1+(1+h)A_3}) + C_1 \alpha_c (e^{(2+h)A_1+2hA_3} - e^{(1+2h)A_1+(1+h)A_3}) + e^{(1+h)A_1+2hA_3} (A_1^2 - A_3^2) \right)$$

$$/ ((e^{2A_3} - e^{2hA_3})(A_1^2 - A_3^2)(B + A_3)),$$

$$C_7 = e^{-(1+h)(A_1-A_2)} \left(-C_4 \left(e^{h(A_1-A_2+A_4)} - e^{(A_1-A_2+hA_4)} \right) + C_3 \left(-e^{(2+h)(A_1-A_2+A_4)} - e^{(1+2h)(A_1-A_2+hA_4)} \right) \right)$$

$$\left((A_1 - A_2) \alpha_c - B (A_1^2 - A_2^2 - A_4^2) (C_4 e^{h(A_1-A_2+A_4)} \alpha_c (1 - C_3 e^2) + \alpha_c (C_4 e^{(A_1-A_2+hA_4)} \right.$$

$$\left. + C_3 e^{(1+2h)(A_1-A_2+hA_4)}) + -e^{(1+h)(A_1-A_2+A_4)} + e^{(1+h)(A_1-A_2+hA_4)} \right) / (e^{2A_4} - e^{2hA_4}) (A_1^2 - A_2^2 - A_4^2) (-B + A_4),$$

$$C_8 = e^{-(1+h)(A_1-A_2+A_4)} \left(-C_4 \left(e^{h(A_1-A_2+2hA_4)} - e^{(A_1-A_2+(1+h)A_4)} \right) + C_3 \left(-e^{(2+h)(A_1-A_2+2hA_4)} + e^{(1+2h)(A_1-A_2+(1+h)A_4)} \right) \right)$$

$$\left((A_1 - A_2) \alpha_c + B \left(e^{h(A_1-A_2+2hA_4)} \alpha_c (-C_4 - C_3 e^2) + \alpha_c (C_4 e^{(A_1-A_2+(1+h)A_4)} + C_3 e^{(1+2h)(A_1-A_2+(1+h)A_4)}) - e^{(1+h)(A_1-A_2+A_4)} \right) c \right)$$

$$\left(-e^{(1+h)(A_1-A_2+2hA_4)} (A_1^2 - A_2^2 - A_4^2) \right) / ((e^{2A_4} - e^{2hA_4}) (A_1^2 - A_2^2 - A_4^2) (B + A_4))$$

$$C_9 = \frac{1}{K(1+\gamma)(A_5^2 - A_1^2)} e^{hA_5} (-K(1+\gamma)(A_5^2 - A_1^2)) \left(\frac{A_6 \gamma (c_2 e^{-A_1} + c_1 e^{A_1})}{(A_1^2 - A_3^2) K(1+\beta)(A_5^2 - A_1^2)} + \frac{G_r K \gamma^2 (C_5 e^{A_3} - C_6 e^{-A_3})}{A_7} \right.$$

$$\left. + \frac{A_6 \gamma (c_1 e^{hA_1} + (C_2 e^{-hA_1-A_5}))}{(A_1^2 - A_3^2)} + \left(\frac{G_r K \gamma^2 (c_6 e^{-hA_3} + c_5 e^{hA_3})}{(A_1^2 - A_3^2)} \right) / (e^{-(1-h)A_5} - e^{-(1+h)A_5}),$$

$$C_{10} = \frac{1}{-K(1+\gamma)(A_5^2 - A_1^2)} e^{A_5} \left(K(1+\gamma)(A_5^2 - A_1^2) \left(\frac{A_6\gamma(c_1 e^{A_1} + c_2 e^{-A_1})}{(A_1^2 - A_3^2)k(1+\beta)(A_5^2 - A_1^2)} + \frac{G_r k \gamma^2 (C_5 e^{A_5} + C_6 e^{-A_5})}{A_7} \right) - (C_2 e^{((2-h)A_5 - A_1)}) A_6 \gamma \right) / (A_1^2 - A_3^2)$$

$$+ \frac{c_1 e^{A_1} A_6 \gamma}{(A_1^2 - A_3^2) K(1+\gamma)(A_5^2 - A_1^2)} + \left(\frac{e^{-A_1} G_r K \gamma^2 (c_6 + c_5)}{(A_1^2 - A_3^2)} \right) + e^{-A_5} \left(\frac{A_6 \gamma (c_2 e^{-hA_1} + c_1 e^{hA_1})}{(A_1^2 - A_3^2) K(1+\gamma)(A_5^2 - A_1^2)} \right) + \left(\frac{G_r K \gamma^2 (C_6 e^{-hA_5} + C_5 e^{hA_5})}{A_7} \right) / 2e^{-A_5(1+h)},$$

$$C_{11} = -\left(e^{-hA_8} \left(\frac{G_r K \gamma^2 (C_6 e^{-A_4} + C_5 e^{A_4})}{A_{10}} + \frac{K \gamma A_9 (C_4 e^{-(A_1 - A_2)} + C_3 e^{(A_1 - A_2)})}{(A_1^2 - A_2^2 - A_4^2) (K(1+\gamma)(A_5^2 - A_1^2) + A_2^2(1+\gamma) - n\gamma)} \right) - e^{-A_8} \left(\frac{G_r K \gamma^2 (C_6 e^{-hA_4} + C_5 e^{hA_4})}{A_7} + \frac{K A_9 \gamma (C_4 e^{-h(A_1 - A_2)} + C_3 e^{h(A_1 - A_2)})}{(A_1^2 - A_2^2 - A_4^2) (K(1+\gamma)(A_5^2 - A_1^2) + A_2^2(1+\gamma) - n\gamma)} \right) \right) / (e^{A_8(1-h)} - e^{-A_8(1-h)}),$$

$$C_{12} = -e^{-hA_8} \left(\frac{G_r K \gamma^2 (C_6 e^{-hA_4} + C_5 e^{hA_4})}{A_{10}} \right) + \frac{K \gamma A_9 (C_4 e^{-h(A_1 - A_2)} + C_3 e^{h(A_1 - A_2)})}{(A_1^2 - A_2^2 - A_4^2) (K(1+\gamma)(A_5^2 - A_1^2) + A_2^2(1+\gamma) - n\gamma)} + \left(e^{2hA_8} (e^{-hA_8} \left(\frac{G_r K \gamma^2 (C_6 e^{-A_4} + C_5 e^{A_4})}{A_{10}} + \frac{K \gamma A_9 (C_4 e^{-(A_1 - A_2)} + C_3 e^{(A_1 - A_2)})}{(A_1^2 - A_2^2 - A_4^2) (K(1+\gamma)(A_5^2 - A_1^2) + A_2^2(1+\gamma) - n\gamma)} \right) - e^{-A_8} \left(\frac{G_r K \gamma^2 (C_6 e^{-hA_4} + C_5 e^{hA_4})}{A_{10}} + \frac{K \gamma A_9 (C_4 e^{-h(A_1 - A_2)} + C_3 e^{h(A_1 - A_2)})}{(A_1^2 - A_2^2 - A_4^2) (K(1+\gamma)(A_5^2 - A_1^2) + A_2^2(1+\gamma) - n\gamma)} \right) \right) / (e^{A_8(1-h)} - e^{-A_8(1-h)}),$$

4.4 Results and Discussion

This section demonstrates graphical results for the shear stress, the Nusselt number and the Sherwood number and physical behavior of various involved parameters on momentum, temperature and mass concentration. The values of the parameters $K_r = 2$,

$\alpha_c = 2, \alpha_r = 2, G_r = 2, G_c = 1, Pr = 0.71, B_i = 0.5, F = 1, S_c = 0.96, t = 2, \varepsilon = 2, h(x) = 1 + \varepsilon A \cos kx$ are kept fixed except the varying one. Figure 4.2 reveals that the velocity u decelerates with the imposition of the Biot number for both Newtonian and Casson fluids in cooling case as we are taking $G_r > 0$.

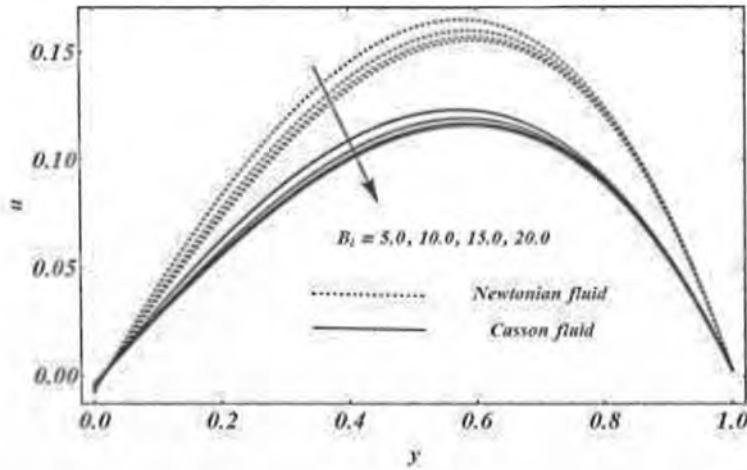


Figure 4.2: Velocity distribution for various inputs of Biot number B_i

The effects of variation in radiation absorption parameter α_c on velocity profile are illustrated in figure 4.3. By enhancing the value of the radiation absorption parameter α_c , the velocity field rises. Figure 4.4 depicts that the thermal radiation parameter and velocity are inversely related.

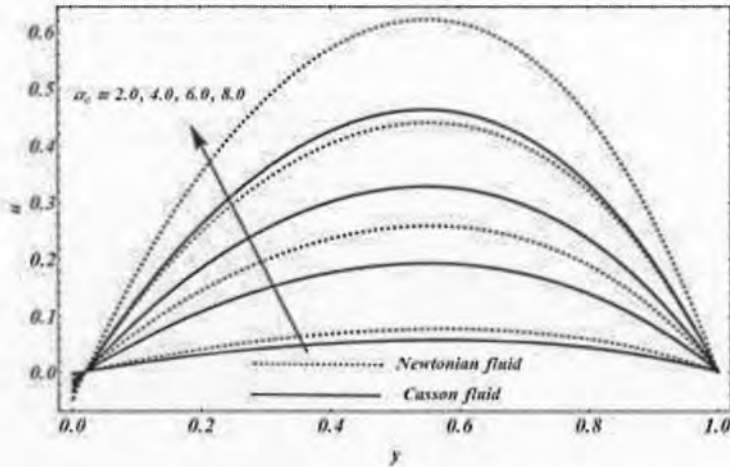


Figure 4.3: Velocity distribution for various inputs of radiation absorption parameter α_c

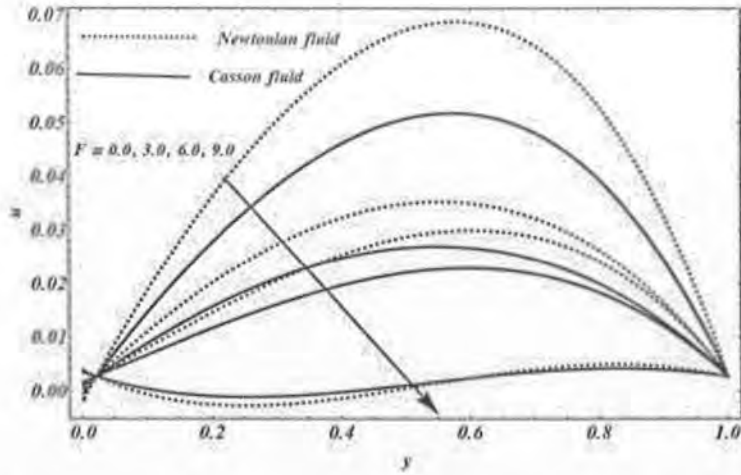


Figure 4.4: Velocity distribution for various inputs of thermal radiation parameter F

Figure 4.5 shows the influence of solutal Grashof number on velocity field. An increase in the solutal Grashof number dominates species buoyancy on viscous hydrodynamic force and as a result velocity enhances significantly both for Casson and Newtonian fluids. The positive value of the Grashof number which physically represents the cooling of the plates. Actually, buoyant force suppresses viscous force and presence of this buoyancy force complicates the flow problem, due to coupling with thermal and mass problems. Therefore, flow accelerates on the imposition of thermal Grashof number G_r due to enhancement of buoyancy force as shown in figure 4.6. Overall, we noticed that the velocity of Newtonian fluid is higher than the velocity of Casson fluid due to the reason that Casson fluid has a large viscosity as compared to the Newtonian fluid.

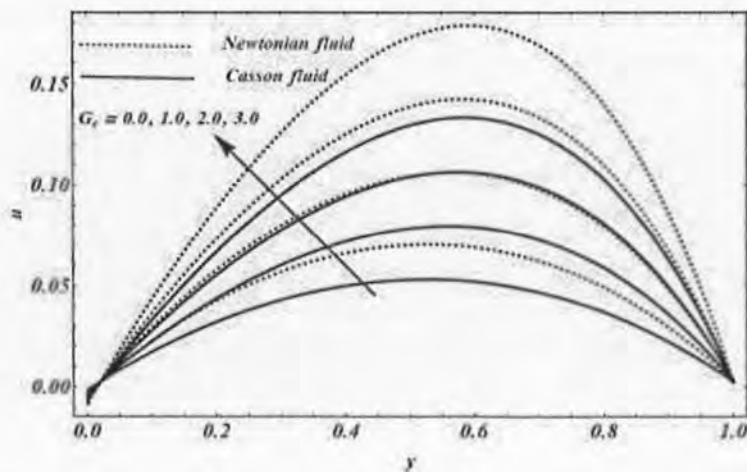


Figure 4.5: Velocity distribution for various inputs solutal Grashof number G_c

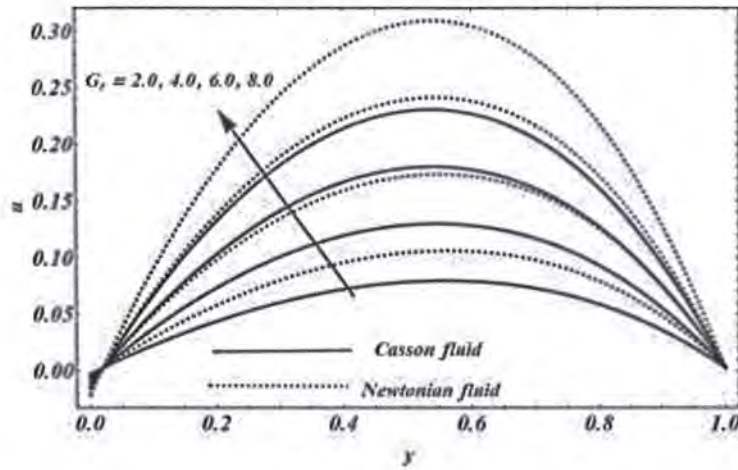


Figure 4.6: Velocity distribution for various inputs of thermal Grashof number G_r ,

Figure 4.7 depicts that the mass concentration and chemical reaction parameter are inversely related. This was expected because the chemical reaction reduces the salute boundary layer thickness which ultimately decreases the mass transfer. Figure 4.8 shows the graph of mass concentration for different inputs of the Schmidt number. Mass concentration decreases with the increase of Schmidt number because Schmidt number and molecular diffusivity are inversely related.

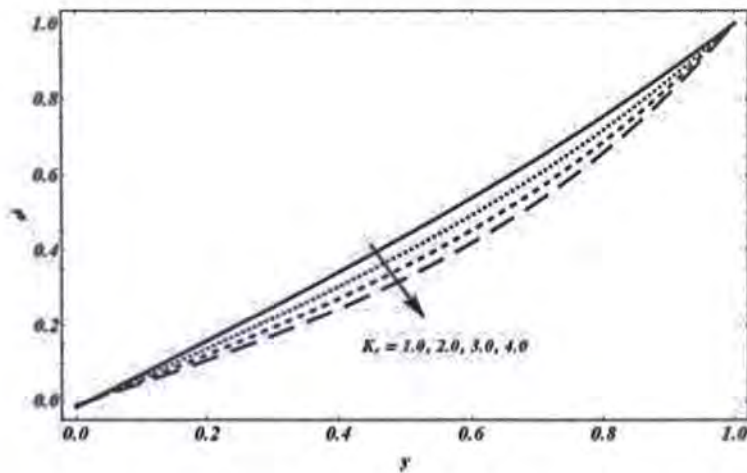


Figure 4.7: Mass concentration distribution for various inputs of chemical reaction parameter K_r ,



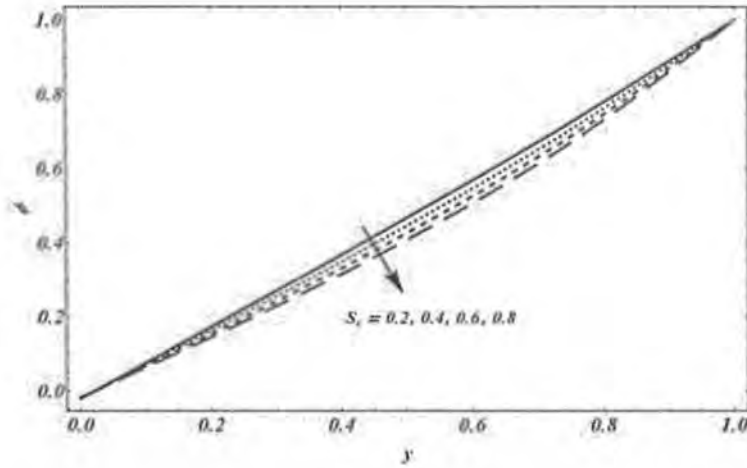


Figure 4.8: Mass concentration distribution for various inputs of Schmidt number S_c

Figure 4.9 shows the plots for temperature profile versus y for different inputs of B_i . It is noted that with the increase of Biot number fluid temperature falls. Rise in the value of Biot number results an enhancement in convective heat transfer of the fluid. Moreover, when the Biot number approaches to infinity the convective boundary conditions will become the prescribed wall temperature case [94].

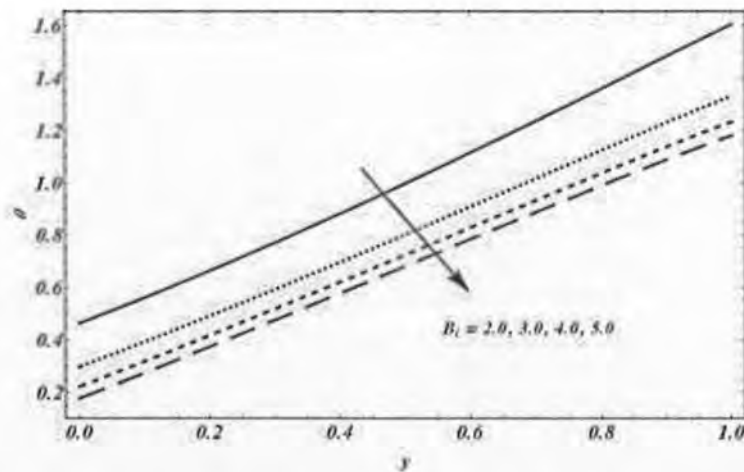


Figure 4.9: Temperature distribution for various inputs of Biot number B_i

Tables 4.1-4.3 illustrate the variation of Nusselt number, the shear stress and the Sherwood number at the wavy wall $y=h$ and at the flat wall $y=1$ respectively for various inputs of parameters. The numerical values of shear stress augment by enhancing the numerical value of casson fluid parameter β , the Biot number B_i , the Grashof number G_r , heat absorption

parameter α_T and drops by enhancing the numerical value of K_r , the Schmidt number S_c , the solutal Grashof number G_c , the thermal Grashof number G_T and the thermal radiation F at the wavy wall $y=h$. Moreover, the shear stress increases by increasing the numerical value of K_r, S_c, G_c, G_T and F and decrease by increasing the numerical value M, B_i and α_T at the flat wall $y=1$. Table 4.1 depicts this phenomena clearly.

Table 4.2 explains that the numerical values of the Nusselt number Nu enhance due to increase in the value of chemical reaction parameter K_r , Schmidt number S_c and Biot number B_i but decreases due to rise in thermal radiation parameter F and heat absorption parameter α_T at the wavy wall $y=h$, while Nusselt number enhances due to increase in the values of K_r, S_c, B_i but there is a drop in the values of F and α_T at the flat wall $y=1$.

Table 4.3 represents the numerical values of the Sherwood number Sh for different inputs of the chemical reaction parameter K_r and Schmidt number S_c . Sherwood number Sh is a measure of mass transfer rate from the channel wall to the fluid. It is noticed that chemical reaction parameter K_r and Schmidt number S_c enhances mass transfer rate at the wavy wall $y=h$ whereas has declining effect on mass transfer rate at $y=1$.

Table 4.1: Variation of shear stress at $y = h$ and $y = 1$ while taking values of parameters

$$S_c = 0.96, t = 2, G_c = 2, G_r = 2, Pr = 0.71, K_r = 2, \alpha_T = 2, \alpha_c = 2, M = 2, B_i = 0.2.$$

		C_{f0}	C_{f1}			C_{f0}	C_{f1}
γ	2.0	0.03699	0.01833	S_c	0.96	0.03699	0.01833
	3.0	0.04127	0.02063		1.1	0.03276	0.02342
	4.0	0.04380	0.02200		1.6	0.01895	0.03985
B_i	0.1	-0.52833	0.77119	G_c	1.0	0.01895	0.03985
	0.5	-0.33294	0.55765		2.0	-0.03943	0.19738
	0.8	0.0547	0.02385		3.0	-0.09783	0.35491
K_r	2.0	0.03699	0.01833	G_r	2.0	0.01895	0.03985
	2.0	0.02317	0.03496		3.0	0.05763	0.6696
	3.0	0.01094	0.0494		4.0	0.09631	0.78155
M	2.0	0.03699	0.01833	F	1.0	-0.33461	0.56753
	3.0	0.03455	0.01819		1.5	-0.39184	0.62778
	4.0	0.03196	0.01768		3.0	-0.46017	0.69941
α_T	1.0	0.01895	0.10407				
	1.5	0.07918	0.08691				
	3.0	0.21713	0.03985				

Table 4.2: Variation of Nusselt number at $y = h$ and $y = 1$ while taking the values of parameters are $S_c = 0.96, t = 2, G_C = 2, G_r = 2, Pr = 0.71, K_r = 2, \alpha_T = 2, M = 2, Bi = 0.2, \alpha_c = 2$.

		Nu_0	Nu_1			Nu_0	Nu_1
B_i	0.1	-0.06969	0.01358	F	1.0	-0.3442	0.05323
	0.5	-0.16295	0.29647		1.5	-0.04479	0.04147
	0.8	0.1993	1.5053		3.0	-0.0572	0.02753
K_R	2.0	-0.16295	-0.29647	α_T	1.0	0.080405	0.70356
	3.0	-0.13705	0.33888		1.5	-0.64166	0.52166
	4.0	0.11460	0.37577		3.0	-0.16295	0.296
S_c	0.96	-0.16295	0.29647				
	1.1	-0.15500	0.30949				
	1.6	-0.12922	0.35173				

Table 4.3: Variation of Sherwood number at $y = h$ and $y = 1$ while taking values of the parameters are $M = 2, B_i = 0.2, G_C = 2, G_r = 2, Pr = 0.71, K_r = 2, \alpha_T = 2, S_c = 0.96, t = 2, \alpha_c = 2$.

		Sh_0	Sh_1			Sh_0	Sh_1
K_r	2.0	-0.76324	-1.5819	S_c	0.96	-0.76324	-1.5819
	3.0	-0.76322	-1.8235		1.1	-0.73343	-1.6546
	4.0	-0.58695	-2.0456		1.6	-0.63898	-1.8995

4.5 Concluding Remarks

The problem of unsteady, incompressible Casson fluid flow in an irregular channel is discussed by taking convective boundary conditions. The perturbation method is used to solve the equations. In the light of present investigation, the following conclusions can be drawn.

- The Newtonian fluid velocity is higher than Casson fluid velocity for all parameters.
- The velocity profile increases with increase in radiation absorption parameter α_c .
- Mass concentration decreases due to increase in Schmidt number S_c .
- An increase in Biot number B_i results in drop in velocity and temperature profiles.
- Higher values of chemical reaction parameter K_r decrease concentration profile.
- The velocity augments due to rise in the value of thermal radiation parameter G_r and solutal Grashof number G_c .
- Decreasing behavior in velocity is noticed by enhancing the value of thermal radiation F .

Chapter 5

Unsteady Flow and Heat Transfer in an Inclined Composite Channel with an Oscillating Wall

5.1 Introduction

In this chapter, a complete thermodynamical analysis has been made for an unsteady, fully developed and laminar flow in an inclined composite channel with upper oscillating wall. The considered problem is modelled by using Darcy Brinkman model. Analytical and numerical schemes are used to solve the governing equations. An asymptotic series solution is calculated by regular perturbation method. For numerical scheme the Backward time central spacing approximation is used to discretize the PDEs. The momentum and temperature fields, entropy generation rate and the Bejan number are discussed qualitatively and quantitatively with respect to pertinent physical parameters.

5.2 Mathematical Formulation

Consider an unsteady, fully developed and laminar flow of an incompressible viscous fluid between two inclined parallel plates separated by a distance $2h$ and inclined at an angle α . The region-1 ($-h < y < 0$) and the region-2 ($0 < y < h$) are occupied with porous space and clear viscous fluid respectively. The diagram of the considered problem can be seen in figure 5.1. The mathematical model of the problem is developed by using Darcy-Brinkman model. The upper and lower walls of the parallel plate channel are maintained at temperatures T_{w_1} and T_{w_2} respectively. The viscous and Darcy dissipation effects are also taken into consideration. It is also supposed that except pressure all physical variables depend on y and t .

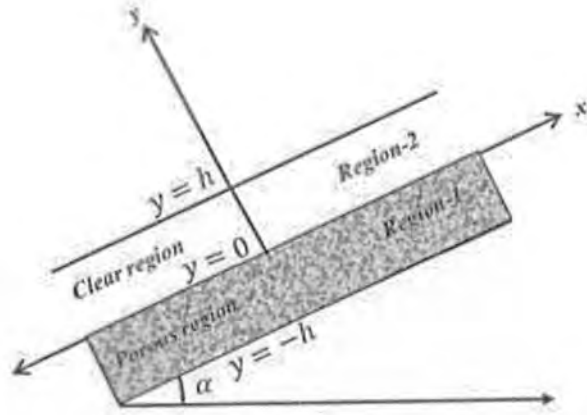


Figure 5.1: Geometry of the considered problem

Further assume that the fluid flows due to a constant pressure gradient $(\partial p / \partial x)$ in both regions of the channel. Initially, the plates are static. At $t > 0$ the upper plate suddenly starts to vibrate with velocity $U = u_0(1 + \varepsilon A e^{i\omega t})$. The no-slip boundary conditions for velocity are taken into account and the walls temperature are assumed to be isothermal. Moreover, the velocity, temperature, shear stress and heat flux at the interface are continuous. Under these considerations, the equations of motion and temperature are given by

Region-1 (Porous region)

$$\frac{\partial v_1}{\partial y} = 0, \quad (5.1)$$

$$\rho \left(\frac{\partial u_1}{\partial t} + v_1 \frac{\partial u_1}{\partial y} \right) = -\frac{\partial p}{\partial x} + \mu_{eff} \left(\frac{\partial^2 u_1}{\partial y^2} \right) - \frac{\mu_{eff}}{s} u_1 + g \beta (T_1 - T_{w_2}) \sin \alpha, \quad (5.2)$$

$$\rho C_p \left(\frac{\partial T_1}{\partial t} + v_1 \frac{\partial T_1}{\partial y} \right) = K_{eff} \frac{\partial^2 T_1}{\partial y^2} + \mu_{eff} \left(\frac{\partial u_1}{\partial y} \right)^2 + \frac{\mu_{eff}}{s} u_1^2. \quad (5.3)$$

Region-2 (Clear region)

$$\frac{\partial v_2}{\partial y} = 0, \quad (5.4)$$

$$\rho \left(\frac{\partial u_2}{\partial t} + v_2 \frac{\partial u_2}{\partial y} \right) = -\frac{\partial p}{\partial x} + \mu \left(\frac{\partial^2 u_2}{\partial y^2} \right) + g \beta (T_2 - T_{w_2}) \sin \alpha, \quad (5.5)$$

$$\rho C_p \left(\frac{\partial T_2}{\partial t} + v_2 \frac{\partial T_2}{\partial y} \right) = K \frac{\partial^2 T_2}{\partial y^2} + \mu \left(\frac{\partial u_2}{\partial y} \right)^2, \quad (5.6)$$

where u_1 and u_2 are the x-components of velocities, v_1 and v_2 are the y-components of velocity. T_1 and T_2 are the temperatures of the fluid for porous and clear regions, respectively.

The interface and boundary conditions become

$$u_1(-h) = 0, \quad T_1(-h) = T_{w_1}, \quad u_2(h) = U = u_0(1 + \epsilon A e^{I\omega t}), \quad T_2(h) = T_{w_2}, \quad (5.7)$$

$$\begin{cases} u_1(0) = u_2(0), \\ \mu_{eff} \frac{\partial u_1}{\partial y} \Big|_{y=0} = \mu \frac{\partial u_2}{\partial y} \Big|_{y=0}, \\ T_1(0) = T_2(0), \\ K_{eff} \frac{\partial T_1}{\partial y} \Big|_{y=0} = K \frac{\partial T_2}{\partial y} \Big|_{y=0}. \end{cases} \quad (5.8)$$

The continuity equations for both porous and viscous regions can be reduced to

$$v_1 = v_2 = v = u_0 \left(1 + \epsilon A e^{I\omega t} \right), \quad (5.9)$$

where v_1 and v_2 are functions of time only.

The equations (5.1)-(5.6) along with boundary conditions (5.7)-(5.8) are made dimensionless by introducing following set of non-dimensional variables

$$y^* = \frac{y u_0}{\nu}, \quad u_i^* = \frac{u_i}{u_0}, \quad v_i^* = \frac{v_i}{u_0}, \quad t^* = \frac{t u_0^2}{\nu}, \quad \theta_i = \frac{T - T_{w_2}}{T_{w_1} - T_{w_2}}. \quad (5.10)$$

Using equation (5.10) and dropping asterisk (*) for simplicity, the continuity equations (5.1) and (5.4) are identically satisfied and equations (5.2)-(5.6) in dimensionless form become

Region-1 (Porous region)

$$\frac{\partial u_1}{\partial t} + v_1 \frac{\partial u_1}{\partial y} = P + m \frac{\partial^2 u_1}{\partial y^2} - \sigma^2 u_1 + \lambda \sin \alpha \theta_1, \quad (5.11)$$

$$\frac{\partial \theta_1}{\partial t} + v_1 \frac{\partial \theta_1}{\partial y} = \frac{k}{Pr} \frac{\partial^2 \theta_1}{\partial y^2} + m Ec \left(\frac{\partial u_1}{\partial y} \right)^2 + Ec \sigma^2 u_1^2. \quad (5.12)$$

Region-2 (Clear region)

$$\frac{\partial u_2}{\partial t} + v_2 \frac{\partial u_2}{\partial y} = -P + \frac{\partial^2 u_2}{\partial y^2} + \lambda \sin \alpha \theta_2, \quad (5.13)$$

$$\frac{\partial \theta_2}{\partial t} + v_2 \frac{\partial \theta_2}{\partial y} = \frac{k}{Pr} \frac{\partial^2 \theta_2}{\partial y^2} + Ec \left(\frac{\partial u_2}{\partial y} \right)^2, \quad (5.14)$$

where $\lambda = \frac{Gr}{Re^3}$ and $Gr = \frac{g \beta \Delta T h^3}{\nu^2}$ are the mixed convection parameter and Grashof number respectively.

The interfacial and boundary conditions take the form

$$\begin{cases} u_1(-1) = 0, u_2(1) = 1 + \varepsilon A e^{I\omega t}, \theta_1(-1) = 1, \theta_2(1) = 0, u_1(0) = u_2(0), \\ m \frac{\partial u_1}{\partial y} \Big|_{y=0} = \frac{\partial u_2}{\partial y} \Big|_{y=0}, k \frac{\partial \theta_1}{\partial y} \Big|_{y=0} = \frac{\partial \theta_2}{\partial y} \Big|_{y=0}, \theta_1(0) = \theta_2(0). \end{cases} \quad (5.15)$$

5.3 Solution of the Problem

5.3.1 Analytical Method

Adopting the same procedure as used in previous chapters velocity and temperature fields are expanded by the following series

$$u_i(y, t) = u_{i0}(y) + \varepsilon A e^{I\omega t} u_{i1}(y) + O(\varepsilon A)^2, \quad \text{for } i = 1, 2, \quad (5.16)$$

$$\theta_i(y,t) = \theta_{i0}(y) + \varepsilon A e^{I\omega t} \theta_{i1}(y) + O(\varepsilon A)^2, \quad \text{for } i=1,2. \quad (5.17)$$

By substituting equations (5.16)-(5.17) into equations (5.11)-(5.14), equating the periodic and non-periodic terms and ignoring the higher order terms, one can obtain the following pair of equations for (u_{i0}, θ_{i0}) and (u_{i1}, θ_{i1}) .

Non-Periodic Coefficient $O(\varepsilon^0)$

$$A_i \frac{\partial^2 u_{i0}}{\partial y^2} - \frac{\partial u_{i0}}{\partial y} - \chi \sigma^2 u_{i0} + \lambda \sin \alpha \theta_{i0} = P, \quad (5.18)$$

$$B_i \frac{\partial^2 \theta_{i0}}{\partial y^2} - \frac{\partial \theta_{i0}}{\partial y} + \text{Ec} A_i \left(\frac{\partial u_{i0}}{\partial y} \right)^2 + \chi \text{Ec} \sigma^2 u_{i0}^2 = 0. \quad (5.19)$$

Periodic Coefficient $O(\varepsilon^1)$

$$A_i \frac{\partial^2 u_{i1}}{\partial y^2} - \chi \sigma^2 u_{i1} - I \omega u_{i1} + \lambda \sin \alpha \theta_{i1} = 0, \quad (5.20)$$

$$B_i \frac{\partial^2 \theta_{i1}}{\partial y^2} - \frac{\partial \theta_{i0}}{\partial y} - \frac{\partial \theta_{i1}}{\partial y} - I \omega \theta_{i1} + 2 \text{Ec} A_i \left(\frac{\partial u_{i0}}{\partial y} \right) \left(\frac{\partial u_{i1}}{\partial y} \right) + 2 \chi \text{Ec} \sigma^2 u_{i0} u_{i1} = 0, \quad (5.21)$$

where

$$A_i = \begin{cases} m, & \text{for } i = 1, \\ 1, & \text{for } i = 2, \end{cases}$$

$$B_i = \begin{cases} k / Pr, & \text{for } i = 1, \\ 1 / Pr, & \text{for } i = 2, \end{cases}$$

where $i = 1, 2$ gives the momentum and heat transfer equations for porous and clear regions, respectively. Using equations (5.16)-(5.17), the boundary and interface conditions (5.15) take the form

$$\begin{cases} u_{1i}(-1) = 0, & u_{20}(1) = 1, & u_{21}(1) = 1, \\ u_{1i}(0) = u_{2i}(0), & m \frac{\partial u_{1i}}{\partial y} \Big|_{y=0} = \frac{\partial u_{2i}}{\partial y} \Big|_{y=0}, \end{cases} \quad (5.22)$$

$$\begin{cases} \theta_{1i}(-1) = 1 - \delta_{1i}, & \theta_{2i}(1) = 0, \\ \theta_{1i}(0) = \theta_{2i}(0), & k \frac{\partial \theta_{1i}}{\partial y} \Big|_{y=0} = \frac{\partial \theta_{2i}}{\partial y} \Big|_{y=0}, \end{cases} \quad (5.23)$$

where $i = 0, 1$ gives the boundary and interfacial conditions for $O(\varepsilon A)$ and $O(\varepsilon A)^1$ respectively.

5.3.2 Numerical Method

The nonlinear partial differential equations (5.11)-(5.14) along with conditions (5.15) are resolved numerically using finite difference method to compare the obtained result with the help of regular perturbation method. The Backward Time Central Spacing (BTCS) is used to discretize these PDEs. The discretized form of momentum and heat transfer equations are given by

$$\frac{u_i(l,n) - u_i(l,n-1)}{k_{1i}} + v_i \frac{u_i(l,n) - u_i(l-1,n)}{h_{1i}} - p - A_i \frac{u_i(l+1,n) - 2u_i(l,n) + u_i(l-1,n)}{h_{1i}^2} - \lambda \sin \alpha \theta_i(l,n) + \chi \sigma^2 u_i(l,n) = 0, \quad (5.24)$$

$$\frac{\theta_i(l,n) - \theta_i(l,n-1)}{k_{2i}} + v_i \frac{\theta_i(l,n) - \theta_i(l-1,n)}{h_{2i}} - B_i \frac{\theta_i(l+1,n) - 2\theta_i(l,n) + \theta_i(l-1,n)}{h_{2i}^2} - Ec A_i \left(\frac{u_i(l,n) - u_i(l-1,n)}{h_{1i}} \right)^2 - \chi Ec \sigma^2 (u_i(l,n))^2 = 0, \quad (5.25)$$

where $i = 1, 2$ gives equations for region-1 and region-2, respectively. The boundary and interface conditions (5.15) take the form

$$\left\{ \begin{array}{l} u_1(-1,n) = 0, \quad u_2(1,n) = 1 + \varepsilon A e^{l\omega n}, \\ \theta_1(-1,n) = 0, \quad \theta_1(1,n) = 0, \\ u_1(0,n) = u_2(0,n), \\ \theta_1(0,n) = \theta_2(0,n), \\ u_2(l-1,n) - m u_2(l-1,n) + (m-1)u_2(l,n) = 0, \\ \theta_2(l-1,n) - k \theta_2(l-1,n) + (k-1)\theta_2(l,n) = 0. \end{array} \right. \quad (5.26)$$

The symbolic software Mathematica is used to do the computation by taking $h_{11} = h_{21} = 0.1$,

$$\omega t = \frac{\pi}{3}, \quad \varepsilon A = 0.2, \quad Pr = .2, \quad Ec = 2, \quad \omega = 5, \quad m = .5, \quad k = 2, \quad Gr = 1, \quad \alpha = \pi / 6,$$

$k_{11} = k_{21} = 5$. The system of algebraic equations that are formed are then solved by using Gauss Seidel method.

5.4 Entropy Generation Analysis

The entropy generation for porous and clear regions in a composite channel is given as

Region-1 (Porous region)

$$(S_G)_1 = \frac{K_{eff}}{T_w^2} \left(\frac{\partial T_1}{\partial y} \right)^2 + \frac{\mu_{eff}}{T_w^2} \left(\frac{\partial u_1}{\partial y} \right)^2 + \frac{\mu}{s} u_1^2. \quad (5.27)$$

Region-2 (Clear region)

$$(S_G)_2 = \frac{K}{T_w^2} \left(\frac{\partial T_2}{\partial y} \right)^2 + \frac{\mu}{T_w} \left(\frac{\partial u_2}{\partial y} \right)^2. \quad (5.28)$$

According to Bejan [95], in order to non-dimensionalize equations (5.27)-(5.28), the volumetric rate of entropy generation S_G is divided by characteristic entropy generation rate S_{G0} . Thus, in non-dimensional form, the entropy generation number can be rewritten as

Region-1 (Porous region)

$$(Ns)_1 = \frac{(S_G)_1}{(S_{G0})_1} = \left(\frac{\partial \theta_1}{\partial y} \right)^2 + \frac{(Br)}{\Omega} \left(\frac{\partial u_1}{\partial y} \right)^2 + \frac{(Br)}{\Omega} \sigma^2. \quad (5.29)$$

Region-2 (Clear region)

$$(Ns)_2 = \frac{(S_G)_2}{(S_{G0})_2} = \left(\frac{\partial \theta_2}{\partial y} \right)^2 + \frac{(Br)}{\Omega} \left(\frac{\partial u_2}{\partial y} \right)^2, \quad (5.30)$$

$$Ns = (Ns)_1 + (Ns)_2, \quad (5.31)$$

where $\Omega = \frac{(\Delta T)^2}{(T_w)^2}$, $Br = EcPr$, $(S_{G0})_1 = \frac{k \Delta T u_0^4}{T_w^2 \nu^2}$ and $(S_{G0})_2 = \frac{k_{eff} \Delta T u_0^4}{T_w^2 \nu^2}$ are the dimensionless temperature difference, Brinkman number, the characteristic entropy generation rates for the porous region and clear region, respectively.

The Bejan number Be is a physical parameter which determines whether heat transfer entropy effects are dominant over fluid friction or vice versa. Its value changes from 0 to 1. The value $Be = 0$ means that the viscous dissipation entropy effects dominate over heat transfer entropy effects, whereas $Be = 1$ shows that the heat transfer entropy effects dominant over viscous dissipation entropy effects. When heat transfer entropy effects equal to viscous dissipation entropy effects the value of Be is equal to 0.5.

5.5 Results and Discussion

This section is about the effects of pertinent parameters on the momentum, temperature and entropy generation effects. Analytical and numerical solutions of the considered problem are found for the momentum and temperature. These expressions are used to find the Bejan number and the entropy generation number. During the study, the numerical values of the different pertinent parameters except the varying one are kept constant at $\sigma = .2$,

$$\omega t = \frac{\pi}{3}, \varepsilon A = 0.2, Pr = .2, Ec = 2, \omega = 5, m = .5, k = 2, Gr = 1, \alpha = \pi / 6.$$

Figure 5.2 describes the effects of porosity parameter on velocity profile when the values of other parameters are fixed as mentioned above. It can be viewed that by rising the value of porosity parameter enhances the frictional drag resistance against the flow motion, which ultimately results in fall in velocity profile in the porous region. While, the velocity component also decreases in clear region due to the dragging effect across the interface. It is worth mentioning that the flow may be laminar for the large value of porosity parameter. Figure 5.3 presents the velocity plots for different values of angle of inclination α . Velocity and angle of inclination are directly related due to increase in buoyancy force. Physically, rise in the values of mixed convection parameter results an increase of buoyancy which enhances fluid motion and, in addition, an increase in an angle of inclination also augments the influence of driving buoyancy by a term $\text{Sin}(\alpha)$. Hence velocity climbs up due to rise in the values of mixed convection parameter as plotted in figure 5.4.

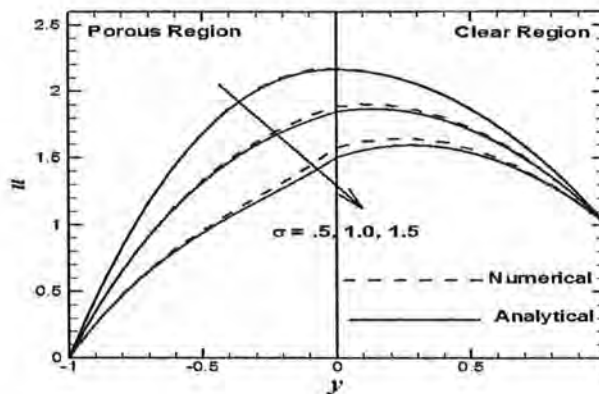


Figure 5.2: Influence of porosity parameter σ on the velocity profile

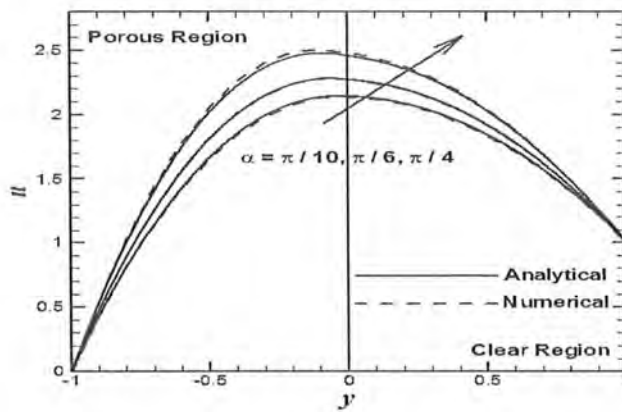


Figure 5.3: Influence of inclination angle α on the velocity profile

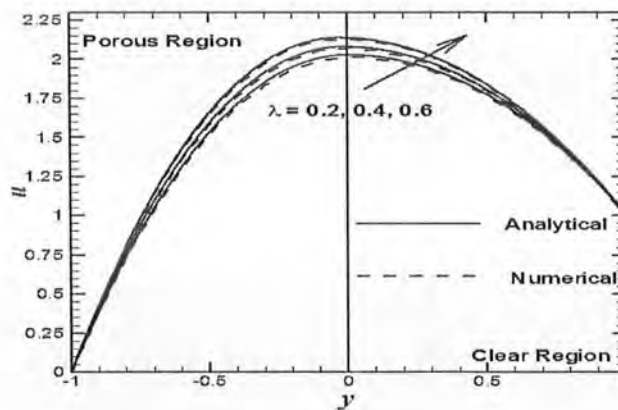


Figure 5.4: Influence of mixed convection parameter λ on the velocity profile

Temperature fields for various inputs of porosity parameter σ , angle of inclination α , mixed convection parameter λ and Eckert number Ec are presented in figures 5.5-5.8. Figure 5.5 depicts that an rise in the value of porosity parameter results in drop in temperature. An expected behavior is observed because porous matrix creates an obstacle to flow and therefore temperature reduces. Moreover, it is quite clear that the temperature in clear region is less than that if in porous region. With an increase in angle of inclination α as shown in figure 5.6, the fluid falls with more velocity which increases the friction within the fluid which ultimately rises the temperature. Figure 5.7 shows that as the value of the mixed convection parameter λ rises temperature enhances. The driving source of buoyancy in the momentum equation, is an increase of mixed convection parameter. Therefore, the effect of dissipation rises, which ultimately

enhances the temperature profile in both regions. The plot of temperature field for different inputs of the Eckert number Ec is displayed in figure 5.8. A rise in temperature is observed as Ec increases due to presence of viscous dissipation. It is noteworthy from the figures 5.2-5.8 that the values obtained from both numerical and analytical methods are in excellent agreement with each other which validates our present solution methodology.

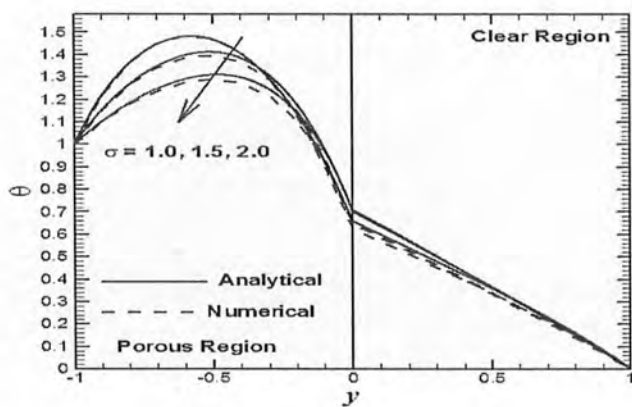


Figure 5.5: Influence of porosity parameter σ on the temperature profile

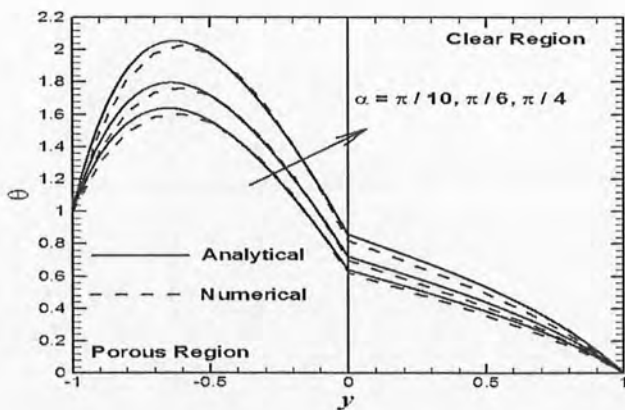


Figure 5.6: Influence of inclination angle α on the temperature profile

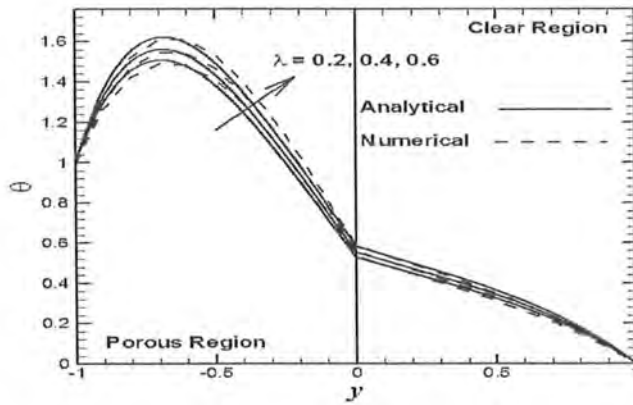


Figure 5.7: Influence of mixed convection parameter λ on the temperature profile

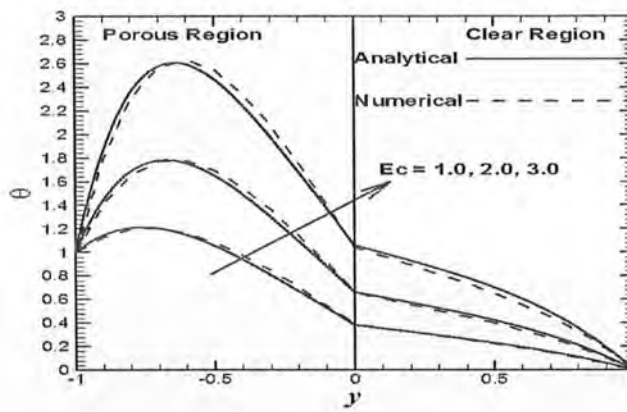


Figure 5.8: Influence of the Eckert number Ec on the temperature profile

The effects of various physical parameters for entropy generation number N_s are shown in figures 5.9-5.11. Figure 5.9 depicts the influence of the angle of inclination α on heat generation number. It is noted that entropy accelerates due to increase in inputs of the inclination angle. The impact of group parameter Br/Ω on the entropy generation number N_s is displayed in figure 5.10. The entropy generation is maximum at the walls of the channel and augments as Br/Ω increases. This increase in the value of entropy generation number N_s is more prominent in the porous region due to pores resistance to the flow which ultimately results in more production of entropy. Figure 5.11 shows the impact of variation of mixed convection parameter λ on the entropy generation number N_s . It can be seen that rise in the value of λ augments the entropy production. It can be observed from all the above figures that entropy generation number

is higher in the vicinity of the channel walls and is very low in the central part of the channel. The entropy generation number is pronounced near the walls due to high velocity and temperature gradient there. While, in the middle part of the channel velocity and temperature gradient decreases, so a very low entropy generation is observed there.

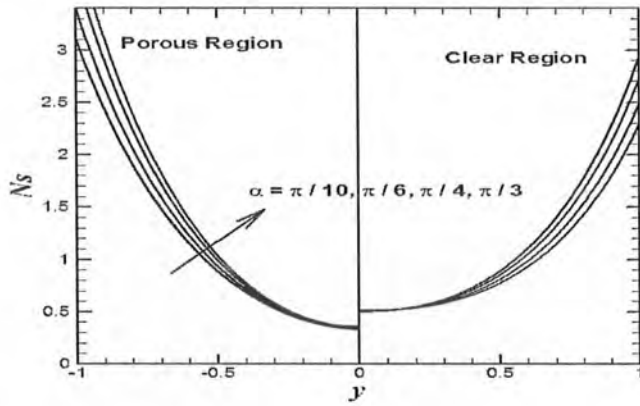


Figure 5.9: Influence of inclination angle α on the entropy generation number

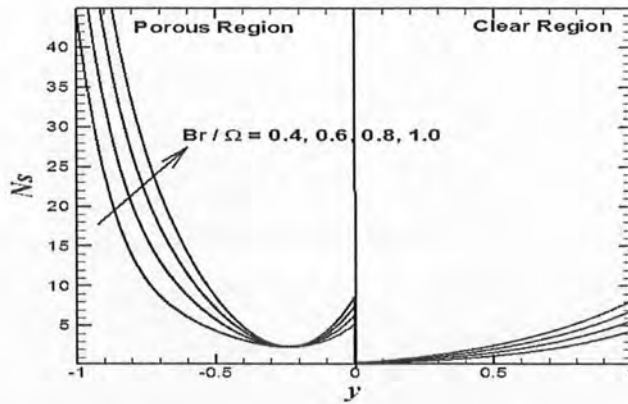


Figure 5.10: Influence of group parameter Br / Ω on the entropy generation number

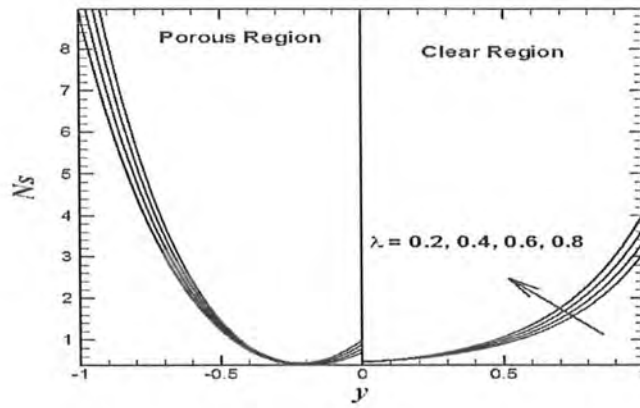


Figure 5.11: Influence of mixed convection parameter λ on the entropy generation number

The Bejan number is plotted from figures 5.12-5.14 to get an insight whether heat transfer entropy effects are dominant over fluid friction entropy effects or vice versa. It is noticed from all these figures that in the porous region, the fluid friction effects are in full dominant, whereas in the clear region, due to transfer of heat the roll of entropy is significant.

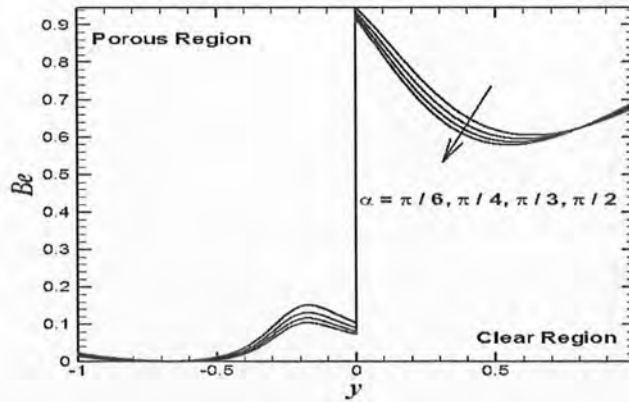


Figure 5.12: Influence of inclination angle α on the Bejan number

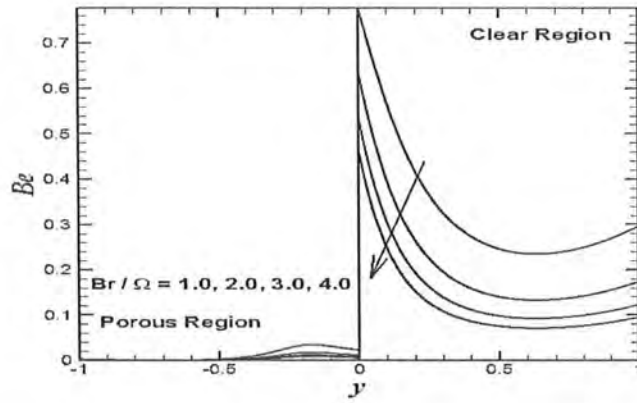


Figure 5.13: Influence of group parameter Br / Ω on the Bejan number

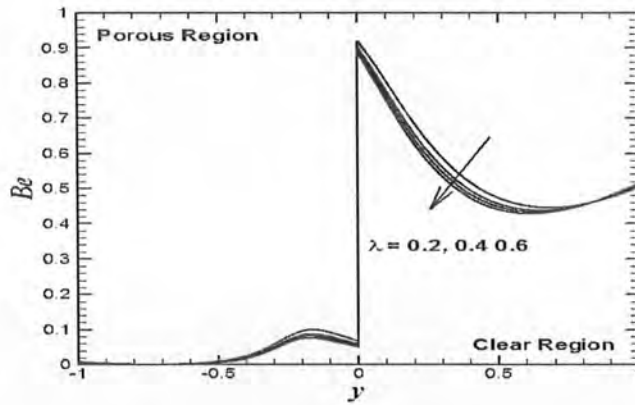


Figure 5.14: Influence of mixed convection parameter λ on the Bejan number

5.6 Concluding Remarks

A mathematical model for unsteady fluid flow between two inclined parallel plates composite channel has been demonstrated. The obtained momentum and temperature fields are used to calculate the entropy generation. The main observations are as follows

- Due to the continuity of velocity and shear stress at the interface, the effect of each physical parameter remains same for both regions.
- The temperature profiles show similar behavior for both regions due to the reason of the continuity of heat flux and temperature at the interface.

- The velocity profile is inversely related to porosity parameter but directly related to mixed convection parameter and inclination angle.
- The temperature profile is directly related to porosity parameter, an inclination angle, mixed convection parameter and Eckert number.
- The total entropy generation rate is directly related to mixed convection parameter, inclination angle and the group parameter.
- The total entropy generation number has maximum values near the walls of the channel.
- All the Bejan number profiles attain maximum values at the upper plate of the channel and minimum values at the lower plate.

Chapter 6

Flow and Heat Transfer Analysis in an Inclined Channel with Embedded Region of Porous Medium

6.1 Introduction

This chapter emphasizes on examining the momentum and heat transfer of an electrically conducting fluid in an inclined channel in which porous medium is sandwiched between viscous fluids. Joule and viscous dissipation are assumed to be present here. The obtained non-linear PDEs that govern the velocity and heat transfer phenomenon have been examined analytically by regular perturbation method. The approximate series solution is confirmed by solving the equations numerically by finite difference method. The solution expression is used to find the local skin friction, entropy generation number and Nusselt number. The comparison between the results obtained by two different techniques is demonstrated with the help of graphs.

6.2 Mathematical Modeling

Consider the unsteady, fully developed, unidirectional and laminar flow in a parallel plate inclined channel in which porous media is sandwiched between two clear regions filled with viscous fluid are shown in figure 6.1. The region-1 ($-h \leq y \leq 0$) and region-3 ($h \leq y \leq 2h$) are occupied with clear viscous fluid while region-2 ($0 \leq y \leq h$) have with porous media. The temperature of lower and upper plate is maintain at T_{w1} and T_{w2} respectively.

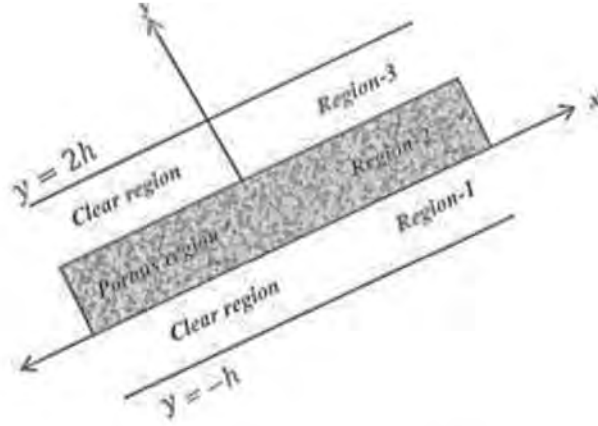


Figure 6.1: Schematic Diagram and coordinate system

The fluid flow in three regions is due to constant pressure gradient $\frac{\partial P}{\partial x}$. Initially, static plates are assumed and at some later time $t > 0$ the upper plate suddenly start to vibrate with the velocity $u_3(2h) = U = u_0(1 + \varepsilon A e^{i\omega t})$. The continuity, momentum and heat transfer equations for three regions are given by

$$\frac{\partial v_i}{\partial y} = 0, \quad (6.1)$$

$$\rho \left(\frac{\partial u_i}{\partial t} + v_i \frac{\partial u_i}{\partial y} \right) = -\frac{\partial p}{\partial x} + \chi_\mu \left(\frac{\partial^2 u_i}{\partial y^2} \right) - \chi \frac{\mu}{s} u_i - \sigma B_0^2 u_i + g\beta(T_i - T_{w2}) \sin \alpha, \quad (6.2)$$

$$\rho C_p \left(\frac{\partial T_i}{\partial t} + v_i \frac{\partial T_i}{\partial y} \right) = \chi_k \frac{\partial^2 T_i}{\partial y^2} - \chi_\mu \left(\frac{\partial u_i}{\partial y} \right)^2 + \sigma B_0^2 u_i^2 + \chi \frac{\mu}{s} u_i^2, \quad (6.3)$$

The index $i=1$ gives equations for region-1 (clear region), $i=2$ gives equations for region-2 (porous region) and $i=3$ gives equations for region-3 (clear region). No-slip boundary conditions are taken into account for the velocity field and walls are supposed to be isothermal. Moreover, the velocity, temperature and their gradients at the interface point are continuous. The interfacial and boundary conditions are as follow

$$u_1(-h) = 0, T_1(-h) = T_{w1}, u_3(2h) = U = u_0(1 + \varepsilon A e^{i\omega t}), T_2(2h) = T_{w2}, \quad (6.4)$$

$$u_1(0) = u_2(0), \quad \mu \frac{\partial u_1}{\partial y} \Big|_{y=0} = \mu_{eff} \frac{\partial u_2}{\partial y} \Big|_{y=0}, \quad T_1(0) = T_2(0), \quad K \frac{\partial T_1}{\partial y} \Big|_{y=0} = K_{eff} \frac{\partial T_2}{\partial y} \Big|_{y=0}, \quad (6.5)$$

$$\begin{cases} u_2(h) = u_3(h), \quad T_2(h) = T_3(h), \\ \mu_{eff} \frac{\partial u_2}{\partial y} \Big|_{y=h} = \mu \frac{\partial u_3}{\partial y} \Big|_{y=h}, \quad K_{eff} \frac{\partial T_2}{\partial y} \Big|_{y=h} = K \frac{\partial T_3}{\partial y} \Big|_{y=h}, \end{cases} \quad (6.6)$$

Equation (6.1) shows that v_1 and v_2 are function of time only and independent of y . So that we can take

$$v_i = v_0 (1 + \varepsilon A e^{i\omega t}). \quad (6.7)$$

Introducing non-dimensional variables

$$y^* = \frac{y}{\nu}, \quad u_i^* = \frac{u_i}{u_0}, \quad v_i^* = \frac{v_i}{v_0}, \quad t^* = \frac{t u_0^2}{\nu}, \quad \theta_i = \frac{T_i - T_{w_2}}{T_{w_2} - T_{w_1}}. \quad (6.8)$$

Using equation (6.8) and dropping asterisk for simplicity, equations (6.2)-(6.3) in dimensionless form become

$$\frac{\partial u_i}{\partial t} + v_i \frac{\partial u_i}{\partial y} = P + A_i \frac{\partial^2 u_i}{\partial y^2} + \lambda \sin \alpha \theta_i - \frac{M^2}{Re^2} u_i - \chi \sigma^2 u_i, \quad (6.9)$$

$$\frac{\partial \theta_i}{\partial t} + v_i \frac{\partial \theta_i}{\partial y} = B_i \frac{\partial^2 \theta_i}{\partial y^2} + Ec A_i \left(\frac{\partial u_i}{\partial y} \right)^2 + \frac{M^2 Ec}{Re^2} u_i^2 + \chi Ec \sigma^2 u_i^2, \quad (6.10)$$

$$A_i = \begin{cases} 1, & i=1, \\ m, & i=2, \\ 1, & i=3, \end{cases}$$

where

$$B_i = \begin{cases} 1/Pr, & i=1, \\ k/Pr, & i=2, \\ 1/Pr, & i=3, \end{cases}$$

where $\lambda = \frac{Gr}{Re^3}$, $Gr = \frac{g \beta \Delta T h^3}{\nu^2}$ and $Re = \frac{u_0 h}{\nu}$ are the mixed convection parameter, Grashof number and Reynold number respectively. The interface and boundary conditions reduces to

$$\begin{cases} u_1(-1) = 0, \quad \theta_1(-1) = 1, \quad \theta_3(2) = 0, \quad u_3(2) = 1 + \varepsilon A e^{I\omega t}, \\ u_1(0) = u_2(0), \quad \theta_1(0) = \theta_2(0), \quad u_2(1) = u_3(1), \quad \theta_2(1) = \theta_3(1), \end{cases} \quad (6.11)$$

$$\begin{cases} \left. \frac{\partial u_1}{\partial y} \right|_{y=0} = m \left. \frac{\partial u_2}{\partial y} \right|_{y=0}, \quad \left. \frac{\partial \theta_1}{\partial y} \right|_{y=0} = k \left. \frac{\partial \theta_2}{\partial y} \right|_{y=0}, \\ \left. k \frac{\partial \theta_2}{\partial y} \right|_{y=1} = \left. \frac{\partial \theta_3}{\partial y} \right|_{y=1}, \quad m \left. \frac{\partial u_2}{\partial y} \right|_{y=1} = \left. \frac{\partial u_3}{\partial y} \right|_{y=1}. \end{cases} \quad (6.12)$$

6.3 Solution Methodologies

6.3.1 Analytical Solution

The coupled partial differential equations of velocity and heat transfer equations (6.9) and (6.10) with boundary conditions (6.11)-(6.12) are solved analytically by regular perturbation technique. Let

$$u_i(y,t) = u_{i0}(y) + \varepsilon A e^{I\omega t} u_{i1}(y) + O(\varepsilon A)^2, \quad \text{for } i=1,2,3, \quad (6.13)$$

$$\theta_i(y,t) = \theta_{i0}(y) + \varepsilon A e^{I\omega t} \theta_{i1}(y) + O(\varepsilon A)^2, \quad \text{for } i=1,2,3. \quad (6.14)$$

Plugging equations (6.13)-(6.14) into equations (6.9)-(6.10) with boundary conditions (6.11)-(6.12) and equating periodic and non-periodic coefficient, one can find system of ODEs which can be solved easily.

Non-Periodic Coefficient $O(\varepsilon^0)$

$$v_0 \frac{\partial u_{i0}}{\partial y} = P + A_i \frac{\partial^2 u_{i0}}{\partial y^2} + \lambda \sin \alpha \theta_{i0} - \frac{M^2}{\text{Re}^2} u_{i0} - \chi \sigma^2 u_{i0}, \quad (6.15)$$

$$v_0 \frac{\partial \theta_{i0}}{\partial y} = B_i \frac{\partial^2 \theta_{i0}}{\partial y^2} + Ec A_i \left(\frac{\partial u_{i0}}{\partial y} \right)^2 + \frac{M^2 Ec}{\text{Re}^2} (u_{i0})^2 + \chi Ec \sigma^2 (u_{i0})^2. \quad (6.16)$$

Periodic Coefficient $O(\varepsilon^1)$

$$I\omega u_{i1} + v_0 \frac{\partial u_{i0}}{\partial y} + v_0 \frac{\partial u_{i1}}{\partial y} = A_i \frac{\partial^2 u_{i1}}{\partial y^2} - \chi \sigma^2 u_{i1} + \lambda \sin \alpha \theta_{i1} - \frac{M^2}{\text{Re}^2} u_{i1}, \quad (6.17)$$

$$I\omega \theta_{i1} + v_0 \frac{\partial \theta_{i1}}{\partial y} + v_0 \frac{\partial \theta_{i0}}{\partial y} = B_i \frac{\partial^2 \theta_{i1}}{\partial y^2} + 2Ec A_i \frac{\partial u_{i1}}{\partial y} \frac{\partial u_{i0}}{\partial y} + 2 \frac{M^2 Ec}{\text{Re}^2} u_{i0} u_{i1} + 2\chi Ec \sigma^2 u_{i0} u_{i1}. \quad (6.18)$$

The corresponding interface and boundary conditions are given by

$$\begin{cases} u_{1i}(-1) = 0, & u_{20}(1) = 1, & u_{21}(1) = 1, \\ u_{1i}(0) = u_{2i}(0), & m \frac{\partial u_{1i}}{\partial y} \Big|_{y=0} = \frac{\partial u_{2i}}{\partial y} \Big|_{y=0}, \\ u_{2i}(1) = u_{3i}(1), & \theta_{2i}(1) = \theta_{3i}(1), \end{cases} \quad (6.19)$$

$$\begin{cases} \theta_{1i}(-1) = 1 - \delta_{1i}, & \theta_{3i}(1) = 0, \\ \theta_{1i}(0) = \theta_{2i}(0), & k \frac{\partial \theta_{1i}}{\partial y} \Big|_{y=0} = \frac{\partial \theta_{2i}}{\partial y} \Big|_{y=0}, \end{cases} \quad (6.20)$$

$$\begin{cases} \left. \frac{\partial u_{1i}}{\partial y} \right|_{y=0} = m \left. \frac{\partial u_{2i}}{\partial y} \right|_{y=0}, & \left. \frac{\partial \theta_{1i}}{\partial y} \right|_{y=0} = k \left. \frac{\partial \theta_{2i}}{\partial y} \right|_{y=0}, \\ \left. k \frac{\partial \theta_{2i}}{\partial y} \right|_{y=1} = \left. \frac{\partial \theta_{3i}}{\partial y} \right|_{y=1}, & m \left. \frac{\partial u_{2i}}{\partial y} \right|_{y=1} = \left. \frac{\partial u_{3i}}{\partial y} \right|_{y=1}, \end{cases} \quad (6.21)$$

where $i = 0, 1$ give the interface and boundary conditions for $O(\varepsilon A)^0$ and $O(\varepsilon A)^1$ respectively.

6.3.2 Numerical Scheme

The above analytical solutions are useful only for small values of parameter εA , the perturbation method does not give solution for large values of εA , so we resort to numerical solutions. The partial differential equations (6.9)-(6.10) with the boundary and interface conditions equations (6.11) -(6.12) are discretized by using BTCS (Backward time central spacing).

$$\begin{aligned} & \frac{u_i(l,n) - u_i(l,n-1)}{k_{1i}} + v_i \frac{u_i(l,n) - u_i(l-1,n)}{h_{1i}} - p - A_i \frac{u_i(l+1,n) - 2u_i(l,n) + u_i(l-1,n)}{h_{1i}^2} + \lambda \sin \alpha \theta_i(l,n) \\ & - \frac{M^2}{\text{Re}^2} u_i(l,n) - \chi \sigma^2 u_i(l,n) = 0, \end{aligned} \quad (6.22)$$

$$\begin{aligned} & \frac{\theta_i(l,n) - \theta_i(l,n-1)}{k_{2i}} + v_i \frac{\theta_i(l,n) - \theta_i(l-1,n)}{h_{2i}} - B_i \frac{\theta_i(l+1,n) - 2\theta_i(l,n) + \theta_i(l-1,n)}{h_{2i}^2} \\ & - Ec A_i \left(\frac{u_i(l,n) - u_i(l-1,n)}{h_{1i}} \right)^2 - \frac{M^2 Ec}{\text{Re}^2} (u_i(l,n))^2 - \chi Ec \sigma^2 (u_i(l,n))^2 = 0, \end{aligned} \quad (6.23)$$

$$\begin{cases} u_1(-1,k) = 0, & u_3(2,n) = 1 + \varepsilon A e^{i\omega n} \\ \theta_1(-1,k) = 0, & \theta_3(2,n) = 0, \end{cases} \quad (6.24)$$

$$\begin{cases} u_1(0,n) = u_2(0,n), & u_2(1,n) = u_3(1,n), \\ \theta_1(0,n) = \theta_2(0,n), & \theta_2(1,n) = \theta_3(1,n), \end{cases} \quad (6.25)$$

$$\begin{cases} u_2(l-1, n) - mu_2(l-1, n) + (m-1)u_2(l, n) = 0, \\ \theta_2(l-1, n) - k\theta_2(l-1, n) + (k-1)\theta_2(l, n) = 0, \\ u_3(l-1, n) - mu_2(l-1, n) + (m-1)u_2(l, n) = 0, \\ \theta_3(l-1, n) - k\theta_2(l-1, n) + (k-1)\theta_2(l, n) = 0. \end{cases} \quad (6.26)$$

6.4 Quantities of Physical Interest

6.4.1 Skin Friction

The skin friction in cartesian coordinate system for the lower plate is

$$\tau_w = \mu \left. \frac{\partial u}{\partial y} \right|_{y=-1}. \quad (6.27)$$

The local skin friction coefficient C_f on the wall is given by

$$C_f = \frac{\tau_w}{\rho u_0^2}, \quad (6.28)$$

and the skin friction in dimensionless form for the lower plate is given by

$$C_f = \left. \frac{du}{dy} \right|_{y=-1}. \quad (6.29)$$

6.4.2 Nusselt Number

The Nusselt number is given as

$$Nu = \frac{Nu^* d}{k \Delta T}, \quad (6.30)$$

where ΔT and Nu^* are the temperature difference between the walls and heat transfer rate at the surface and can be written as

$$Nu^* = -k \left. \frac{\partial T}{\partial y} \right|_{y=-1}. \quad (6.31)$$

The Nusselt number for the lower plate in dimensionless form after using (6.8) in (6.30) with (6.31) is given by

$$Nu = -\theta'(-1). \quad (6.32)$$

6.4.3 Entropy

The local entropy generation rate per unit volume for a viscous, incompressible and MHD flow in a composite channel can be written by

$$(S_G)_i = \underbrace{\frac{K}{T_{wi}^2} \left(\frac{\partial T_i}{\partial y} \right)^2}_{\substack{\text{irreversibility} \\ \text{due to} \\ \text{heat transfer}}} + \underbrace{\frac{\mu}{T_{wi}} \left(\frac{\partial u_i}{\partial y} \right)^2}_{\substack{\text{entropy effects} \\ \text{due to} \\ \text{viscous dissipation}}} + \underbrace{\frac{\sigma^2 B_0^2}{T_{wi}} (u_i)^2}_{\substack{\text{entropy effects} \\ \text{due to} \\ \text{magnetic field}}} + \underbrace{\psi \frac{\mu}{s} (u_i)^2}_{\substack{\text{entropy effects} \\ \text{due to} \\ \text{porous region}}}. \quad (6.33)$$

The dimensionless form of equation (6.33) after using equation (6.8) take the form

$$(N_s)_i = \left(\frac{\partial \theta_i}{\partial y} \right)^2 + \frac{Br}{\Omega} \left(\frac{\partial u_i}{\partial y} \right)^2 + \frac{M^2 Br}{\Omega Re^2} (u_i)^2 + \psi \frac{Br}{\Omega} \sigma^2, \quad (6.34)$$

$$(N_s)_i = (N_H)_i + (N_f)_i + (N_m)_i = (N_H)_i + (N_F)_i, \quad (6.35)$$

where $i=1,2,3$ gives entropy generation for three regions of the channel. $Br = EcPr$ and $\Omega = \Delta T / T_{w1}$ represent the Brinkman number and dimensionless temperature difference respectively. $(N_H)_i$ represents the entropy generation due to heat transfer and $(N_f)_i$ denotes the entropy generation due to fluid friction. $(N_m)_i$ is the entropy generation due to magnetic field.

The Bejan number tells that whether fluid friction and magnetic field effects are dominant over heat transfer entropy effects or vice versa and is given as

$$(Be)_i = \frac{(N_H)_i}{(Ns)_i}. \quad (6.36)$$

The value of Bejan number changes from 0 to 1. $Be=1$ tells that the irreversibility due to heat transfer is dominant, $Be=0$ shows that the irreversibility due to viscous dissipation is prominent. While, $Be=0.5$ demonstrates that irreversibility due to viscous dissipation is equal to heat transfer.

6.5 Results and Discussion

The impact of different physical parameters is analyzed by plotting graphs, while the inputs of various pertinent parameters $Ec=0.5$, $\alpha = \pi/6$, $M=0.5$, $P=-2$, $\sigma=0.2$, $m=0.5$, $Re=2$, $Gr=5$, $Pr=0.2$, $k=0.5$ are kept fixed except the varying one. Figure 6.2 shows that the velocity and magnetic field parameter M are inversely related due to resistive action of the Lorentz forces. Figure 6.3 indicates that velocity decreases due to rise in the values of porosity parameter σ . Increase in the values of the porosity parameter, the friction between the fluid particles enhances. Consequently, a fall in fluid velocity is noticed in the porous region. The impact of porosity parameter in the clear regions remains same due to the stability of velocity and shear stress at the interface. It is depicted in figure 6.4 that in forward directional flows, the velocity increases as the favorable pressure gradient increases. While an opposite behavior is noticed in figure 6.5 for adverse pressure gradient. Figure 6.6 represents that by rising the values of inclination angle α , the velocity accelerates, due to the reason of the effect of driving force which support the motion.

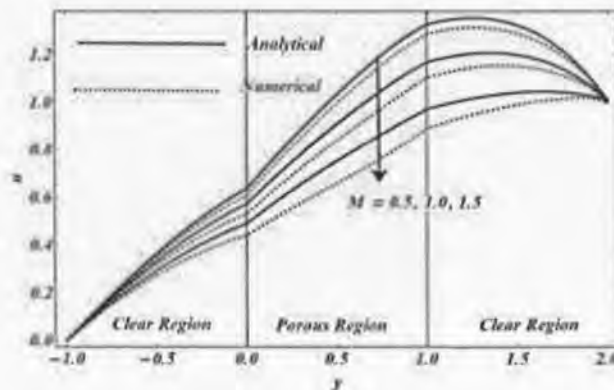


Figure 6.2: Velocity profile for variation in the magnetic field M

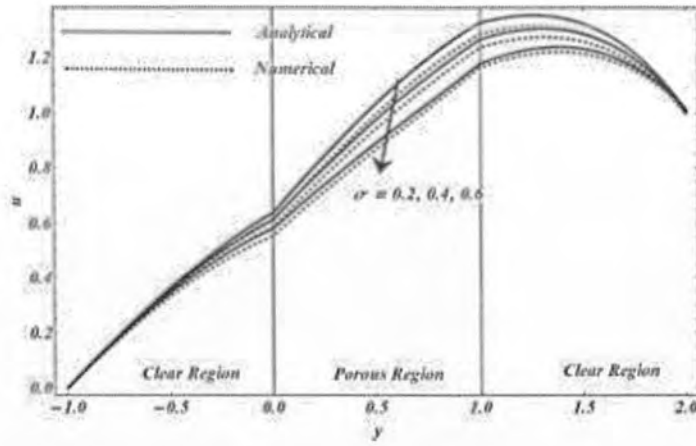


Figure 6.3: Velocity profile for variation in the porosity parameter σ

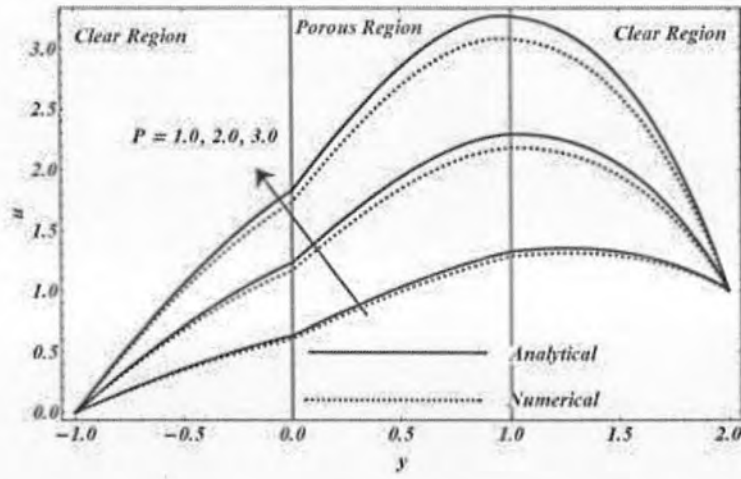


Figure 6.4: Velocity profile for variation in the favorable pressure gradient P

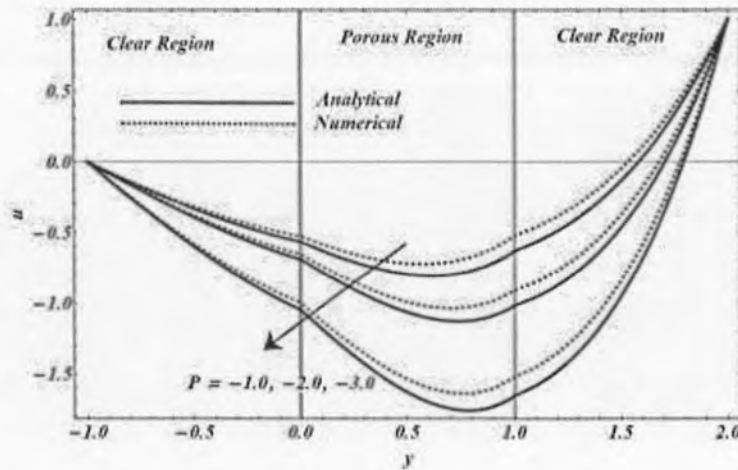


Figure 6.5: Velocity profile for for variation in the adverse pressure gradient P

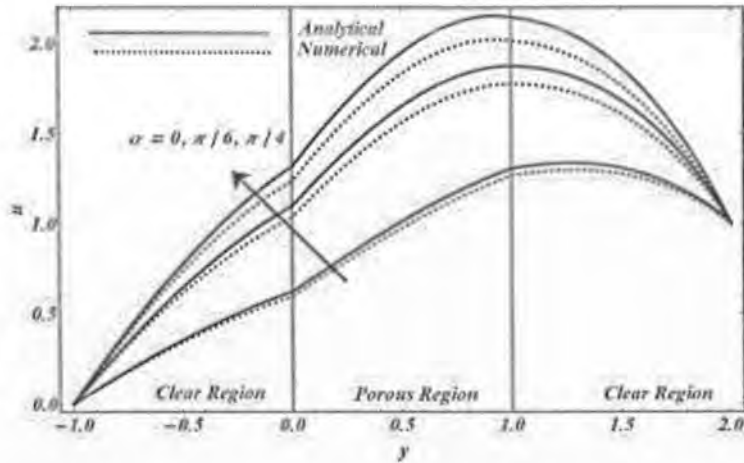


Figure 6.6: Velocity profile for variation in the inclination angle α

The temperature are inversely related to the favorable pressure gradient due to process of convection as illustrated in figure 6.7. Figure 6.8 represents the temperature distribution for different values of Pr. It is observed that Prandtl number and temperature are inversely related in the whole flow region. It was expected since when we increase the values of Pr, thermal conduction process reduces and there is a decrease in the molecular motion of the fluid elements. Consequently, the temperature reduces in the parallel plate channel. The temperature and magnetic field parameter are directly related due to the existence of Lorentz force which produces flow resistance. This fact can be observe in figure 6.9. As the velocity gradient increases, the influence of dissipation increases, due to which temperature increases. When we increase the inclination angle, fluid velocity increases as a result friction between the fluid particles enhanced. Ultimately, temperature of the fluid increases as shown in figure 6.10.

Figures 6.2-6.10 of velocity and temperature profiles for different parameters also give a comparison of analytical and numerical solutions. It is observed that for small values of the physical parameters, results are very close and show excellent agreement but difference increases as the values of the physical parameters increase.

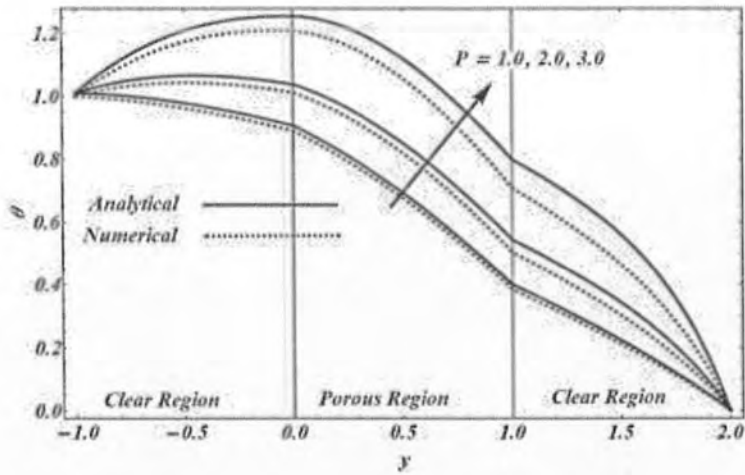


Figure 6.7: Temperature profile for variation in the favorable pressure gradient P

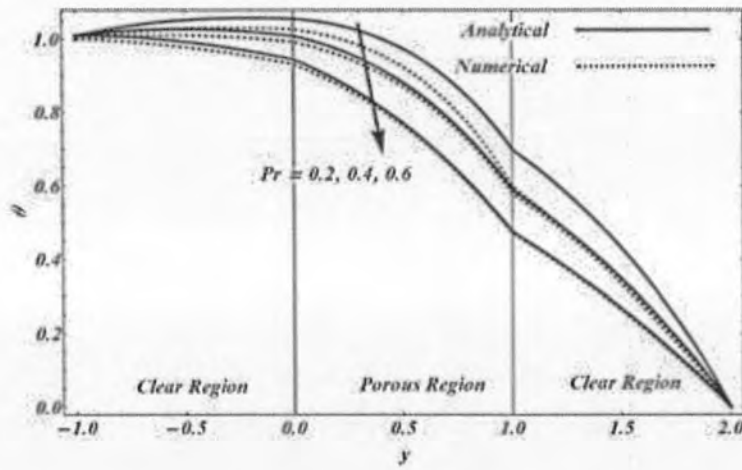


Figure 6.8: Temperature profile for variation in the Prantdl number Pr

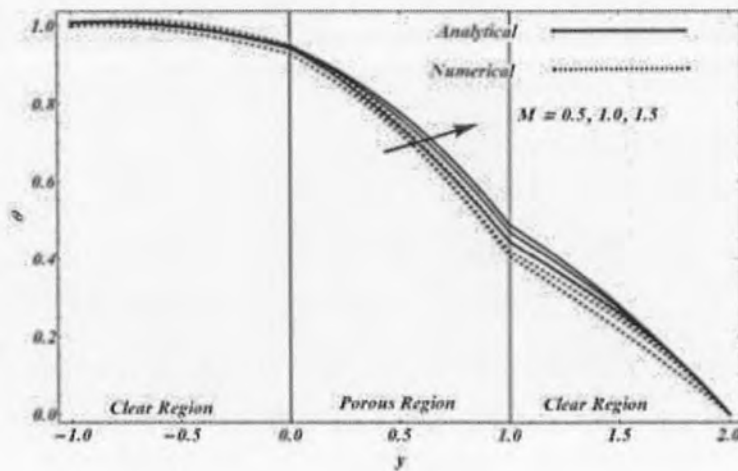


Figure 6.9: Temperature profile for variation in magnetic field parameter M

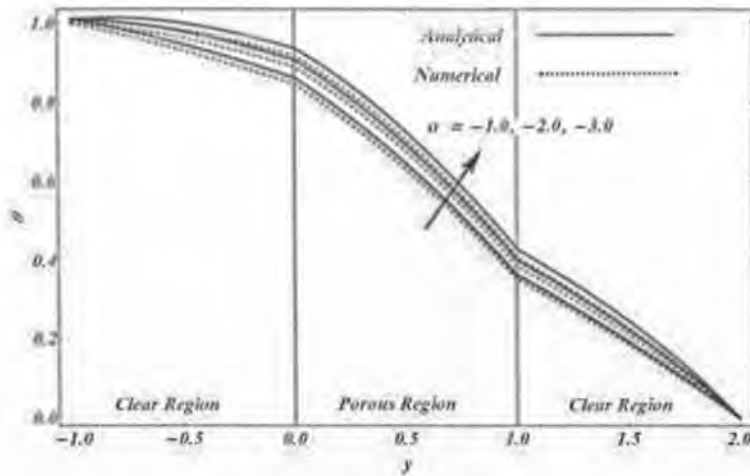


Figure 6.10: Temperature profile for variation in the inclination angle α

The variation in the local entropy generation number and the Bejan number for different values of the physical parameters like group parameter, magnetic field parameter, porosity parameter and inclination angle have been demonstrated from figures 6.11-6.18. Figure 6.11 depicts that by enhancing the value of group parameter Br/Ω , the variations in the entropy generation number also rises. It indicates the frictional heating in the system. Figure 6.12 shows that variation in the Bejan number Be for different values of group parameter Br/Ω is somewhat cumbersome. Figure 6.13 indicates the entropy generation number for different values of magnetic field parameter. Due to the presence of Lorentz force, increase in entropy generation is seen near the clear-porous interface while reverse trend is noticed in the upper part of the channel. Figure 6.14 depicts the effect of M on the Bejan number in a channel in which porous substrate is sandwiched between viscous fluids. The Bejan number increases considerably at both clear-porous interfaces, while the reverse trend is observed near the upper wall of the channel. It is also observed from the figure 6.14 that impact of fluid friction and magnetic field are dominant from $y = -1$ to $y = 0$ (clear region) and $y = 0$ to $y = 1$ (porous region). While, heat transfer effects are dominant near the upper plate in clear region. Figure 6.15 demonstrates that entropy production reduces due to increase in the values of porosity parameter, while the Bejan number increases due to rise in the values of porosity parameters as represented in figure 6.16. In the porous region of the channel, the effects of entropy generation due to heat transfer irreversibility are negligible. While, the influence of fluid friction near the lower plate show dominant behavior and near the upper wall of the channel heat transfer effects are dominant. Figures 6.17 and 6.18

show the local entropy generation number and the Bejan number profiles for different values of inclination angle α . Entropy production rises due to increase in the values of the inclination angle while the Bejan number decreases due to rise in the values of the inclination angle. Moreover, entropy effects due to fluid friction and magnetic field become prominent in first two regions. While, near the upper plate in clear region heat transfer entropy effects are prominent with the increase in the values of inclination angle. The sharp jump in entropy generation number at the clear-porous interface is noticed. It is also found that entropy generation effects are higher in regions adjacent to the walls. One may conclude that the walls of the channel serve as sources to entropy generation. Furthermore, it is also noted that $Be < 1$ throughout the channel for different values of group parameter, inclination angle, porosity parameter and magnetic field parameter.

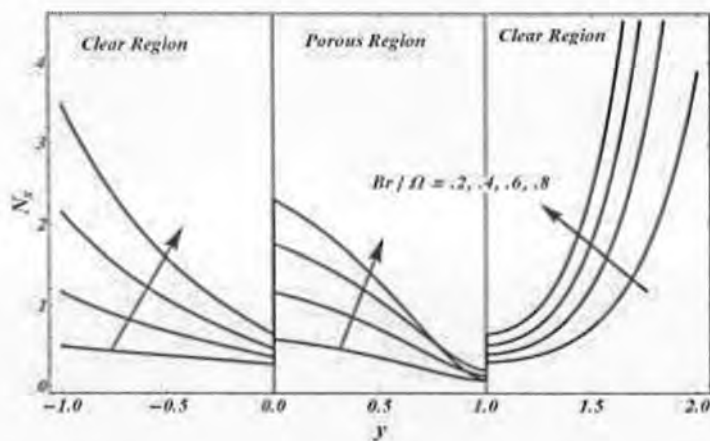


Figure 6.11: Entropy generation for variation in group parameter Br / Ω

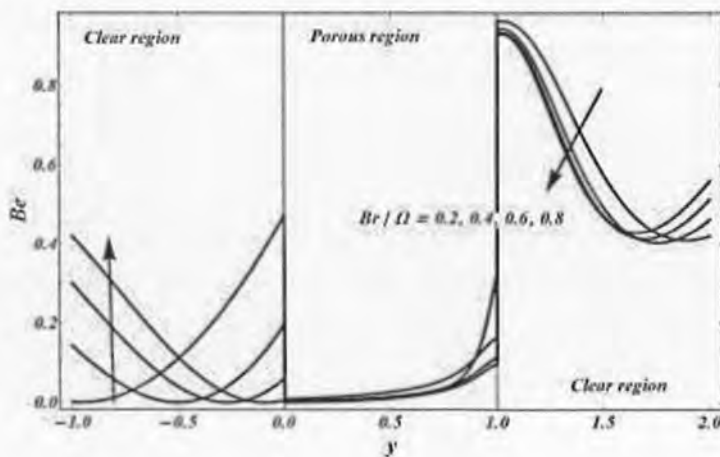


Figure 6.12: Bejan number for variation in group parameter Br / Ω

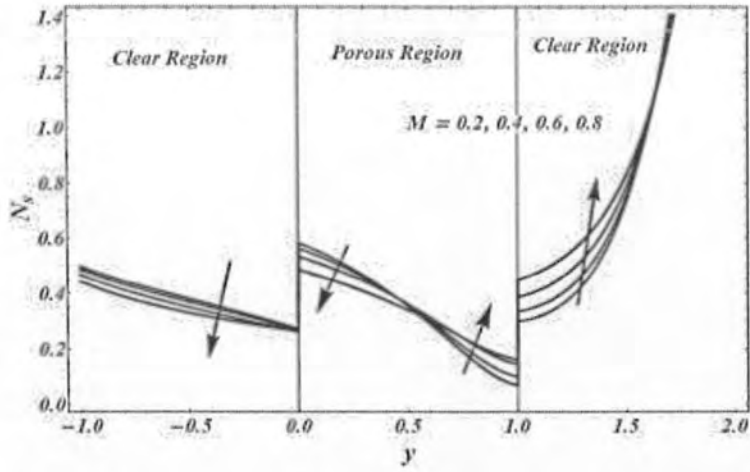


Figure 6.13: Entropy generation for variation in magnetic field parameter M

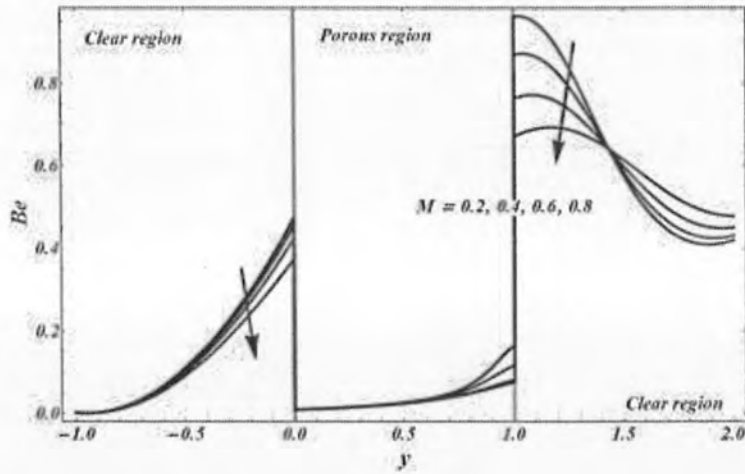


Figure 6.14: Bejan number for variation in magnetic field parameter M

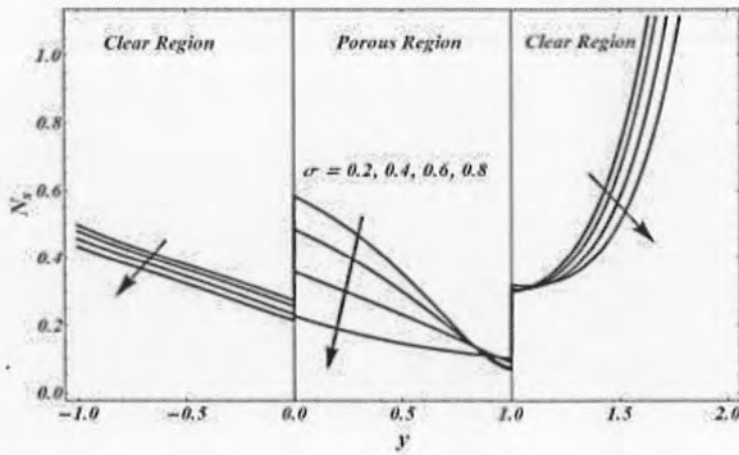


Figure 6.15: Entropy generation for variation in porosity parameter σ

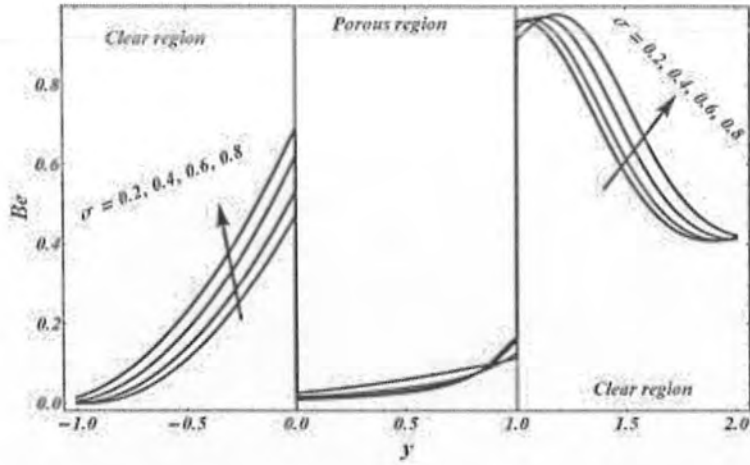


Figure 6.16: Bejan number for variation in porosity parameter σ

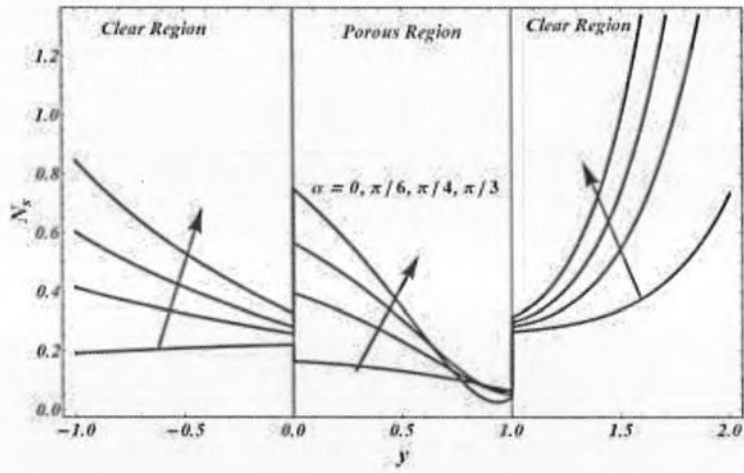


Figure 6.17: Entropy generation for variation in the inclination angle α

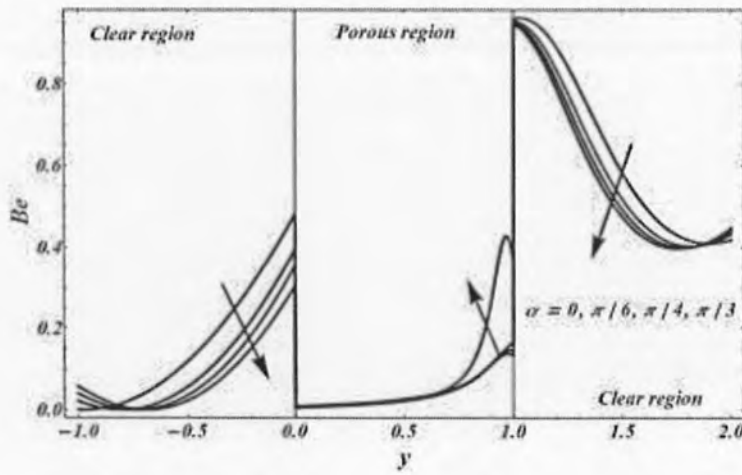


Figure 6.18: Bejan number for variation in the inclination angle α

Figures 6.19 and 6.20 show the effects of skin friction for inclination angle and porosity parameter at the lower wall of the channel. It has been found that skin friction enhances due to rise in the values of inclination angle and reduces due to rise in the values of magnetic field. But, Skin friction decreases due to rise in the values of porosity parameter as shown in figure 6.20. Figures 6.21 and 6.22 show the effect of Nusselt number for various inputs of the inclination angle and porosity parameter. The Nusselt number drops due to increase in the values of the inclination angle and enhances due to rise in the values of magnetic field. While, opposite effects are seen in case of porosity parameter.

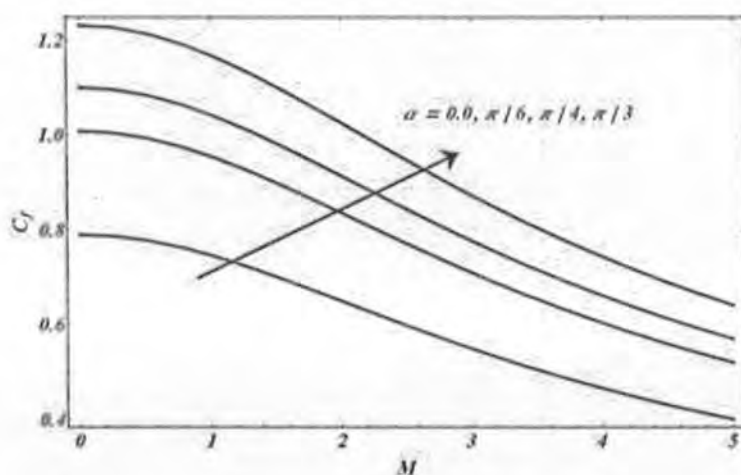


Figure 6.19: Skin friction for variation in the both inclination angle and magnetic field

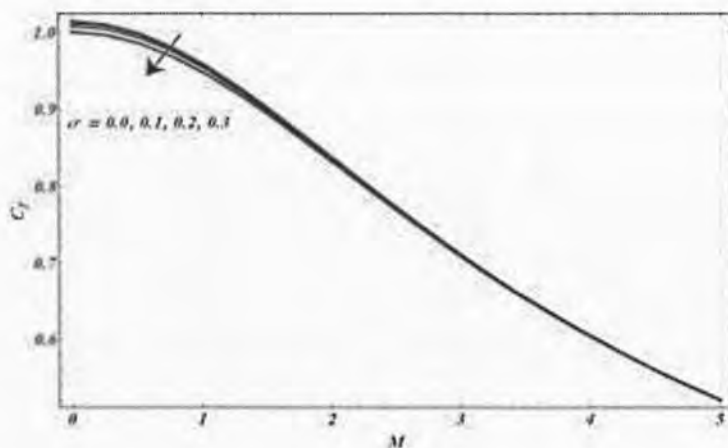


Figure 6.20: Skin friction for various inputs of the both porosity parameter and magnetic field

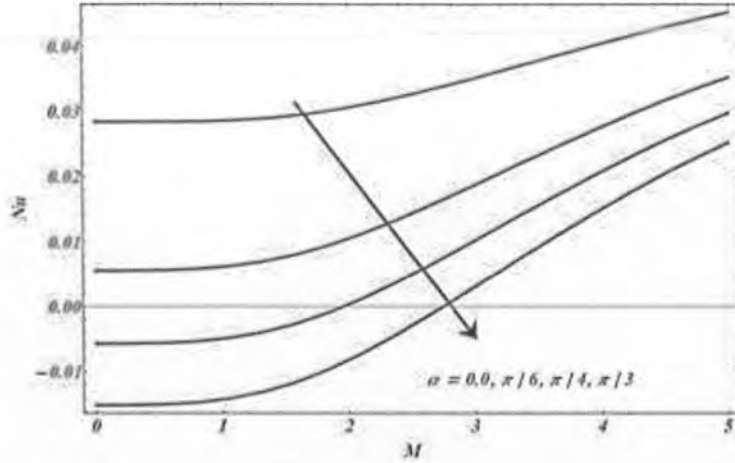


Figure 6.21: The Nusselt number for variation in the both inclination angle and magnetic field

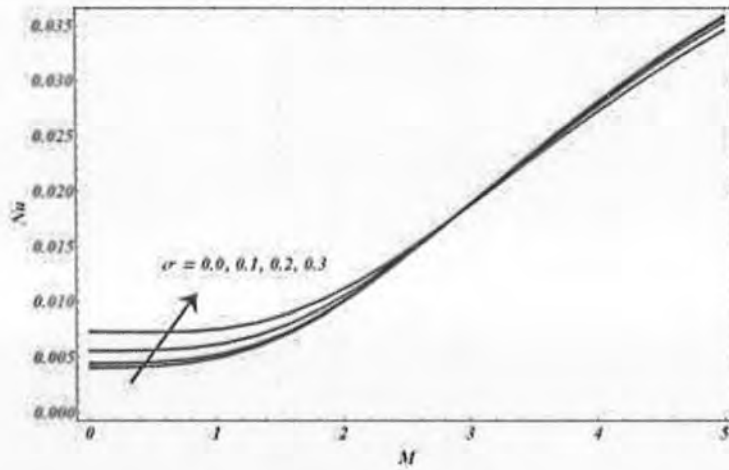


Figure 6.22: The Nusselt number for various values of the both porosity parameter and magnetic field

6.6 Concluding Remarks

The velocity and heat transfer characteristics are analyzed for an incompressible, laminar flow in an inclined parallel plate channel in which porous substrate is sandwiched between viscous fluids. The Darcy-Brinkmann model is used to model the problem. The obtained non-linear PDEs are solved numerically and analytically. This study leads to following conclusions.

- Velocity is inversely related to both magnetic field parameter and porosity parameter.
- Velocity profile increases due to rise in the values of favorable pressure gradient,

reverse behavior is noticed for the case of temperature profile.

- Increase in the values of Prandtl number reduces the temperature.
- Temperature augments due to rise in the value of magnetic field parameter.
- Entropy generation number enhances in the clear regions adjacent to the walls with the increasing values of group parameter and magnetic field parameter while the reverse behavior is observed for increasing values of porosity parameter.
- The entropy generation effects are higher in regions adjacent to the walls.
- The Bejan number increases due to rise in the values of porosity parameter and reduces for various values of magnetic field parameter.
- Skin friction is directly related with an inclination angle while inversely related to porosity parameter.
- Nusselt number falls due to increase in the value of inclination angle while grows due to rise in the values of porosity parameter.

Chapter 7

Conclusion and Future Work

7.1 Concluding Remarks

Investigation of laminar flow with heat transfer gives a physical insight of the factors effective for the flows in the channel with emphasis to composite channel/annulus. It was noticed that the presence of porous medium in the channel flow has its own significance, introducing important effects on the laminar flow and heat transfer. During the study carried out in this thesis, it is also noticed that favorable pressure gradient accelerates the process of convection. Moreover, the Prandtl number, the Eckert number, the mixed convection parameter, the inclination angle and the ratio of thermal conductivity accelerate the temperature of the fluid in the channel. The important fact experienced, that the effects of all physical parameters remain invariant in the study of composite channel too. Nevertheless, the existence of magnetic field in the composite channel is responsible for slowing down the velocity and raising the temperature due to Lorentz force.

The study of a non-Newtonian fluid (Casson fluid) flow in an irregular channel proves that the Newtonian fluid velocity is more than the Casson fluid velocity for all physical parameters with convective boundary conditions. It is observed that mass concentration is reduced due to rise in the values of Schmidt number while velocity decreases subject to rise in the value of thermal radiation parameter.

The remarkable achievement in the accomplishment of the thesis is the study of entropy production of an incompressible laminar flow in an inclined composite channel. The expression of entropy can be conveniently obtained from the momentum and heat transfer equations. The highest entropy production number is closer to the channel walls and lowest at the middle of the channel. For the flow in a composite channel, it is found that fluid friction entropy effects are prominent near the central region and heat transfer entropy effects are dominant closer to the channel walls. The total entropy generation is directly proportional to the mixed convection

parameter, the inclination angle and the group parameter. The magnetic field plays a vital role for the generation of entropy in the channel in which porous medium is sandwiched between viscous fluids and develops an opposing force in the transverse direction to the surface responsible for the deceleration of the fluid motion and in enhancement of the temperature field. Thus, decrease in entropy is observed near the lower clear porous interface along with the increase in magnetic field parameter while reverse trend is upper clear porous interface. The increase in magnetic field parameter depicts that the entropy due to fluid friction are more dominant than the heat transfer entropy effects while contrasting effects is observed near the upper wall of the channel.

7.2 Future Work

The flow and heat transfer phenomenon investigated in this thesis provide useful information and to extend the work in various dimensions. The current work could be extended to various rheological fluids. Now a days, nano-fluids are also considered as the helpful agent in enhancing the heat transfer processes. The role of shear stress jump condition for non-Newtonian nano-fluid would be an interesting topic for the new investigators.

Bibliography

1. Pfitzner, J., *Poiseuille and his law*. Anaesthesia, 1976. **31**(2): p. 273-275.
2. Siegel, R. and M. Perlmutter, *Heat transfer for pulsating laminar duct flow*. ASME J. Heat Transfer, 1962. **84**(2): p. 111-123.
3. Berman, A.S., *Laminar flow in channels with porous walls*. Journal of Applied Physics, 1953. **24**(9): p. 1232-1235.
4. Wah, T., *Laminar flow in a uniformly porous channel*. The Aeronautical Quarterly, 1964. **15**(3): p. 299-310.
5. Brady, J., *Flow development in a porous channel and tube*. The Physics of fluids, 1984. **27**(5): p. 1061-1067.
6. Kaviany, M., *Laminar flow through a porous channel bounded by isothermal parallel plates*. International Journal of Heat and Mass Transfer, 1985. **28**(4): p. 851-858.
7. Yuan, S., *Further investigation of laminar flow in channels with porous walls*. Journal of Applied Physics, 1956. **27**(3): p. 267-269.
8. White, F., *Laminar flow in a uniformly porous tube*. Journal of Applied Mechanics, 1962. **29**(1): p. 201-204.
9. Cox, S.M., *Analysis of steady flow in a channel with one porous wall, or with accelerating walls*. SIAM Journal on Applied Mathematics, 1991. **51**(2): p. 429-438.
10. Cox, S.M. and J. King, *Large-Reynolds-Number Asymptotics of the Berman Problem*. Studies in Applied Mathematics, 2004. **113**(3): p. 217-243.
11. Sellars, J.R., *Laminar flow in channels with porous walls at high suction Reynolds numbers*. Journal of Applied Physics, 1955. **26**(4): p. 489-490.
12. Lu, C., A.D. MacGillivray, and S.P. Hastings, *Asymptotic behaviour of solutions of a similarity equation for laminar flows in channels with porous walls*. IMA journal of Applied Mathematics, 1992. **49**(2): p. 139-162.
13. Taylor, C., et al., *Three-dimensional flow in a porous channel*. The Quarterly Journal of Mechanics and Applied Mathematics, 1991. **44**(1): p. 105-133.
14. Andersson, H. and L. Holmedal, *Start-up flow in a porous medium channel*. Acta Mechanica, 1995. **113**(1): p. 155-168.

15. Skalak, F.M. and C.Y. Wang, *On the nonunique solutions of laminar flow through a porous tube or channel*. SIAM Journal on Applied Mathematics, 1978. **34**(3): p. 535-544.
16. Terrill, R. and G. Shrestha, *Laminar flow in a uniformly porous channel with an applied transverse magnetic field*. Applied Scientific Research, Section B, 1965. **12**(3): p. 203-211.
17. Wang, C., *Flow through a finned channel filled with a porous medium*. Chemical Engineering Science, 2010. **65**(5): p. 1826-1831.
18. Choudhury, R. and U.J. Das, *Heat transfer to MHD oscillatory viscoelastic flow in a channel filled with porous medium*. Physics Research International, 2012. **2012**.
19. Khodadadi, J., *Oscillatory fluid flow through a porous medium channel bounded by two impermeable parallel plates*. Journal of Fluids Engineering, 1991. **113**(3): p. 509-511.
20. Kim, S.Y., B.H. Kang, and J.M. Hyun, *Heat transfer from pulsating flow in a channel filled with porous media*. International Journal of Heat and Mass Transfer, 1994. **37**(14): p. 2025-2033.
21. Neale, G. and W. Nader, *Practical significance of Brinkman's extension of Darcy's law: coupled parallel flows within a channel and a bounding porous medium*. The Canadian Journal of Chemical Engineering, 1974. **52**(4): p. 475-478.
22. Kim, S. and W.B. Russel, *Modelling of porous media by renormalization of the Stokes equations*. Journal of Fluid Mechanics, 1985. **154**: p. 269-286.
23. Al-Hadhrami, A., L. Elliott, and D. Ingham, *Combined free and forced convection in vertical channels of porous media*. Transport in Porous Media, 2002. **49**(3): p. 265-289.
24. Batchelor, G.K., *An introduction to fluid dynamics*. 2000: Cambridge university press.
25. Jankowski, T.A. and J. Majdalani, *Laminar flow in a porous channel with large wall suction and a weakly oscillatory pressure*. Physics of Fluids, 2002. **14**(3): p. 1101-1110.
26. Chamkha, A.J., *Non-Darcy fully developed mixed convection in a porous medium channel with heat generation/absorption and hydromagnetic effects*. Numerical Heat Transfer, Part A Applications, 1997. **32**(6): p. 653-675.
27. Pantokratoras, A. and T. Fang, *Flow of a weakly conducting fluid in a channel filled with a porous medium*. Transport in Porous Media, 2010. **83**(3): p. 667-676.
28. Sarpkaya, T., *Flow of non-Newtonian fluids in a magnetic field*. AIChE Journal, 1961. **7**(2): p. 324-328.

29. Chow, A.W. and G.G. Fuller, *Some experimental results on the development of Couette flow for non-Newtonian fluids*. Journal of Non-Newtonian Fluid Mechanics, 1985. **17**(2): p. 233-243.
30. Ghosh, N., B. Ghosh, and L. Debnath, *The hydromagnetic flow of a Dusty Visco-Elastic fluid between two infinite parallel plates*. Computers & Mathematics with Applications, 2000. **39**(1-2): p. 103-116.
31. Kasim, A., N. Mohammad, and S.S. Aurangzaib, *Natural convection boundary layer flow of a viscoelastic fluid on solid sphere with Newtonian heating*. World Academy of Science, Engineering and Technology (64), 2012: p. 628-633.
32. Kavitha, K. and C.V.R. Murthy, *Mixed convection flow of a second grade fluid in an inclined porous channel*. International Journal of Physics and Mathematical Sciences, 2011. **1**: p. 120-139.
33. Ariel, P.D., *On exact solutions of flow problems of a second grade fluid through two parallel porous walls*. International Journal of Engineering Science, 2002. **40**(8): p. 913-941.
34. Gireesha, B. and B. Mahanthesh, *Perturbation solution for radiating viscoelastic fluid flow and heat transfer with convective boundary condition in nonuniform channel with hall current and chemical reaction*. ISRN Thermodynamics, 2013. **2013**.
35. Hayat, T., et al., *Three-dimensional mixed convection flow of viscoelastic fluid with thermal radiation and convective conditions*. Plos one, 2014. **9**(3): p. e90038.
36. Hayat, T., et al., *Mixed convection stagnation point flow of Casson fluid with convective boundary conditions*. Chinese Physics Letters, 2012. **29**(11): p. 114704.
37. Sivaraj, R. and B.R. Kumar, *Chemically reacting dusty viscoelastic fluid flow in an irregular channel with convective boundary*. Ain Shams Engineering Journal, 2013. **4**(1): p. 93-101.
38. Sivaraj, R. and B.R. Kumar, *Unsteady MHD dusty viscoelastic fluid Couette flow in an irregular channel with varying mass diffusion*. International Journal of Heat and Mass Transfer, 2012. **55**(11): p. 3076-3089.
39. Srinivasacharya, D. and K. Kaladhar, *Soret and Dufour effects on free convection flow of a couple stress fluid in a vertical channel with chemical reaction*. Chemical Industry and Chemical Engineering Quarterly/CICEQ, 2013. **19**(1): p. 45-55.

29. Chow, A.W. and G.G. Fuller, *Some experimental results on the development of Couette flow for non-Newtonian fluids*. Journal of Non-Newtonian Fluid Mechanics, 1985. **17**(2): p. 233-243.
30. Ghosh, N., B. Ghosh, and L. Debnath, *The hydromagnetic flow of a Dusty Visco-Elastic fluid between two infinite parallel plates*. Computers & Mathematics with Applications, 2000. **39**(1-2): p. 103-116.
31. Kasim, A., N. Mohammad, and S.S. Aurangzaib, *Natural convection boundary layer flow of a viscoelastic fluid on solid sphere with Newtonian heating*. World Academy of Science, Engineering and Technology (64), 2012: p. 628-633.
32. Kavitha, K. and C.V.R. Murthy, *Mixed convection flow of a second grade fluid in an inclined porous channel*. International Journal of Physics and Mathematical Sciences, 2011. **1**: p. 120-139.
33. Ariel, P.D., *On exact solutions of flow problems of a second grade fluid through two parallel porous walls*. International Journal of Engineering Science, 2002. **40**(8): p. 913-941.
34. Gireesha, B. and B. Mahanthesh, *Perturbation solution for radiating viscoelastic fluid flow and heat transfer with convective boundary condition in nonuniform channel with hall current and chemical reaction*. ISRN Thermodynamics, 2013. **2013**.
35. Hayat, T., et al., *Three-dimensional mixed convection flow of viscoelastic fluid with thermal radiation and convective conditions*. Plos one, 2014. **9**(3): p. e90038.
36. Hayat, T., et al., *Mixed convection stagnation point flow of Casson fluid with convective boundary conditions*. Chinese Physics Letters, 2012. **29**(11): p. 114704.
37. Sivaraj, R. and B.R. Kumar, *Chemically reacting dusty viscoelastic fluid flow in an irregular channel with convective boundary*. Ain Shams Engineering Journal, 2013. **4**(1): p. 93-101.
38. Sivaraj, R. and B.R. Kumar, *Unsteady MHD dusty viscoelastic fluid Couette flow in an irregular channel with varying mass diffusion*. International Journal of Heat and Mass Transfer, 2012. **55**(11): p. 3076-3089.
39. Srinivasacharya, D. and K. Kaladhar, *Soret and Dufour effects on free convection flow of a couple stress fluid in a vertical channel with chemical reaction*. Chemical Industry and Chemical Engineering Quarterly/CICEQ, 2013. **19**(1): p. 45-55.

40. Adesanya, S.O. and O.D. Makinde, *Heat transfer to magnetohydrodynamic non-Newtonian couple stress pulsatile flow between two parallel porous plates*. Zeitschrift für Naturforschung A, 2012. **67**(10-11): p. 647-656.
41. Adesanya, S.O., *Steady magnetohydrodynamic visco-elastic heat generating/absorbing slip flow through a porous medium with radiation effect*. International Journal of Heat and Technology, 2012. **30**(1): p. 69-74.
42. Hassanizadeh, S.M. and W.G. Gray, *Boundary and interface conditions in porous media*. Water Resources Research, 1989. **25**(7): p. 1705-1715.
43. Ochoa-Tapia, J.A. and S. Whitaker, *Momentum transfer at the boundary between a porous medium and a homogeneous fluid—I. Theoretical development*. International Journal of Heat and Mass Transfer, 1995. **38**(14): p. 2635-2646.
44. Deng, C. and D.M. Martinez, *Viscous flow in a channel partially filled with a porous medium and with wall suction*. Chemical Engineering Science, 2005. **60**(2): p. 329-336.
45. Beavers, G.S. and D.D. Joseph, *Boundary conditions at a naturally permeable wall*. Journal of Fluid Mechanics, 1967. **30**(1): p. 197-207.
46. Kuznetsov, A., *Analytical investigation of the fluid flow in the interface region between a porous medium and a clear fluid in channels partially filled with a porous medium*. Applied Scientific Research, 1996. **56**(1): p. 53-67.
47. Kuznetsov, A., *Influence of the stress jump condition at the porous-medium/clear-fluid interface on a flow at a porous wall*. International Communications in Heat and Mass Transfer, 1997. **24**(3): p. 401-410.
48. Kuznetsov, A., *Fluid flow and heat transfer analysis of Couette flow in a composite duct*. Acta Mechanica, 2000. **140**(3): p. 163-170.
49. Kuznetsov, A., *Analytical investigation of Couette flow in a composite channel partially filled with a porous medium and partially with a clear fluid*. International Journal of Heat and Mass Transfer, 1998. **41**(16): p. 2556-2560.
50. Al-Nimr, M. and A. Khadrawi, *Transient free convection fluid flow in domains partially filled with porous media*. Transport in Porous Media, 2003. **51**(2): p. 157-172.
51. Chauhan, D.S. and R. Agrawal, *Effects of Hall current on MHD flow in a rotating channel partially filled with a porous medium*. Chemical Engineering Communications, 2010. **197**(6): p. 830-845.

52. Chauhan, D.S. and V. Kumar, *Three-Dimensional Couette flow in a composite channel partially filled with a porous medium*. Applied Mathematical Sciences, 2010. 4(54): p. 2683-2695.
53. Kuznetsov, A., *Influence of thermal dispersion on forced convection in a composite parallel-plate channel*. Zeitschrift für Angewandte Mathematik und Physik (ZAMP), 2001. 52(1): p. 135-150.
54. Kuznetsov, A., *Numerical modeling of turbulent flow in a composite porous/fluid duct utilizing a two-layer $k-\epsilon$ model to account for interface roughness*. International Journal of Thermal Sciences, 2004. 43(11): p. 1047-1056.
55. Umavathi, J., et al., *Unsteady oscillatory flow and heat transfer in a horizontal composite porous medium channel*. Nonlinear analysis: Modelling and Control, 2009. 14(3): p. 397-415.
56. Umavathi, J., *Free convection of composite porous medium in a vertical channel*. Heat Transfer—Asian Research, 2011. 40(4): p. 308-329.
57. Umavathi, J., J.P. Kumar, and K. Sridhar, *Flow and heat transfer of Poiseuille-Couette flow in an inclined channel for composite porous medium*. International Journal of Applied Mechanics and Engineering, 2010. 15(1): p. 249-266.
58. Huang, X. and C. Liu, *The developing flow in a channel filled with porous media*. International Communications in Heat and Mass Transfer, 1996. 23(1): p. 123-132.
59. Li, H., et al., *Analysis of fluid flow and heat transfer in a channel with staggered porous blocks*. International Journal of Thermal Sciences, 2010. 49(6): p. 950-962.
60. Gireesha, B., et al., *Three-dimensional Couette flow of a dusty fluid with heat transfer*. Applied Mathematical Modelling, 2012. 36(2): p. 683-701.
61. Leong, K. and L. Jin, *An experimental study of heat transfer in oscillating flow through a channel filled with an aluminum foam*. International Journal of Heat and Mass Transfer, 2005. 48(2): p. 243-253.
62. Vafai, K. and S. Kim, *Fluid mechanics of the interface region between a porous medium and a fluid layer—an exact solution*. International Journal of Heat and Fluid Flow, 1990. 11(3): p. 254-256.

63. Huang, P. and K. Vafai, *Internal heat transfer augmentation in a channel using an alternate set of porous cavity-block obstacles*. Numerical Heat Transfer, 1994. **25**(5): p. 519-539.
64. Chikh, S., et al., *Analytical solution of non-Darcian forced convection in an annular duct partially filled with a porous medium*. International Journal of Heat and Mass Transfer, 1995. **38**(9): p. 1543-1551.
65. Geindreau, C. and J.-L. Auriault, *Magnetohydrodynamic flows in porous media*. Journal of Fluid Mechanics, 2002. **466**: p. 343-363.
66. Marques, F., J. Sanchez, and P. Weidman, *Generalized Couette–Poiseuille flow with boundary mass transfer*. Journal of Fluid Mechanics, 1998. **374**: p. 221-249.
67. Terrill, R., *Flow through a porous annulus*. Applied Scientific Research, 1967. **17**(3): p. 204-222.
68. Vafai, K., *Convective flow and heat transfer in variable-porosity media*. Journal of Fluid Mechanics, 1984. **147**: p. 233-259.
69. Hinch, E.J., *Perturbation methods*. 1991: Cambridge university press.
70. Holmes, M.H., *Introduction to perturbation methods*. Vol. 20. 2012: Springer Science & Business Media.
71. Hayat, T., Y. Wang, and K. Hutter, *Hall effects on the unsteady hydromagnetic oscillatory flow of a second-grade fluid*. International Journal of Non-Linear Mechanics, 2004. **39**(6): p. 1027-1037.
72. Bejan, A., *Entropy generation minimization: The new thermodynamics of finite-size devices and finite-time processes*. Journal of Applied Physics, 1996. **79**(3): p. 1191-1218.
73. Eegunjobi, A. and O. Makinde, *Entropy generation analysis in a variable viscosity MHD channel flow with permeable walls and convective heating*. Mathematical Problems in Engineering, 2013. **2013**.
74. Adesanya, S.O. and O.D. Makinde, *Effects of couple stresses on entropy generation rate in a porous channel with convective heating*. Computational and Applied Mathematics, 2015. **34**(1): p. 293-307.
75. Mahmud, S. and R.A. Fraser, *Flow, thermal, and entropy generation characteristics inside a porous channel with viscous dissipation*. International Journal of Thermal Sciences, 2005. **44**(1): p. 21-32.

76. Chinyoka, T. and O.D. Makinde, *Analysis of entropy generation rate in an unsteady porous channel flow with Navier slip and convective cooling*. Entropy, 2013. **15**(12): p. 2081-2099.
77. Hooman, K., F. Hooman, and S.R. Mohebpour, *Entropy generation for forced convection in a porous channel with isoflux or isothermal walls*. International Journal of Exergy, 2008. **5**(1): p. 78-96.
78. Morosuk, T., *Entropy generation in conduits filled with porous medium totally and partially*. International Journal of Heat and Mass Transfer, 2005. **48**(12): p. 2548-2560.
79. Cimpean, D. and I. Pop, *Parametric analysis of entropy generation in a channel filled with a porous medium*. Recent Researches in Applied and Computational Mathematics, WSEAS ICACM, 2011: p. 54-59.
80. Chauhan, D.S. and V. Kumar, *Effects of slip conditions on forced convection and entropy generation in a circular channel occupied by a highly porous medium: Darcy extended Brinkman-Forchheimer model*. Turkish Journal of Engineering and Environmental Sciences, 2010. **33**(2): p. 91-104.
81. Srinivasacharya, D. and K.H. Bindu, *Entropy generation in a micropolar fluid flow through an inclined channel*. Alexandria Engineering Journal, 2016. **55**(2): p. 973-982.
82. Sparrow, E. and R. Cess, *The effect of a magnetic field on free convection heat transfer*. International Journal of Heat and Mass Transfer, 1961. **3**(4): p. 267-274.
83. Raptis, A. and N. Kafousias, *Heat transfer in flow through a porous medium bounded by an infinite vertical plate under the action of a magnetic field*. International Journal of Energy Research, 1982. **6**(3): p. 241-245.
84. Tasnim, S.H., M. Shohel, and M.A.H. Mamun, *Entropy generation in a porous channel with hydromagnetic effect*. Exergy, An International Journal, 2002. **2**(4): p. 300-308.
85. Kumar, V., et al., *Entropy generation in poiseuille flow through a channel partially filled with a porous material*. Theoretical and Applied Mechanics, 2015. **42**(1): p. 35-51.
86. Umavathi, J., et al., *Unsteady flow and heat transfer of porous media sandwiched between viscous fluids*. Applied Mathematics and Mechanics, 2010. **31**(12): p. 1497-1516.

87. Kaur, P.P., S. Agrawal, and A. Kumar, *Finite Difference Technique for Unsteady MHD Periodic Flow of Viscous Fluid through a Planer Channel*. American Journal of Modeling and Optimization, 2013. **1**(3): p. 47-55.
88. Shanker, B. *Magneto-hydrodynamic effects on the flow of blood through a porous channel*. IEEE Engineering in Medicine and Biology Society and 14th Conference of the Biomedical Engineering Society of India. An International Meeting, Proceedings of the First Regional Conference., IEEE. 1995: IEEE.
89. Jha, B.K., A.K. Samaila, and A.O. Ajibade, *Unsteady/steady free convective couette flow of reactive viscous fluid in a vertical channel formed by two vertical porous plates*. ISRN Thermodynamics, 2012. **2012**.
90. Jha, B.K. and J. Odengle, *Unsteady couette flow in a composite channel partially filled with porous material: A Semi-analytical Approach*. Transport in Porous Media, 2015. **107**(1): p. 219-234.

From QAU Theses (CL QAU)

- Processed on 14-Jan-2019 14:33 PKT
- ID: 1063915873
- Word Count: 26659

Similarity Index
18%
Similarity by Source

Internet Sources:
11%
Publications:
10%
Student Papers:
5%

M. Nasir
14/01/2019
Focal person (Turnitin)
Quaid-i-Azam University
Islamabad

sources:

- 1 1% match (Internet from 17-Jul-2010)
<http://www.lana.lt/journal/34/Umvathi.pdf>
- 2 1% match (publications)
Vyas, Paresh, and Nupur Srivastava. "Entropy Analysis of Generalized MHD Couette Flow Inside a Composite Duct with Asymmetric Convective Cooling". *Arabian Journal for Science and Engineering*. 2015.
- 3 < 1% match (publications)
"Applications of Fluid Dynamics". Springer Nature. 2018
- 4 < 1% match (publications)
Donald A. Nield, Adrian Bejan. "Convection in Porous Media". Springer Nature. 2017
- 5 < 1% match (student papers from 24-Jun-2014)
Submitted to Universiti Teknologi Petronas on 2014-06-24
- 6 < 1% match (Internet from 21-Nov-2017)
<https://link.springer.com/content/pdf/10.1007/978-3-319-49562-0.pdf>
- 7 < 1% match (student papers from 09-Feb-2018)
Submitted to Higher Education Commission Pakistan on 2018-02-09
- 8 < 1% match (publications)
M.D. Shamshuddin, S.R. Mishra, Q. Anwar Bég, A. Kadiri. "Unsteady reactive magnetic radiative micropolar flow, heat and mass transfer from an inclined plate with joule heating: A". *Proceedings of the Institution of Mechanical Engineers, Part C: Journal of Mechanical Engineering Science*. 2018
- 9 < 1% match (Internet from 02-Sep-2013)
<http://www.kikiwi.fr/uploads/data/Picali/Picali901.dat>
- 10 < 1% match (Internet from 24-Nov-2017)
https://www.cambridge.org/core/services/aop-cambridge-core/content/view/B111AF4AB1D4D6DEED64605DDDFCEFC4/S1727749112018003a.pdf/poiseuillecouette_flow_and_heat_transfer_in_an_incl
- 11 < 1% match (Internet from 29-Aug-2017)
<http://www.proba.jussieu.fr/pageperso/fournier/a63.pdf>
- 12 < 1% match (Internet from 14-Apr-2016)
<http://journals.tubitak.gov.tr/engineering/issues/muh-09-33-2/muh-33-2-2-0903-9.pdf>
- 13 < 1% match (publications)
J. C. Umavathi. "Free convection of composite porous medium in a vertical channel". *Heat Transfer-Asian Research*. 06/2011
- 14 < 1% match (publications)
Bult, Adnan Saeed, Asif Ali, and Ahmer Mehmood. "Numerical investigation of magnetic field effects on entropy generation in viscous flow over a stretching cylinder embedded in a porous

Khalid Mirza
KHALID MISHRANIRZA
Assistant Librarian
DRSM LIBRARY
Quaid-i-Azam University
ISLAMABAD